A CALIBRATION PROCEDURE FOR THE MEASUREMENT OF TRANSVERSE VORTICITY USING HOT-WIRE ANEMOMETRY

By

Casey Lynn Klewicki

A THESIS

Submitted to

Michigan State University

in partial fulfillment of the requirements

for the degree of

MASTER OF SCIENCE

Department of Mechanical Engineering

1983

ABSTRACT

A CALIBRATION PROCEDURE FOR THE MEASUREMENT OF TRANSVERSE VORTICITY USING HOT-WIRE ANEMOMETRY

By

Casey Lynn Klewicki

A technique to obtain an irregular time series of the transverse vorticity from the four measured hot-wire voltages of a vorticity probe is presented. The complete technique involves several calculation schemes, including those for the calibration and the flow field data. The schemes are presented in detail and demonstration data, from a large plane shear layer, are used to demonstrate them.

ACKNOWLEDGMENTS

I would like to express my appreciation to my parents for their continual support and encouragement throughout my entire college career.

I would like to recognize the support of Lockheed of Georgia Co., grant monitor: Dr. A. S. W. Thomas and the support of NASA Langley Research Center, grant monitor: Dr. J. Yu. I am pleased to acknowledge the substantial contribution of Mr. Peter J. Disimile to the clarification and organization of flow charts for the vorticity algorithms during their initial development stages. I would like to express my gratitude and appreciation to my thesis advisor, Dr. John F. Foss, for his guidance throughout my graduate program.

TABLE OF CONTENTS

LIST OF TABLES

LIST OF FIGURES

LIST OF SYMBOLS

A	Collis and Williams parameter
b	modified Collis and Williams parameter
B	Collis and Williams parameter
n	Collis and Williams parameter
E	anemometer output voltage
E_a	voltage from designated angle-wire (slant wire 1 or 2)
E_s	voltage from designated speed-wire (slant wire 1 or 2)
Gr	Grashoff number
Q	velocity
Q_p	velocity determined from output voltage of parallel array
Q_x	velocity determined from output voltage of x-array
Q_{xp}	defined by eq. 3.9
Re	Reynolds number
s-n	local micro-circulation domain coordinates
U_{oo}	free stream velocity
u,v,w	velocity components relative to laboratory coordinates
u_s, u_n	velocity components relative to micro-domain coordinates
x,y,z	laboratory coordinates
α	angle between pitch angle γ and laboratory x-coordinate
β	angle of hot wire; defined in Figure 2.2a
δt	incremental time between data samples: 1/sample rate
δs	incremental convection length

Δ	distance between straight wires of the parallel array (mm)
$\Delta\gamma^{o}$	convergence check for Q,γ iteration scheme
γ	pitch angle of velocity vector relative to probe axis
λ	data-day correction factor
Ω	angular velocity
τ	psuedo-time variable as defined by eq. 2.9
θ	angle between probe axis and laboratory x-axis
ω_z	transverse vorticity
ω_x	streamwise vorticity

subscripts

a	identified with angle-wire
c	identified with (master) calibration of the vorticity probe
d	identified with data-day
i	counter for τ
j	counter for t (data sampled at t_j)
p	identified with parallel array
s	identified with speed-wire
x	identified with x-array

CHAPTER 1

INTRODUCTION

The concept of vorticity is fundamental to the understanding of turbulent flows. Fluctuating, three-dimensional, components of vorticity are a necessary condition for a flow to be labeled turbulent; hence, vorticity ($\vec{\omega}$) is a primitive variable of turbulent flows. Corrsin and Kistler[1] considered this in their study of the boundary region between a turbulent and non-turbulent flow. A signal from a pyramidal configuration of four hot-wires, responding primarily to the streamwise component of vorticity, was used to detect the passage of the turbulent - non-turbulent boundary. More recently Kibens, Kovasznay and Oswald [2] have developed an anolog circuit for the detection in real time of the boundary. Several input signals to the detector were considered. The signal chosen was that used by Corrsin and Kistler (a signal proportional to ω_x) since it offered the most contrast between the turbulent and non-turbulent regions. Hardin [3] has used the concept of vorticity to model and predict the far field noise associated with turbulent jets. Willmarth and Bogar [4], in their investigation of the near wall region of a turbulent boundary layer, used the concept of pressure gradients at the wall as a source of vorticity. They attempted to measure the streamwise component of vorticity in order to gain understanding of the turbulent structures

and mechanisms that result in an increase or decrease of drag. Several other studies, Brown and Roshko[5], Blackwelder and Eckelmann[6], Eckelmann, Nychas, Brodkey, and Wallace[9], Signor and Falco[7], Falco and Lovett[8], etc have also used vorticity in attempts to understand phenomena associated with turbulent flows, i.e., coherent structures (typical eddies), bursting phenomenon, mixing, etc. Thus an accurate measurement of the instantaneous vorticity would be most useful in experimental fluid mechanics.

1.0 Historical Review of Techniques to Measure Vorticity

The measurement of vorticity is much more difficult than measuring velocity. Each component of vorticity involves spatial gradients in two different directions of two different velocity components. Hence, the measuring instruments (hot-wire anemometry, hot films, LDV) tend to be complex, both geometrically and electrically. Typically if hot-wires are used, more than one probe is involved, which suggests multichannels and simultaneous measurements. Even so, the final measurement is usually one or two out of the three components of vorticity.

Kovasznay [10], 32 years ago, developed a streamwise vorticity meter. (Since then, it has been commonly referred to as the Kovasznay-type probe). It consists of four hot-wires mounted on four prongs, which form a Wheatstone Bridge when operated as a constant current anemoneter. The output voltage across opposite prongs is proportional to the streamwise vorticity, ω_x. Some of the earliest users

were Uberoi and Corrsin[11] for studies of the propagation of a turbulence into non-turbulent regions. At that time the probe was assumed to be insensitive to cross-stream velocities. Since that time Kastrinakis, Eckelmann and Willmarth[12] have investigated the influence the effect of these transverse velocities on the ω_x measured by the Kovasznay probe. The authors concluded that instantaneous measurements of vorticity in flows of high turbulence levels is impossible since the influence of the transverse velocity fluctuations (u', v') cannot be corrected for; simultaneous knowledge of both u' and v' is unavailable. Also the effect of these components of velocity can not be ignored since they may be of the same order of magnitude as the vorticity signal being observed. To allow for the measurement of all three velocity components and their influence on ω_x, Vukoslavcevic and Wallace[13] constructed a probe with the same configuration as the Kovasznay probe but supported each wire by a separate pair of prongs (a total of 8), and electrically operated each wire independently. In effect the configuration is 2 x-arrays in perpendicular planes which are parallel to the flow. It was concluded that the instantaneous ω_x measurment was badly in error whether transverse velocity components were accounted for or not, since the effects of the velocity gradients introduced large errors in their measurement. The errors could be reduced by decreasing the spacing between wires, but thermal cross talk then becomes a problem.

In an investigation of the vortex structures associated with the bursting phenomenon, Blackwelder and Eckelmann[6] developed a technique to obtain a measure two vorticity components in the near wall

region. Two hot film sensors in a v-configuration were flush mounted to the wall with a hot-wire located directly above, the signals were considered to be proportional to ω_x and ω_z.

The importance of making direct measurements of vorticity is attested to by the novel concepts that have been developed for this purpose. Two of these are noted in the following. Frish and Webb[14] developed an optical method to directly measure vortictiy in fluid flows. Spherical particles imbedded with crystal mirrors were suspended in a liquid. The vorticity was obtained directly by measuring the time required for laser reflections from the mirrors to rotate through small angles, $\Omega=.5\omega$. The technique is limited by sensitivity of the optics and electronics to noise and the technique can only determine the vorticity of one sign. Lang and Dimotakis[15] have used a laser doppler velocimeter technique to measure the circumferential velocity components at the 4 vertices of a small diamond shaped region. These velocity components can be related to the curl of V, i.e. through the use of Stokes theorem. Smoothing and interpolation procedures are required since the probability of obtaining four simultaneously sampled velocities at the four vertices, is relatively small.

Foss, in a series of publications[16,17,18] presents the development of a technique to obtain a measure of the transverse component of vorticity using a 4 wire array. The present manuscript reports important revisions and improvements of the technique and calculation schemes. The technique lends itself to flows in which large pitch

angles are encountered; free shear flows, outer regions of boundary layers and wakes. Specifically, this writing presents the theory and computational schemes involved in obtaining a time series of the transverse vorticity, strain rate, and velocity components for a small sample domain in a flow field. The influence of the transverse velocity, w, on the measurements is analytically described and a technique to correct for its existance is presented and it is applied to a body of data. Experimental data, obtained in a free shear flow, have been used to demonstrate the complete technique. An organizational flow chart of the complete technique used to obtain the values for the time series of vorticity, strain rate and velocity components from the vorticity probe response voltages, E_1, E_2, E_3, E_4, is shown in Figure 1.1. Each rectangular box represents a supporting calculation scheme used in determining the time series values. Note that these calculation schemes utilize various functions which are defined from a complete calibration data set.

CHAPTER 2

VORTICITY MEASUREMENT

2.0 Introduction

A regular time series of voltages from an array of four hot wires is used to obtain an irregular time history of vorticity. The computational scheme used to determine the time history of vorticity has the same basic structure as the scheme described in Foss [21] but with important additions and revisions. The complete method is described herein.

2.1 A Qualitative Description of the Micro-Circulation Domain

The quantities derived from the four wire probe are to be spatially averaged values over a small domain ($\lesssim$ 1mm). The domain will be referred to as the 'micro-circulation' domain. These spatially averaged values approach 'point measures' in the flow field for situations where the scale of the micro-circulation domain is sufficiently smaller than the scales of the motion being studied. An example of such a flow field is shown in Figure 2.1a; the measurements, taken in the intermittent region of the free shear layer with a hot-wire probe, approach point measures since the length scale of the probe is much smaller than that of the energetic turbulent motion. For the smaller

scales, the scheme acts as a low pass spatial filter; ie; the smallest scale that can be measured is limited by the length scale of the micro-circulation domain.

In constructing a value for the transverse vorticity, ω_z, two spatial velocity gradients are required; $\omega_z = \partial v/\partial x - \partial u/\partial y$. A value for the cross-stream spatial gradient $\partial u/\partial y$ may be obtained by using measurements from two hot wire probes that are parallel to the z-axis and separated by a distance Δy. The measurement of $\partial v/\partial x$, by using two probes that are displaced in the streamwise direction, would be disallowed due to probe interference effects. Hence a streamwise length proportional to (velocity) x (time) is used instead. Foss [16] used $[(1/u)\partial/\partial t] \simeq -\partial/\partial x$; however this formulation does not account for the contribution of $v\partial[\ ]/\partial y$ to the $\partial[\ ]/\partial t$ value. A more accurate description would utilize the total velocity component in the x-y plane as the convection or translation velocity: $(1/Q)\partial[\ ]/\partial t = -\partial[\ ]/\partial s$. An incremental streamwise length: δs, may be defined in this manner and an appropriately defined sum of such lengths may be used to create a micro-domain over which the vorticity (ω_z) is defined as:

$$\langle \omega_z \rangle \Delta A = \int_{\Delta A} \omega_z \, dA \; ; \quad \text{where } \Delta A = \Delta s \Delta n \qquad \text{(eq. 2.1)}$$

A schematic representation of the micro-domain is shown in Figure 2.1b. Note that the width of the domain: Δn, depends upon the spatial orientation of the parallel array with respect to an average of the streamwise directions for the time segment used to define the micro-domain. The time segment is chosen such that the micro-domain

is nominally square: $\Delta s \simeq \Delta n$. As a result of these procedures, the regularly sampled voltages: $\{ E_1(t_j), \ldots E_4(t_j)\}$, are converted to an irregular time series of spatially averaged values over the micro-domain: $\langle u(\tau_i)\rangle, \langle v(\tau_i)\rangle, \langle \omega(\tau_i)\rangle$, and $\langle \varepsilon_{xy}(\tau_i)\rangle$. The irregular time series: τ_i, reflects the variable speed of translation as well as the variable dimensions of the micro-domain.

2.2 The Vorticity Probe

The vorticity probe consists of four hot wires or two arrays: an x-array and a parallel array. A schematic representation of the probe is presented in Figures 2.2a and 2.2b. The slant wires of the x-array are nominally at an angle of 45° with respect to the probe axis. The distance between them is of the order 1mm. The parallel array is located below the x-array and consists of 2 straight wires which are parallel to the z-axis. They are separated by a distance of nominally 1mm. The placement of the parallel array is such that the wires are directly below the active region of the x-array wires; hence, the measurements from the parallel and x-arrays are at the same streamwise location. The distance between centers of the 2 arrays is approximatlely 3.8 mm.

The fundamental, and the most limiting, assumption in the use of the four wire array to define ω_z is that:

$$\partial\gamma/\partial z \simeq 0 \quad \text{for each } t_j \text{ value}$$

The (δz) separation between the two arrays requires that this assumption be made; its validity is dependent upon the instantaneous character of the velocity field. One motivation for the present algorithm, and that of Foss [17] is that the error in: $\partial\gamma/\partial z \simeq 0$, is presumed to be much less than the error in the alternative assumption: $\partial(\partial v/\partial x)/\partial z \simeq 0$, a la Foss [18].

Each of the 4 wires of the vorticity probe is fabricated using the same technique. A representative wire is shown in Figure 2.2.b The wire is 5 μm tungsten which is copper plated on the ends. The copper plating enables the wire to be soft-soldered to the ends of the jeweler's broaches (prongs) and it aerodynamically isolates the active portion of the wire from the prongs. The total wire length is nominally 3mm with an active portion of 1mm, ie $l/d \geq 200$. The minimum spatial resolution that can be expected is greater than or equal to 1mm. No wire length corrections, (e.g., Wyngaard[19]) were utilized in the present algorithms. According to Collis and Williams[20] and others, the effects of bouyancy forces may be neglected if $Gr < Re^2$. For the condition; $Gr \geq Re^2$, the velocity components adjacent to the wire induced by the buoyancy forces become comparable in magnitude with the flow velocity being measured. The relation $Gr < Re^2$ therefore defines the lowest speed at which the hot wire is capable of measuring without ambiguity. For the flow conditions and hot-wires used in the present study the effect of buoyancy forces was insignificant. That is the Grashoff number was of the order 3.5E-06 (using an overheat ratio of 1.7) and the Reynolds number based on the 5μm diameter was of the order .59 for U_{oo}=2m/s. The free convection effects for these

conditions would become significant at a flow speed of .05m/s or less.

2.3 Role of the x-array in the Vorticity Calculation

The primary role of the x-array is to provide a measure of the pitch angle γ at the location of the vorticity probe. This pitch angle information is used at the parallel array location in defining the velocity components and the orientation of the micro-circulation domain with respect to the probe axis. It is assumed that the spatial variations of the pitch angle are sufficiently small that:

$$\gamma(x,y,z+\delta z) \simeq \gamma(x,y + \Delta/2,z)$$
$$\simeq \gamma(x,y - \Delta/2,z)$$

A secondary role of the x-array is to provide the requisite information to allow a correction for the influence of the transverse velocity. Namely, if the velocity magnitude determined from the x-array exceeds the velocity magnitude defined by the parallel array, the difference may be attributed to the existance of a (w^2) influence on the hot wire voltages of the x-array. A technique to correct for this w^2 influence is presented in a later section.

2.4 The Vorticity Calculation

2.4.1 Definiton of the Micro-Circulation Domain

The vorticity calculation scheme yields a time series of spatially averaged quantities; the velocity components ($\langle u \rangle, \langle v \rangle$) and their

derivatives from which the transverse vorticity, and the strain rate are found. The spatial averaging is performed in a region referred to as the micro-circulation domain. This domain has been defined qualitively in section 2.1. The present section provides an operational definition of this domain and specifies the procedures which are used to compute the locally averaged quantities.

A key element in the computational procedure is the use of cumulative averaged quantities for the identification of the length (Δs) and the width (Δn) of the micro-circulation domain. The cumulative averaging procedure can be defined using the terms introduced in Figure 2.3 and the following operational steps.

For a given time step (t_j), the previous and present quantities are used to define an incremental value; e.g., the convection speed for the increment: $t_{j-1} \rightarrow t_j$ is:

$$Q_{convection}(t_j) = 0.5\left[[(Q_3+Q_4)/2](t_j) + [(Q_3+Q_4)/2](t_{j-1})\right] \quad \text{(eq. 2.2)}$$

The locally averaged quantities at time (τ_i) are defined by the incremental values existing between τ_{i-1} and τ_i. For purposes of illustration, consider a time counter: k, such that k=0 at τ_{i-1}. The convection speed: $Q_c(t_k)$, and the cumulative average of γ:

$$\langle\gamma(t_k)\rangle = (\gamma_0 + \gamma_1 + \gamma_2 + \ldots + \gamma_k) \;/\; (k+1), \quad \text{(eq. 2.3)}$$

are used to define an incremental length in the streamwise direction:

$$\delta s(t_k) = Q_c(t_k)\cos(\gamma(t_k) - \langle\gamma(t_k)\rangle)(t_k - t_{k-1}) \qquad \text{(eq. 2.4)}$$

where $\gamma(t_k)$ is the incremental value for $t_{k-1} \rightarrow t_k$.

The corresponding value of the transverse dimension is:

$$\Delta n(t_k) = \Delta\cos(\gamma(t_k) - \langle\gamma(t_k)\rangle). \qquad \text{(eq. 2.5)}$$

Note that the $\Delta n(t_k)$ values will form a convergent series for the expected, i.e., smoothly varying, $\gamma(t_k)$ values.

The nominally square micro-domain is established by comparing, at each time step value, Δn with the cumulative sum of the δs values. Namely, for

$$\Delta s(t_k) = \sum_{k'=1}^{k} \delta s(t_{k'}), \qquad \text{(eq. 2.6)}$$

the computational scheme allow k to increase until the cumulative length first exceeds the current value of the width:

$$\Delta s(t_k) \geq \Delta n(t_k) \qquad \text{(eq. 2.7)}$$

The proper number of time steps (N) is defined as that value which causes Δs to most nearly equal Δn. Specifically, N=k if

$$\left[\Delta s(t_k) - \Delta n(t_k)\right] < \left[\Delta n(t_{k-1}) - \Delta s(t_{k-1})\right]. \qquad \text{(eq. 2.8)}$$

Similarly, N=k-1 if the inequality is reversed. These operations

define the number of time steps to proceed from τ_{i-1} to τ_i; viz.

$$\tau_i = \tau_{i-1} + N\delta t_j \qquad \text{(eq. 2.9)}$$

and the quantities at these two limits will be identified as, for example, $u_n(\tau_i)$ or $u_n(\tau_{i-1})$. It is pertinent to note that the nature of the variable in question defines whether it represents an instantaneous (e.g., $u_n(\tau_i)$), an incremental (e.g., $\delta s(t_k)$), or a cumulative (e.g., $\langle\gamma(\tau_i)\rangle$) value. The procedures to evaluate the spatial average quantities given the correct N value are presented in the following.

2.4.2 Micro-Domain Average Values

The spatial average value for the transverse vorticity over the micro-circulation domain $[\Delta n\Delta s](\tau_i)$, can be expressed as:

$$\langle\omega_z\rangle(\tau_i) = (\Delta s\Delta n)^{-1}\int_A \omega_z \, dn\,ds. \qquad \text{(eq. 2.10)}$$

The area integral in eq. 2.10 is transformed into a contour integral around the circumference of the parallelogram $\Delta s\Delta n$ by applying Stokes Theorem:

$$\langle\omega_z\rangle = (\Delta n\Delta s)^{-1}\left[\int_{n-\Delta n/2}^{n+\Delta n/2}[u_n(s+\Delta s/2) - u_n(s-\Delta s/2))\cos\langle\gamma\rangle]dn/\cos\langle\gamma\rangle - \int_{s-\Delta s/2}^{s+\Delta s/2}[u_s(n+\Delta n/2) - u_s(n-\Delta n/2)]ds\right] \qquad \text{(eq. 2.11)}$$

Figure 2.4 shows a representation of the defined circulation loop around the circumference of the micro domain. The first integral in

equation 2.11 may be interpreted as $\langle \partial u_n/\partial s \rangle$ and the second integral as $\langle \partial u_s/\partial n \rangle$. Hence equation 2.11 may be rewritten in terms of these spatial velocity gradients;

$$\langle \omega_z \rangle = \langle \partial u_n/\partial s \rangle - \langle \partial u_s/\partial n \rangle \qquad \text{(eq. 2.12)}$$

The strain rate, ε_{xy}, may be readily evaluated using these spatial velocity gradients; viz.,

$$\langle \varepsilon_{xy} \rangle = \langle \partial u_n/\partial s \rangle + \langle \partial u_s/\partial n \rangle \qquad \text{(eq. 2.13)}$$

The evaluation of $\langle \partial u_n/\partial s \rangle$ is estimated using the difference between the cross-stream velocity u_n calculated at s and s+Δs and then dividing by Δs_i, ie.;

$$\langle \partial u_n/\partial s \rangle(\tau_i) = [u_n(\tau_{i-1}) - u_n(\tau_i)] \,/\, \Delta s(\tau_i) \qquad \text{(eq. 2.14)}$$

where

$$u_n(\tau_i) = Q_p(\tau_i)\sin(\gamma(\tau_i) - \langle \gamma(\tau_i) \rangle) \qquad \text{(eq. 2.15)}$$

$$u_n(\tau_{i-1}) = Q_p(\tau_{i-1})\sin(\gamma(\tau_{i-1}) - \langle \gamma(\tau_i) \rangle) \qquad \text{(eq.2.16)}$$

and

$$Q_p = (Q_3 + Q_4)/2. \qquad \text{(eq. 2.17)}$$

The factor $\sin(\gamma(\tau_i)-\langle\gamma(\tau_i)\rangle)$ accounts for the difference between the direction of the instantaneous streamwise velocity $[Q_p(t_j)]$ and the mean flow direction: $\langle\gamma(\tau_i)\rangle$, for the averaging time τ_{i-1} to τ_i of the current micro-circulation domain.

The second integral represents $\langle\partial u_s/\partial n\rangle(\tau_i)$ which is analogous to $\langle\partial u/\partial y\rangle$ in laboratory coordinates. The strategy to obtain a value for $\langle\partial u_s/\partial n\rangle(\tau_i)$ utilizes a summation of the incremental values of $\delta u_s(t_k)$; namely, for

$$\partial u_s(t_k) = 0.5\Big[(Q_4-Q_3)\cos(\gamma(t_k)-\langle\gamma(t_k)\rangle) + (Q_4-Q_3)\cos(\gamma(t_{k-1})-\langle\gamma(t_{k-1})\rangle)\Big] \qquad \text{(eq. 2.18)}$$

the $\langle\partial u_s/\partial n\rangle$ value can be written as

$$\langle\partial u_s/\partial n(\tau_i)\rangle = \sum_{k=1}^{N}[\delta u_s(t_k)][\delta s(t_k)] \;/\; [\Delta n(\tau_i)\sum_{k=1}^{N}\delta s(t_k)] \qquad \text{(eq. 2.19)}$$

Note that the factor $\cos(\gamma(t_k)-\langle\gamma(t_k)\rangle)$ aligns each incremental convective length: $\delta s(t_k)$, with the average convection velocity vector of the fluid element. In a similar manner, the spatial average for the two velocity components, $\langle u_s(\tau_i)\rangle$ and $\langle u_n(\tau_i)\rangle$ are also defined over the micro-circulation domain: $\Delta s\Delta n(\tau_i)$, as:

$$\langle u_s(\tau_i)\rangle = (\Delta s)^{-1}\sum_{k=1}^{N} 0.5\Big[Q_p(t_k)\cos(\gamma(t_k)-\langle\gamma(t_k)\rangle) + Q_p(t_{k-1})\cos(\gamma(t_{k-1})-\langle\gamma(t_{k-1})\rangle)\Big]\delta s(t_k) \qquad \text{(eq. 2.20)}$$

$$\langle u_n(\tau_i)\rangle = (\Delta s)^{-1}\sum_{k=1}^{N} 0.5\Big[Q_p(t_k)\sin(\gamma(t_k)-\langle\gamma(t_k)\rangle) + Q_p(t_{k-1})\sin(\gamma(t_{k-1})-\langle\gamma(t_{k-1})\rangle)\Big]\delta s(t_k) \qquad \text{(eq. 2.21)}$$

Thus equations 2.12-21 are used to obtain values for the irregular time series of the spatially averaged quantities: $\langle u_s(\tau_i)\rangle$, $\langle u_n(\tau_i)\rangle$, $\langle \partial u_s/\partial n(\tau_i)\rangle$, $\langle \partial u_n/\partial s(\tau_i)\rangle$, $\langle \omega_z(\tau_i)\rangle$, $\langle \varepsilon_{xy}(\tau_i)\rangle$. These quantities are in terms of the s-n or micro-circulation domain coordinates. A coordinate transformation converts these quantities to laboratory coordinates: x-y; the transformation equations are presented in Appendix B. The vorticity values are independent of this transformation but the strain rate, velocity components and their derivatives are not. Figure 2.5 shows the relation between the s-n coordinates, probe coordinates and the laboratory coordinates. The relative angle between the x-y and s-n coordinate systems of a given micro-circulation domain is given by

$$\alpha(\tau_i) = \theta + \langle\gamma(\tau_i)\rangle \ , \qquad \text{(eq. 2.22)}$$

where θ is the angle between the vorticity probe axis and the x-laboratory coordinate and $\langle\gamma(\tau_i)\rangle$ is the angle between the velocity vector $\langle Q(\tau_i)\rangle$ and the vorticity probe axis.

CHAPTER 3

SUPPORTING SCHEMES FOR THE VORTICITY CALCULATION

3.0 Introduction

The complete scheme to determine the time history of the transverse vorticity involves several intermediate calculations; specifically, the regular time series: $[Q_x(t_j),\gamma(t_j)]$, is computed from the slant wires of the x-array, and a calculation to correct for the influence of the transverse velocity component on the computed Q_x and γ values may be performed. The present section describes these calculation procedures and the extensive processing of the calibration data that is required to support them.

3.1 Determining Q and γ From the x-array Voltages

The response of the x-array, $[E_1,E_2](t_j)$, is used to construct the regular time series of $Q_x(t_j),\gamma(t_j)$. Basically there are three schemes that have been evolved from which the Q_x and γ information may be extracted from the x-array measurements: (1) a two-equation/two-unknown scheme technique (e.g., Bradshaw [21]), (2) a table look-up (e.g. Willmarth and Bogar [4]) and (3) an iterative : speed wire/angle wire procedure (Foss [18]). The data base for the iterative scheme is similar to that required for the table look-up

technique. Smoothing and interpolation operations that are made possible by the use of analytic relationships, are employed in the iterative technique; hence, this method gains accuracy, at the expense of computation time and complexity, with respect to the table look-up scheme.

The two-equation/two-unknown scheme is characterized by the method described by Bradshaw [21]. For $E^2=A+BQ^n_{eff}$ and $Q_{eff}=Q\cos(\beta-\gamma)$, the resulting velocity component equations are:

$$u\cos\beta_1 + v\sin\beta_1 = \left[(E_1^2-A_1)/B_1\right]^{1/n_1} \qquad \text{(eq. 3.1)}$$

$$u\cos\beta_2 + v\sin\beta_2 = \left[(E^2{}_2-A_2)/B_2\right]^{1/n_2} \qquad \text{(eq. 3.2)}$$

where

$$\gamma = TAN^{-1}(v/u) \qquad \text{(eq 3.3)}$$

Thus the regular time series of sampled voltages $[E_1,E_2](t_j)$ from the x-array are used to obtain a regular time series of $u(t_j),v(t_j),\gamma(t_j)$. This calculation scheme is referred to (herein) as COSLAW and is described more fully in Appendix A. Implicitly, it is assumed that the cosine relationship is uniformly valid over a range of angles from the orientation at which the calibration is executed (i.e.; $\gamma=0$ for the present study).

A correction to the basic cosine relationship can extend the range of validity for a given slant wire; for example, Foss [16] considers the available analytical forms. The pitch angle range of validity for the cosine and extended cosine laws for a given slant wire is shown schematically in Figure 3.1. Note that the viable range for an x-array to deliver accurate Q and γ values is limited by the inaccuracy of the analytical form at large $|\beta-\gamma|$ values. The range of pitch angles where the analytical form fails to describe $E=f(Q,\gamma)$ relationship is referred to as the 'outer range'. This inability of a single analytic form to accurately represent $E(Q,\gamma)$ in the 'outer range' motivates the development of an alternative calculation strategy. The strategy involves the designation, for a given data pair $[E_1,E_2]$, of one slant wire as the angle wire and one slant wire as the speed wire. An iterative calculation is used to determine Q_x and γ for each sample time t_j as noted below.

3.1.1 Speed-Wire/Angle-Wire Technique: Iterative

At a given sample time, t_j, one of the slant wires will be oriented at a relatively large value of $|\beta-\gamma|$ while the other will be at a relatively small value of $|\beta-\gamma|$. The wire at the small $|\beta-\gamma|$ value is designated the 'speed wire' since it is predominantly sensitive to the speed Q and minimally sensitive to the pitch angle γ. Likewise, the wire at large $|\beta-\gamma|$ is designated the 'angle wire' and is most sensitive to γ with a reduced sensitivity to Q. Figure 3.2 depicts wire 1 as the speed wire and wire 2 as the angle wire (i.e. $\gamma>0^\circ$).

Given the state shown in Figure 3.2, the pitch angle and flow speed are determined as follows. From the calibration of the x-array the functions: f_a and f_s, are available; specifically,

$$\gamma = f_a(E_a(\gamma)/E_a(0);Q_{jj}) \qquad \text{(eq. 3.4)}$$

$$Q_s = f_s(E_s;\gamma_c) \qquad \text{(eq. 3.5)}$$

where the convention: (a;b) is used to distinguish between an independent variable: 'a', and a parameter: 'b'. Figures 3.3a-c show schematically how these functions are used to obtain the Q_x and γ values. Note that wire 1 is the speed wire and wire 2 is the angle wire for this illustration.

The calculation scheme is initiated with an estimate for the speed ,Q_x, via the COSLAW technique. Using Q_x as a parameter, the pitch angle γ is determined from the functional form given in eq. 3.4, for which $|Q_x-Q_{jj}|$ is minimized. Then, using γ as a parameter, a new value for the speed is determined from the functional form given in eq. 3.5, for which $|\gamma-\gamma_c|$ is minimized. (Note, both Q_{jj} and γ_c are members of the calibration grid; see Figure 4.1.) For values of $\gamma \neq \gamma_c$ the speed is adjusted accordingly by (locally) employing the concept of an effective cooling velocity;

$$Q_x(E_s;\gamma) = Q_s \left[\cos(\beta-\gamma_c)/\cos(\beta-\gamma)\right] \qquad \text{(eq. 3.6)}$$

The value of Q_x, found using eq. 3.6, may then be used as the parameter to re-evaluate γ. The process iterates to convergence wherein $|\gamma_{n+1}-\gamma_n| \leq \Delta\gamma^\circ$. A value of $\Delta\gamma^\circ=.5^\circ$ was used for the present study, but the value may be arbitrarily established. Note that as $\Delta\gamma^\circ \to 0$ the Q,γ values converge to the true values. This convergence was observed numerically and it follows from considering the effect of a perturbation, from the true values, in the sequence of steps shown in Figures 3.3a-c.

The above iterative scheme accurately determines Q_x and γ for large $|\beta-\gamma|$ values. At the smaller $|\beta-\gamma|$ values the accuracy is also maintained but the convergence time is significantly increased with respect to using an explicit two-equation/two-unknown scheme. To maximize the accuracy and efficiency in determining Q_x and γ from the $[E_1,E_2]$ data pairs, the calculation algorithm employs both methods. The initial value of γ is determined using the COSLAW; if it exceeds the $\pm 12^\circ$ range, then the corresponding Q_x value is used as the starting value for the iteration technique. If the initial value of γ is within the $|\gamma| \leq 12^\circ$ range, then this initial value is accepted and the computation continues with the Q_x and γ values provided by the COSLAW calculation.

3.2 Three-Dimensional Effects

3.2.1 Effect of the Transverse Velocity Component on the Q_x and γ Evaluation

Neither the COSLAW nor the iterative scheme accounts for the

effects of a transverse velocity component (w)on the response of slant wires. Neglecting this effect may introduce significant errors in the Q_x and γ values calculated from the "contaminated" x-array voltages. These errors have been observed, for example, by Vukoslavcevic and Wallace [13], Bruun [23] and Kastrinakis, Eckelmann and Willmarth [12] in flows where large turbulence intensities are present. In the analyses of their data, these authors have accounted for the effect of the transverse velocity by including higher order terms in the model for the hot wire response. The following section presents a different technique for determining the magnitude of the transverse velocity (w) and a method to correct for its influence on the calculated values of Q_x and γ.

3.2.2 Detection of the Transverse Velocity

Consider that a z-component velocity (w) is added to the x-y plane velocity magnitude (Q_x). The change in the parallel array voltages would be relatively small, since this component is parallel to these wires; however, the speed-wire and the angle-wire would experience non-neglible changes in their voltages. The speed-wire, angle-wire voltages that would be created by $[Q_x, \gamma]$ will retain their designations as: E_s and E_a respectively. The measured voltages, that include the effect of w, will be designated as $E_s|_m$ and $E_a|_m$ respectively. The effects of w are then designated as the difference (δE) values as:

$$E_s|_m = E_s + \delta E_s \quad \text{and} \quad E_a|_m = E_a + \delta E_a. \qquad \text{(eq. 3.7)}$$

It is pertinent to note that a given w value represents a relatively larger effect on the angle-wire since its additive cooling effect is a larger fraction that that which is provided by (Q_x,γ) acting alone. Specifically,

$$\delta E_a/E_a > \delta E_s/E_s \qquad \text{(eq. 3.8)}$$

Since the x-array voltages are significantly more responsive to the presence of a z-component velocity that are the vlotages of the parallel array, an inequality of the form: $Q_x > Q_p$ may signal the presence of a z-component of velocity. This inequality is not, however, uniquely related to the presence of a non-zero w value as noted below.

The physical separation (δz) between the two arrays and the existance of three-dimensional effects in the flow are sufficient to produce an inequality in the Q_x and Q_p values. These effects alone would create a symmetric distribution for the velocity magnitude difference: $\delta Q=[Q_x-Q_p]$. However, the existance of non-zero w values will give a positive bias to this distribution. A first order technique, to discriminate between the effect of w and the effect of $\partial Q/\partial z \simeq 0$, can be established using the measured frequency distribution that approximates the probability density function (p.d.f.) of the velocity difference: $p(\delta Q)$. A typical frequency distribution is presented in Figure 3.4. The area of the frequency distribution that is associated with $\delta Q<0$ represents the dominance of a negative value of $\partial Q/\partial z$. If it is assumed that $w \simeq 0$, then a symmetrically distributed

area for $\delta Q>0$ would exist since the average value of $\partial Q/\partial x$ is equal to zero. For computational simplicity, the magnitude of a "cut-off" value: $\delta Q_{cut-off}=\delta Q_{xp}$, is defined from the negative values of the δQ distribution. Specifically,

$$\int_{-\delta Q_{xp}}^{0} ap(\delta Q)\,d\alpha = k_c \int_{-\infty}^{0} ap(\delta Q)\,d\alpha \qquad \text{(eq. 3.9)}$$

where k_c may be selected arbitrarily. A nominal value of 0.8 is used in order that extreme values of δQ are not inappropriately weighted. Hence, if δQ is positive and greater than δQ_{xp}, the value of w at the time of the $[E_1,E_2]$ measurement is assumed non-zero. The procedure to correct the measured voltages, for the influence of this w value, is described below.

3.2.3 The w^2 Correction

The strategy for the correction scheme is that for an "inverse problem": Given $\delta Q>\delta Q_{xp}$, what value of the transverse velocity (w), is required to cause δQ to be equal to zero. To answer this question, the effect of w on the x-array response must be investigated. (It is assumed that the magnitude of w is identical at both of the slant wires.)

The concept of an effective cooling velocity in the x-y plane is invoked in order to account for the effect of w. The effective cooling velocity may be thought of as a velocity that is perpendicular to the wire and that provides a cooling effect equal to that of the actu-

al velocity. The effective velocity may therefore be described as:

$$Q_{eff}|_{total} = \left[Q^2_{eff}|_{x-y} + w^2\right]^{1/2} \qquad \text{(eq. 3.10)}$$

where: $Q_{eff}|_{total}$ - cooling effect on the wire including w

$Q_{eff}|_{x-y}$ - cooling effect on the wire from a velocity in the x-y plane only.

An explicit analytic expression for $Q_{eff}|_{x-y}$ is not required; however, the response from each of the slant wires may be used to determine its own effective cooling velocity.

$$Q_{eff}|_{speed-wire} = \left([((E_s+\delta E_s)^2-A(\beta))/B\right]^{2/n(\beta)} - [w^2])^{1/2} \qquad \text{(eq. 3.11)}$$

and

$$Q_{eff}|_{angle-wire} = \left([((E_a+\delta E_a)^2-A(\beta))/B\right]^{2/n(\beta)} - [w^2])^{1/2} \qquad \text{(eq. 3.12)}$$

The above coeffients: A B n, were determined by calibrating the wire at the respective β values for each slant wire. If an initial estimate for w^2 is arbitraily selected, then effective velocities for the speed and angle wires may be computed. Note that these effective velocities are in the x-y plane; hence, the initial estimates for the corrected speed and angle wire voltages may be evaluated by using the equations:

$$E^2_s = A(\beta_s) + B(\beta_s)[Q_{eff}|_s]^{n(\beta_s)} \qquad \text{(eq. 3.13)}$$

$$E^2_a = A(\beta_a) + B(\beta_a)[Q_{eff}|_a]^{n(\beta_a)} \qquad \text{(eq. 3.14)}$$

The corrected voltages represent the response of the x-array given the cooling effect of a velocity that is totally in the x-y plane. These voltages are then used to determine Q_x and γ in the same manner presented previously, i.e., using equations 3.4 and 3.5 and the iterative calculation scheme. A complete utilization of the previously described scheme also accounts for the second order effect of γ on the Q_p calculation; viz,:

$$Q_p = 0.5\left[Q_3(E_3;\gamma) + Q_4(E_4;\gamma)\right] \qquad \text{(eq. 3.15)}$$

The resulting Q_x value is then compared with the Q_p value determined from the parallel array response. If the two are in agreement, it is inferred that the postulated w value is correct; if not, a new w value is selected and the above computation is repeated until $\delta Q=0$.

The above describes an overview of the strategy for determining Q_x and γ from the response of an x-array; this strategy assumes that the proper calibration functions are available. The next section provides the detailed considerations for obtaining the calibration functions and the associated processing algorithms that are required for the complete 'vorticity calculation'.

CHAPTER 4

CALIBRATION OF THE VORTICITY PROBE AND PROCESSING ALGORITHMS

4.0 Introduction

The objective of the vorticity probe calibration is to obtain analytical forms that accurately describe the response of each wire for a range of pitch angles and flow speeds. Specifically the required analytical forms are:

$$\gamma = f_a(E_a(\gamma)/E_a(0) \; ; \; Q_c) \qquad \text{(eq. 4.1)}$$

$$Q_x = f_s(E_s \; ; \; \gamma_c) \qquad \text{(eq. 4.2)}$$

$$Q_{3,4} = f_p(E_{3,4} \; ; \; \gamma_c) \qquad \text{(eq. 4.3)}$$

Equations 4.1 and 4.2 utilize the voltages from the x-array response and equation 4.3 utilizes the parallel array voltages for the range of pitch angles and flow speeds established for the calibration grid. The calibration grid is represented in Figure 4.1. For $|\gamma| \leq 12^\circ$ the coefficients determined from a calibration at $\gamma=0^\circ$ are sufficient to determine Q_x and γ; recall that the COSLAW was shown to provide accurate results for this range of γ values. For $|\gamma| > 12^\circ$ a more elaborate calibration is required to obtain the functions given in equations

4.1-4.3. The following sections present the details of the complete calibration: i.e. the calibration facility and equipment, the data aquisition procedure and the processing of the calibration data to obtain the required analytical functions.

4.1 The Data Acquisition Facility

A complete set of calibration data is obtained by sampling $[E_1,E_2,E_3,E_4]$ at each of the grid points: $[Q_c,\gamma_c]$, shown in Figure 4.1. For the present study, 7 flow speeds: $\simeq 2m/s \leq Q_c \leq \simeq 13m/s$, and 15 pitch angles, ranging from -42° to 42° in increments of 6°, were used. The calibration facility is shown in Figures 4.2a-b. The x and parallel arrays of the vorticity probe are supported by the fixture shown in figure 4.2b. This fixture is mounted on a vertical stem which is attached to a ($\simeq$25cm) horizontal arm. The active portions of the hot-wires are positioned on the axis of rotation of the stem/arm assembly; i.e. the hot wires spatial location (x,y,z) remains constant as the probe body is rotated through the calibration pitch angles. The constant temperature hot wire probes are operated with DISA 55M01 anemometers and the data acquisition system is based upon a TSI 1075X (12-bit A/D , 0-5 volts, matched 50kHz low pas filters) and a Charles River Data LSI-11/23 computer (hereafter referred to as 'the computer'). The rotation of the probe through the set of calibration pitch angles is computer controlled, which insures the precision and repeatability of the orientation for each calibration grid point. The flow speed is monitored using an additional straight wire (referred to as the 'reference wire') which is located near the vorticity probe.

Prior to calibrating the vorticity probe, the reference wire is calibrated using a Validyne DP45-22 pressure transducer and CD12 carrier demodulator over the same range of speeds as that to be used for the probe calibration.

4.2 The Calibration Data

The calibration data set is acquired by sampling the 4 wires of the vorticity probe at each of the 15 angles for the 7 flow speeds. The reference wire voltage is simultaneously recorded. The final data set consists of : $[E_1, E_2, E_3, E_4, E_{ref}]$ taken at each of the conditions defined by the grid points in Figure 4.1.

The flow speeds indicated by the reference wire are used to calibrate one of the straight wires of the parallel array. The selected wire is designated as the 'master-wire'. The remaining 3 wires of the probe are then calibrated using the speed indicated by the master-wire for the particular γ_c value. The selection is based on the best fit (i.e. smallest standard deviation) to the modified Collis and Williams equation:

$$E^2 = A(\gamma_c) + B(\gamma_c)Q^{n(\gamma_c)} \qquad \text{(eq. 4.4)}$$

$$\text{STD}\left[Q_{meas.} - Q\right] = \left[(N-1)^{-1}\sum_{i=1}^{N}[Q_{meas.}-Q]_i^2\right]^{1/2} \qquad \text{(eq. 4.5)}$$

where: Qmeas. is determined from the reference wire and Q is

evaluated from the measured E and the coefficients of equation 4.4. This procedure relates 3 of the measured voltages to the 4th voltage from the designated master-wire. Note that the vorticity is determined as the difference between two quantities which themselves are differences, the relative (and not the absolute) values of the voltages at a given time are of principal importance. Hence, a calibration scheme which maximizes the relative accuracy of the wire responses is both recommended and utilized. At each of the γ_c values, the $[E, Q(E_{master})]$ pairs are fit to the modified Collis and Williams equation (eq. 4.4). This results in 15 sets of the coefficients (ABn) for each of the 4 wires.

4.3 A Measure of the 'Effective' Angle of the Slant Wires

The angle between the wire and the probe axis, (β), is be determined operationally for each of the slant wires of the x-array. That is, when the probe is pitched at $\gamma_c=\pm 12^\circ$ the data provides redundant measures of β_1 and β_2. The cosine law can be used to obtain a relation for β as a function of γ:

$$E^2(\gamma) = A(0) + b(0)Q_{eff}^{n(o)} \qquad \text{(eq. 4.6)}$$

where $Q_{eff} = Q \cos(\beta-\gamma)$.

Equation 4.6 represents a four parameter family of equations; viz, A(0), b(0),n(0) and β. The previously described calibration procedures provide best-fit values for A(0) and n(0); however, b(0) and β must be evaluated using additional information. Note that the compan-

ion value, B(0), may be used with the calibration data from one other angular position to evaluate b(0) and β; specifically,

$$B(0) = b(0)\ \cos^{n(o)}(\beta) \qquad \text{(eq. 4.7)}$$

and, for example,

$$E^2(12^\circ) = A(0) + b(0)\cos^{n(o)}(\beta-12^\circ)Q^{n(o)} \qquad \text{(eq. 4.8)}$$

The second of these equations, i.e.(4.8), may be subjected to an averaging procedure to evaluate the coefficient:

$$K = (1/N_s)\sum_{s=1}^{N_s}[b(0)\cos^{n(o)}(\beta-12^\circ)]_s$$

where N_s = number of speeds used for the calibration (eq. 4.9)

Since E^2, A(0), n(0) and Q are known values, β can be solved for explicitly as that value which satisfies:

$$K = \left[B(0)/\cos^{n(o)}\beta\right]\cos^{n(o)}(\beta-12^\circ) \qquad \text{(eq. 4.10)}$$

The values of β found using equation 4.10 are approximately 3° less than the measured values. Vukoslavcevic and Wallace[13] have also observed this difference and attribute it to the hydrodynamic upstream effect of the prongs on the flow and non-uniform properties of the wires.

4.4 Construction of Calibration Functions

4.4.1 The 'Smoothed' Calibration Data Base

The hot-wire voltages for wires 1 and 2 represent surfaces above the Q,γ plane. In principle, these surfaces monotonically increase in "height" as $\gamma \rightarrow \beta$ and as Q increases. Similarly, the voltages from wires 3 and 4 represent surfaces that monotonically increase in height with increasing Q but are, in principle, not dependent upon γ. (The acceleration around the support prongs does provide a weak dependence upon γ, as shown comparatively in Figures 4.10a-b and 4.12a-b. This effect is also noted in the section 3.2.1 for the w^2 correction scheme.)

The calibration data are acquired at discrete positions in the (Q,γ) plane; see Figure 4.1. To insure the implied differentiability of the $E(Q,\gamma)$ surface, the discrete data samples are replaced with an appropriately selected analytic function. The modified Collis and Williams [20] relationship (eq. 4.4) is used for this purpose. The coefficients are selected by minimizing the standard deviation (eq. 4.5) for discrete values of n:.20,.21,.22, ... .70. Recall that Q is derived from the voltage value of the master-wire and its A,B,n coefficients for that γ value.

The above procedure is uniformly valid for wires 3 or 4 (i.e., the non-master-wire for a given γ) and for wires 1 and 2 in their speed-wire range of γ values. For the angle range, and especially for large $\beta-\gamma$ values, the calibration data may be better fit to equation 4.4 in a piecewise manner. That is, the coefficients A,B,n may vary

for different segments of the velocity range: $Q_{min} \rightarrow Q_{max}$. This can result in a non-differentiable condition at the juncture points of the $E_a(Q;\gamma_c)$ distributions. However, this condition does not present any difficulty since the analytical fit in the angle-wire range need only provide for interpolation between measured velocity values at a given γ. These considerations are explored more fully below.

4.4.2 A Computationally Efficient Form for the Velocity Magnitude Evaluation

A smoothed calibration "data" base is constructed using equation 4.4. for the speed-wire range of wires 1 and 2 and for all γ values of the non-master-wire: 3 or 4. Each wires response (E)is analytically evaluated (using eq. 4.4) at the grid point conditions: (Q_c, γ_c) of Figure 4.1. The smoothness of these "data" is insured by the use of this analytical form.

Drubka and Wlezian [22] have shown that a polynomial fit to such data* can dramatically increase the computational efficiency of evaluating Q from a measured E and with a negligible effect on the accuracy of the E-Q relationship. That is, although eq. 4.4 also offers a relation for $Q=f(E\ \gamma^c)$, the computation time is significantly greater

---

*It is pertinent to note that a polynomial fit to the orginal (i.e., the non-smoothed) data base led to a condition in which the higher derivatives: $(M_{n^s}/M_{Q^n}\gamma \geq_c$ for n 3, did not show a montonic decrease with increasing Q values. In some cases, this led to problems of convergence when the iterative method was employed.

on the computer than using a polynomial of integer powers. The polynomial form is suggested by the inverse form of eq. 4.4: "for a function that is defined and continuous on a closed interval, there exists a polynomial that is close to the given function as desired"(Burden [25]). A 4th order Chebychev polynomial was chosen since it allowed for maximum accuracy at a reduced degree of the approximating polynomial. Specifically,

$$Q(E;\gamma_c) = \sum_{i=1}^{5} a_i \, E^{2(i-1)} \qquad \text{(eq. 4.12)}$$

where a_i are the polynomial coefficients

For each of the slant wires, the approximating polynomial is required only over the range of γ_c for which that wire is designated the speed-wire:

wire 1 - speed-wire: $\gamma_c \geq 0^0$

wire 2 - speed-wire: $\gamma_c \leq 0^0$

For the straight wires, the polynomial coefficients are determined at every γ_c, even though their responses are a very weak function of the pitch angle.

4.4.3 The Angle-Wire Response Functions

The iterative calculation scheme requires that γ be determined from a function of the form:

$$\gamma = f_a(E_a(\gamma)/E_a(0) \; ; \; Q_{jj}) \qquad \text{(eq. 4.13)}$$

where $E_a(\gamma)$ represents the measured voltage, Q_{jj} is a reference velocity that is "close" to that existing at the instant of the measurement and $E_a(0)$ is the corresponding voltage at $\gamma=0^\circ$ for the angle-wire. The calibration data provide the necessary information to develop the function "f_a".

The procedure to interpolate: $E(Q;\gamma_c)$, between the measured Q values at a given γ_c was described in section 4.4.1; from that discussion it is apparent that the subdivision of the velocity range into a set of Q_{jj} values can be accomplished. The Q_{jj} values are described as:

$$Q_{min} \leq Q_{jj} \leq Q_{max} \; ; \quad \delta Q_{jj} = (Q_{max}-Q_{min})/36 \qquad \text{(eq. 4.14)}$$

For convenience, f_a is expressed as a function of η with a parametric dependence upon Q_{jj} as

$$\gamma = f_a(\eta \; ; \; Q_{jj}) \qquad \text{where } \eta = E_a(\gamma)/E_a(0) \qquad \text{(eq. 4.15)}$$

The function: f_a is known from the smoothed calibration data, at the discrete locations described by the γ values of the calibration process: γ_c; viz.,

$|\gamma_c|$ = 12,18,24,30,36,42 degrees.

Cubic splines are used to interpolate between these discrete γ_c values. Figures 4.5 and 4.6 are representative sets of such functions that were fitted to the smoothed and doubly interpolated data set.

4.5 A 'Data-Day' Correction Scheme

From the time of calibration to the time of a data day run, the wires response character may be altered due to corrosion, dust, etc. The calibration coefficients for the Q and γ functions (eq. 4.12 and 4.13) may then become invalid. If the overall changes are small and have only the effect of causing a minor drift in each wire's response, a linear correction may be applied to the data-day voltages. The magnitude of the drift is estimated by assuming that the data-day voltages have shifted by δE^2:

$$E_d^2 = E_c^2 + \delta E^2, \qquad \text{(eq 4.16)}$$

where: E_d - data-day voltage and

E_c - voltage measured at the time of the master calibration time

This expression may be expressed in terms of the coefficient λ as:

$$E_d^2 = E_c^2 (1 + \lambda) \; ; \quad \text{where } \lambda = \delta E^2/E_c^2. \qquad \text{(eq. 4.17)}$$

A 'minor' drift condition is represented by $\lambda \simeq 0$. For this condition the master calibration coefficients are considered to remain valid for the corrected data-day voltages:

$$E_c^2 = E_d^2/(1 + \lambda) \qquad \text{(eq. 4.18)}$$

The correction factor $(1+\lambda)$ is established by calibrating the vorticity probe at the $\gamma_c=0^o$ condition prior to a data run. The set of $[E_d, Q_d]$ pairs are sampled over the same range of flow speeds used for the master calibration; $Q_{c-min} \leq Q_d \leq Q_{c-max}$. At each Q_d the $(1+\lambda)$ factor is determined for each wire using eq. 4.17:

$$1 + \lambda = E^2/(A_c(0) + B_c(0)Q_d^{n_c(o)}) \qquad \text{(eq. 4.19)}$$

The average correction factor is then found for each wire. If the $\langle(1+\lambda)\rangle$ factors are sufficiently different than 1, the vorticity probe must be recalibrated; otherwise the data-day voltages are corrected according to eq. 4.19 before being used in the vorticity algorithm.

4.6 Calibration Curves From Experimental Calibration Data

Actual experimental data was used to produce the curves shown in Figures 4.3-4.8. These curves are of the same form as those shown previously in Figures 3.3a-c. The curves that are used in the iterative scheme for determining Q_x and γ are designated by the angle or speed-wire condition noted for wires 1 and 2. Lack of this designation indicates determination of Q_x and γ by the COSLAW technique (see Appendix A). (two-equation/two-unknown). Figures 4.9-4.12 are calibration curves for the straight wires 3 and 4. Note the slight pitch angle dependence for the $Q=f(E^2)$ curves as identified in section 4.4.1; see Figures 4.10a-b and 4.12a-b. This slight γ dependence is

also apparent in Figures 4.9a-b and 4.11a-b for the $E^2=f(Q^n)$ curves.

CHAPTER 5

DEMONSTRATION DATA

5.0 Introduction

A limited body of experimental data has been acquired to demonstrate the computational procedures described in Chapters 2 and 3. These experimental results, and the relevant observations that are inferred from them, are presented in this chapter.

5.1 Expermental Results

The four-wire array was placed in the intermittent region of a large plane shear layer. The shear layer measurements were taken in the test section of the Free Shear Flow Facility that is shown in Figures 5.1a-b. The probe position: x=1m, y=.099m, was selected to provide an intermittent condition wherein vortical and non-vortical fluid would occupy the probe location. The non-dimensional probe location may be described in terms of $y_{1/2}$ (i.e., the y value such that $u/U_0=.5$) and the apparant origin (x_0) of the linearly growing shear layer: $\delta_\omega=C(x-x_0)$. The vorticity thickness: δ_ω, is defined as:

$$\delta_\omega = U_0 \; / \; (\partial u/\partial y)_{max}.$$

The non-dimensional: $\eta=(y-y_{1/2})/(x-x_0)$, location of the probe was 0.076 and the corresponding value of $\bar{u}/U_0$ was 0.17.

The data were acquired with an imposed probe angle of: $\Theta=-20^{\circ}$; this insured that the large angles of the entrainment stream, with respect to the x-axis, would not exceed the $(\pm)42^{\circ}$ pitch angle of the calibration grid.

The four, hot-wire voltages were simultaneously sampled at a rate of 15,625 hz and the data acquisition computer (see section 4.1) was able to store a continuous record of 8,125 samples per wire. The initial processing made use of the scheme, described in Chapter 3, to convert these voltages to Q_x and γ values at each time value. A value of 0.25 degrees was used for the γ-convergence criterion. A computation time of 42 minutes was required on the 11-23 micro-computer(RT-11 operating system). These (Q_x,γ) values were then combined with the measured (E_3,E_4) values as the inputs to the computational procedures described in Chapter 2. This computation time was 16 minutes. The Q_x and Q_p values were then used to correct E_1 and E_2 for the presence of a transverse velocity: w^2, as described in Chapter 3. The corrected γ values were then used to recompute the micro-domain quantities. The resulting time series for the transverse vorticity, the strain rate and velocity components are presented in Figures 5.2a-5.6a. The influence of the transverse velocity, w on each of these quantities was also determined. The time series using the corrected values are presented in Figures 5.2b-5.6b.

In principle, the transition from the vortical to the non-vortical state can be characterized by the magnitude of the vorticity. In practice, this transition is obscured by the difficulty of providing a measurement of $\vec{\omega}$ that is sufficiently free from uncertainties. For the present demonstration data, it is encouraging that the effect of the w^2 correction has very little influence on the inferred location of the transition. It is also encouraging that the $\omega_z(\tau)$ time series appears to be qualitatively reasonable.

Given the $\omega_z(\tau)$ signal, it is of interest to note that the vortical/non-vortical transition is not readily apparent in the corresponding u and v time series record. This observation is compatible with the motivation for the present effort: that the direct measurement of the transverse vorticity consitutes a significant experimental capability for fluid mechanic investigations.

The frequency distribution in Figure 3.4 showed the occurance of both $Q_x > Q_p$ and $Q_x < Q_p$ in the processed data. it is speculated that for $Q_x > Q_p$, the difference is in part due to the presence of a transverse velocity (w) and in part due to $\partial[]/\partial z \neq 0$. A correction for the w^2 influence on the x-array voltages was made ($k_c = 0.8$ from eq. 3.9) and the resulting time series for the vorticity and velocity components are shown in Figures 5.3b-5.4b. For the present data, the qualitative character of the signals remain unchanged by the application of the w^2 correction. Quantitatively, the magnitude of the vorticity values in the highly fluctuating regions is increased by approximately 400(1/sec). The velocity components, for the corresponding times,

showed a slight decrease (approximately .6 m/s) in magnitude for the large fluctuations of $\langle u \rangle$ and $\langle v \rangle$. The corresponding time series for the strain rate and velocity derivatives are presented in Figures 5.4 to 5.6.

CHAPTER 6

SUMMARY

A method to obtain time series for the transverse vorticity, and the in-plane velocity components from 4 hot-wire voltages has been presented. The method includes several calculation schemes. The iterative scheme, which determines the velocity magnitude (Q_x) and (γ) from the voltages of the x-array, is basically the same as Foss[18]; however several significant improvements have been made in this computation procedure. Specifically, the present scheme utilizes the two-equation two-unknown method (COSLAW) for pitch angles that are within $\pm 12^\circ$ of the probe axis. This modification significantly decreases the computation time, without decreasing the accuracy, and it provides a viable first estimate of the flow speed as required for the iterative procedure ($|\gamma| > 12^\circ$). An evaluation of the iterative method subsequent to the preparation of [18], revealed a very slow convergence at small γ values; hence, the used of the COSLAW solves an inherent problem with the iterative method. The iterative method is found to be relatively efficient at large pitch angle values; when the calibration data are inserted in the (Q_x, γ) calculation scheme. Using Q_x and γ values determined from COSLAW as initial estimates the method converged to the correct values within 3 interations at the large pitch angles for a convergence criterion of $\Delta\gamma = .25^\circ$.

The use of a temporally aligned (s-n), micro-domain in the present computational scheme is considered to be a significant improvement compared with the (x-y) orientation of the previous method. Specifically, the basis for the space (δs)/time (δt_k) correspondence of the convected (u_c) fluid element is more rational if the velocity vector in the x-y plane is used for the convective speed. The variable size and orientation of the micro-domains is compatible with the reconstruction of the time series (τ_i).

The locally defined s-n coordinates require that coordinate transformation techniques be used to evaluate the velocity components and their spatial derivatives in the laboratory, or (x-y), coordinates. These considerations have been used for the demonstration data of the present study and the coordinate transformations account for the pitched probe orientation ($\theta=-20^0$) as well as the s-n orientation with respect to the probe axis.

The calibration of the vorticity probe and the subsequent calibration functions, ($\gamma=f(\eta;Q_{jj})$, $Q=f(E^2,\gamma_c)$) have revealed some interesting characteristics of the vorticity probe. Namely at large $|\beta-\gamma|$ values the aerodynamic influence of the parallel array on the slant wire adjacent to it, is suggested by the consistent appearance of a steepening in the $\gamma=f(\eta;Q_{jj})$ function for $\gamma>36^0$. In the present configuration of the vorticity probe, wire 1 shows this steepening trend, see Figure 4.3a. The same steepening character was found to exist in two previous calibration curves for different wires but in the same position, that is the trend appeared in the x-array wire

directly above the parallel array. A study to determine the minimum distance for which no significant effect is observed would be useful.

The calibration speed functions for the parallel wires showed a slight dependence for specific ranges of pitch angle. These ranges corresponded alternately for the large $|\gamma|$ values in which one wire affected the flow on the other wire. Specifically wire 4 appeared to show the pitch angle dependence for large positive γ and negligible dependence for $\gamma<0$, see Figures 4.12a-b. The opposite trend was observed for wire 3.

The designation of a 'master wire' for the evaluation of the flow speeds during calibration was introduced by Foss[17]. The present calibration scheme utilizes this concept in defining one of the wires of the parallel array as a master wire, for each pitch angle used during the vorticity probe calibration. The straight wire chosen, wire 3 or 4, is based on the minimum STD of the data fit to the response function at a given γ_c. This is in constrast with the technique of [18] which defined on straight wire as the master wire for the entire calibration.

FIGURES

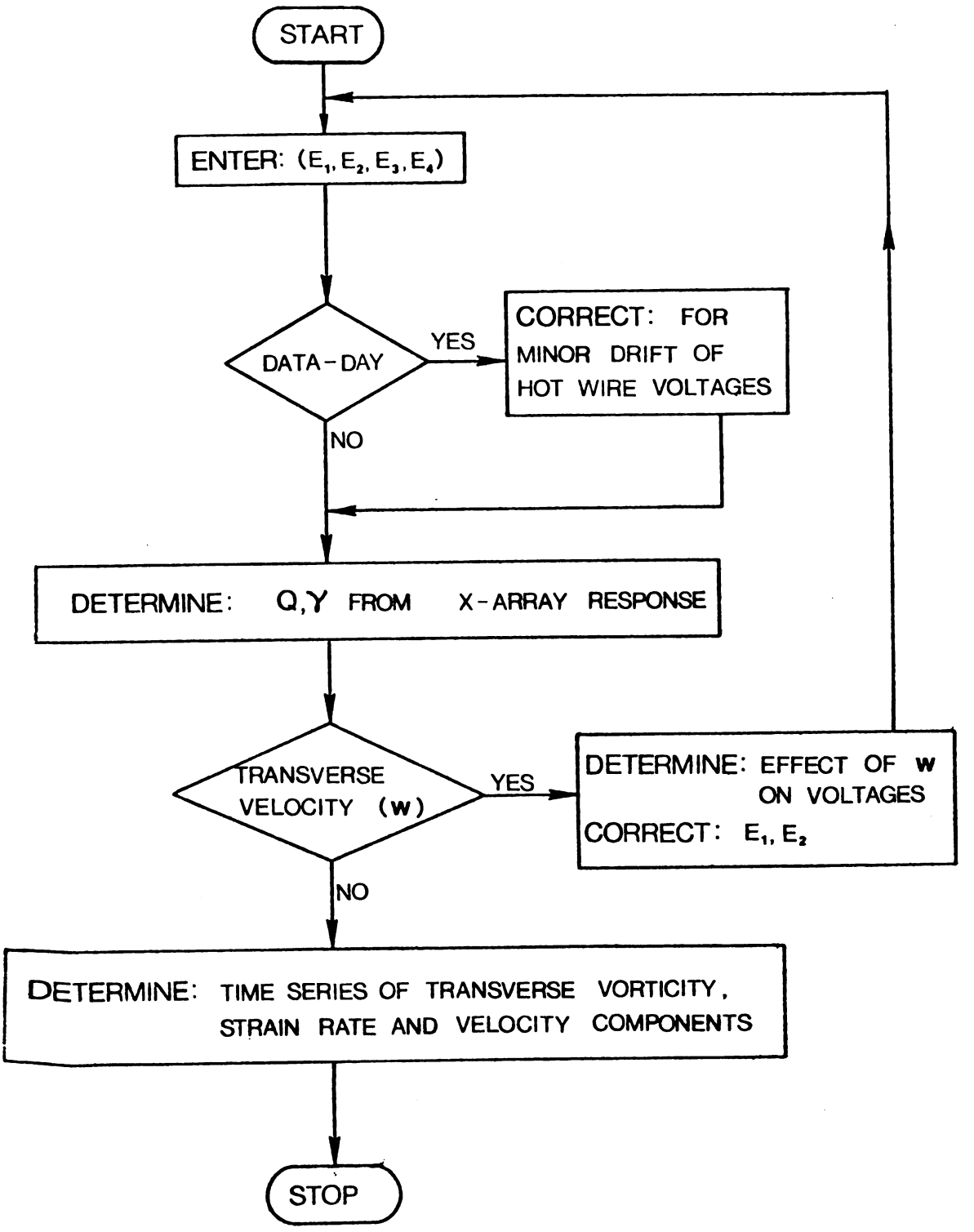

Figure 1.1. Organization Flow Chart of the Technique

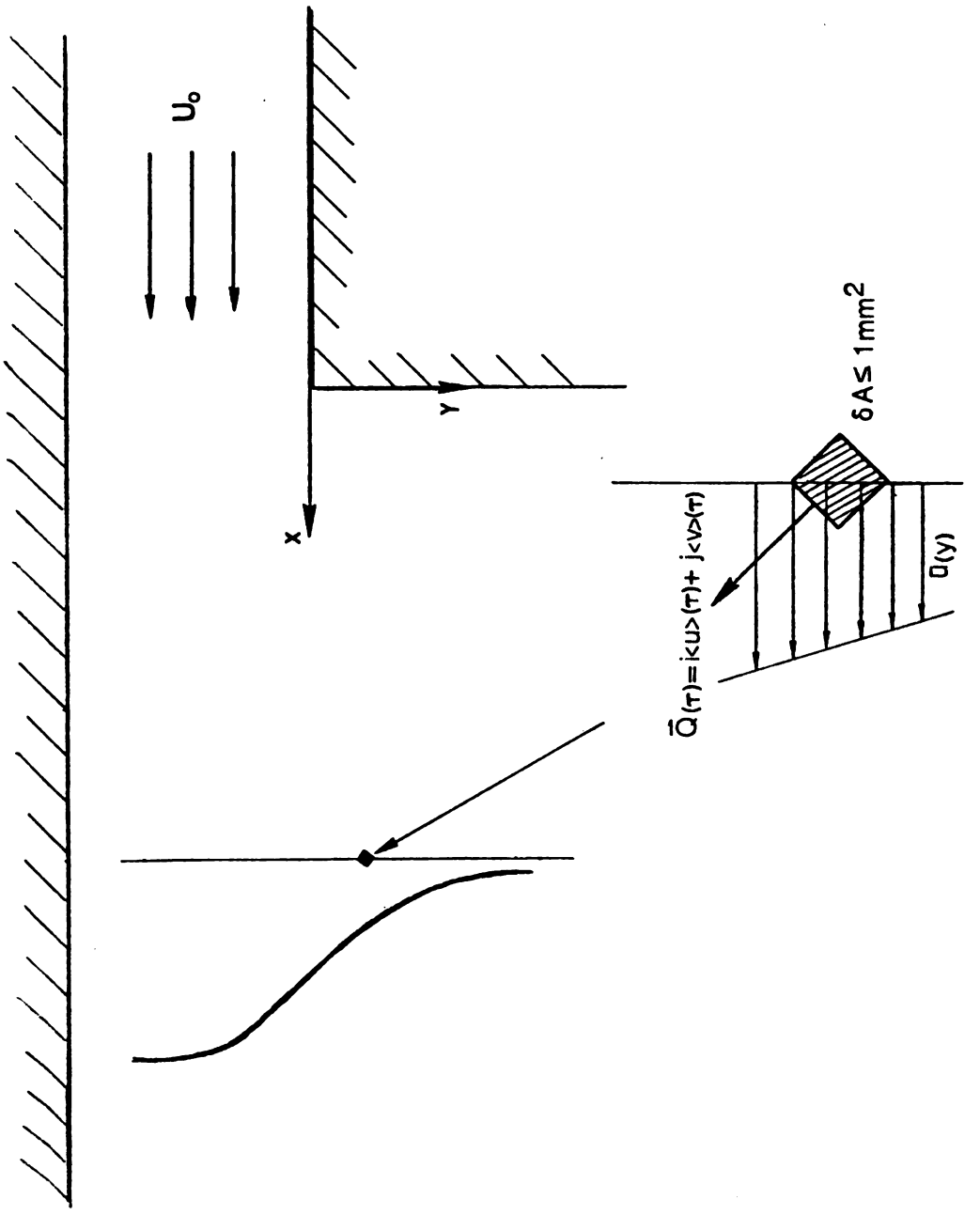

Figure 2.1. The Subject Flow Field

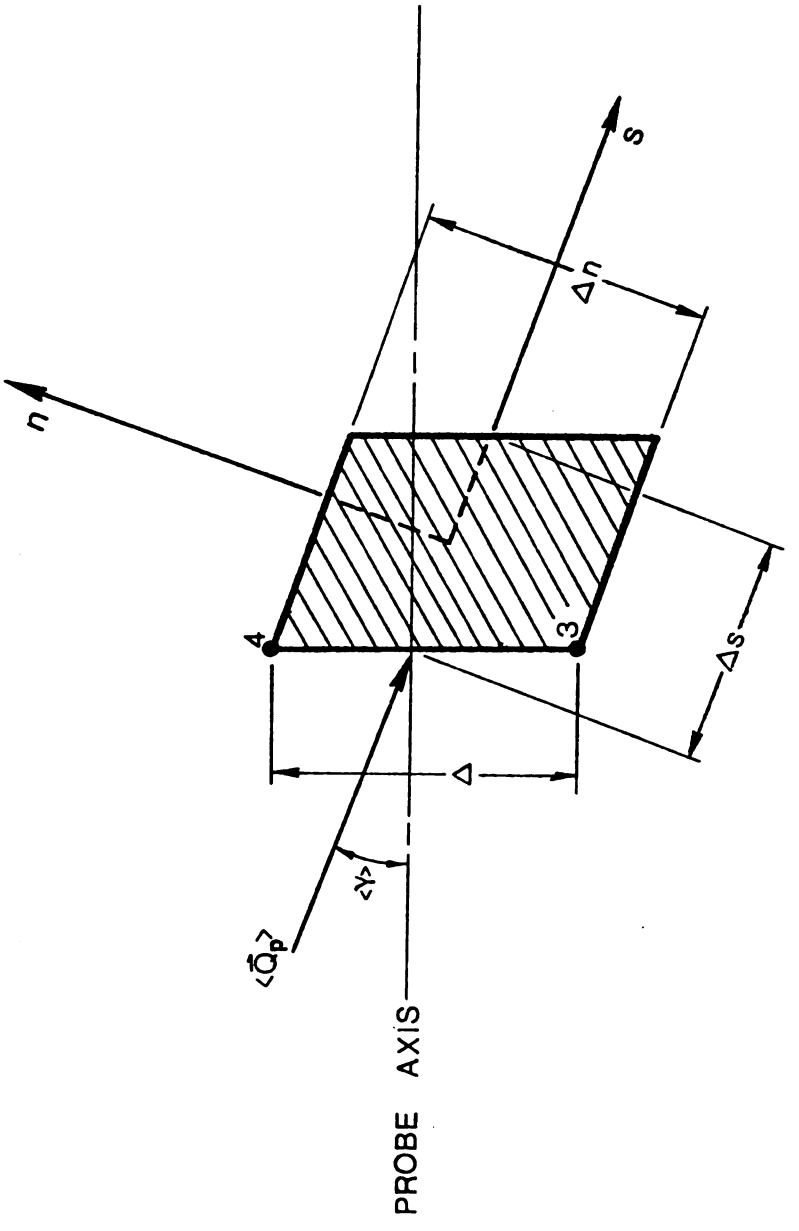

Figure 2.1b. The Micro-Circulation Domain

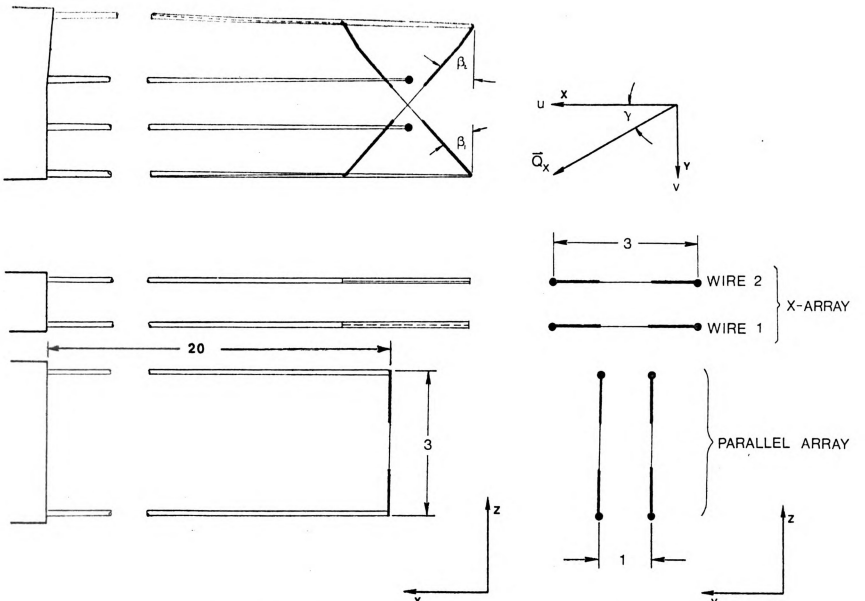

Figure 2.2a. The Vorticity Probe [Dimensions in MM]

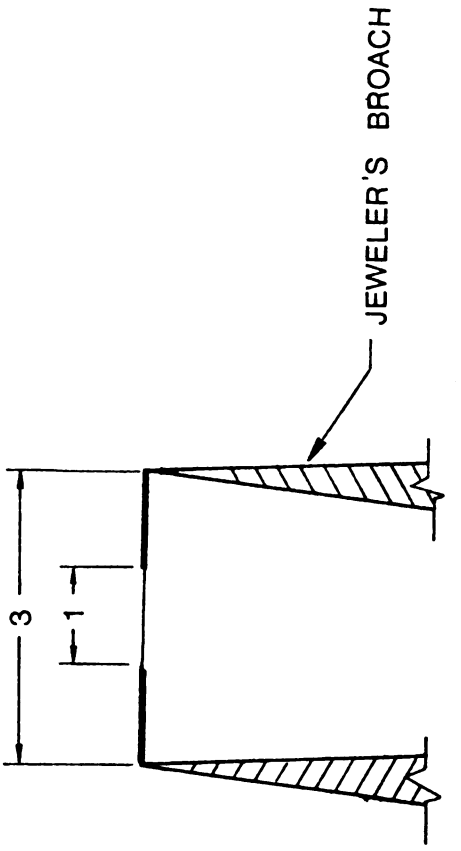

Figure 2.2b. A Typical Hot-Wire Probe [Dimensions in MM]

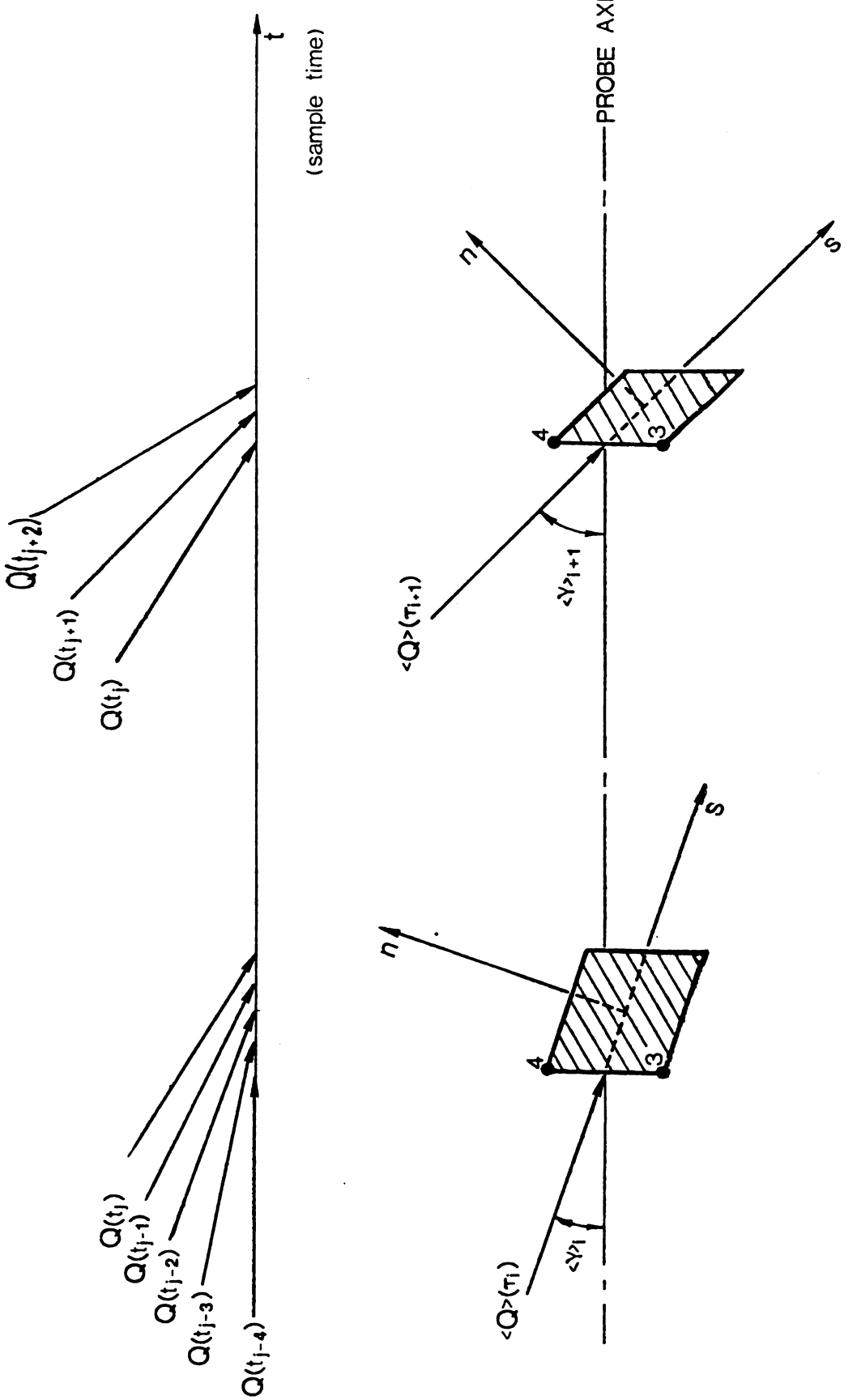

Figure 2.3. Nomenclature for the Cumulative Averaging Scheme

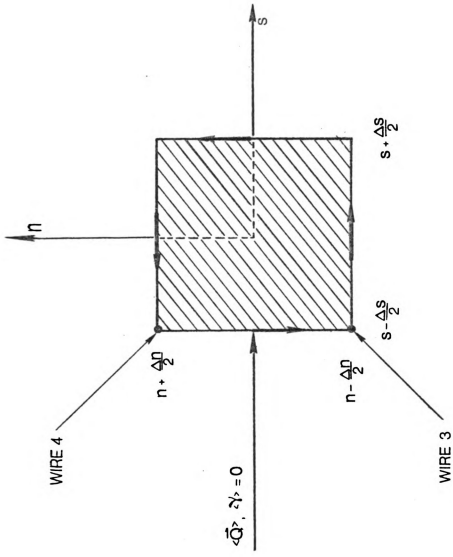

Figure 2.4. Circulation Loop about Micro-Domain

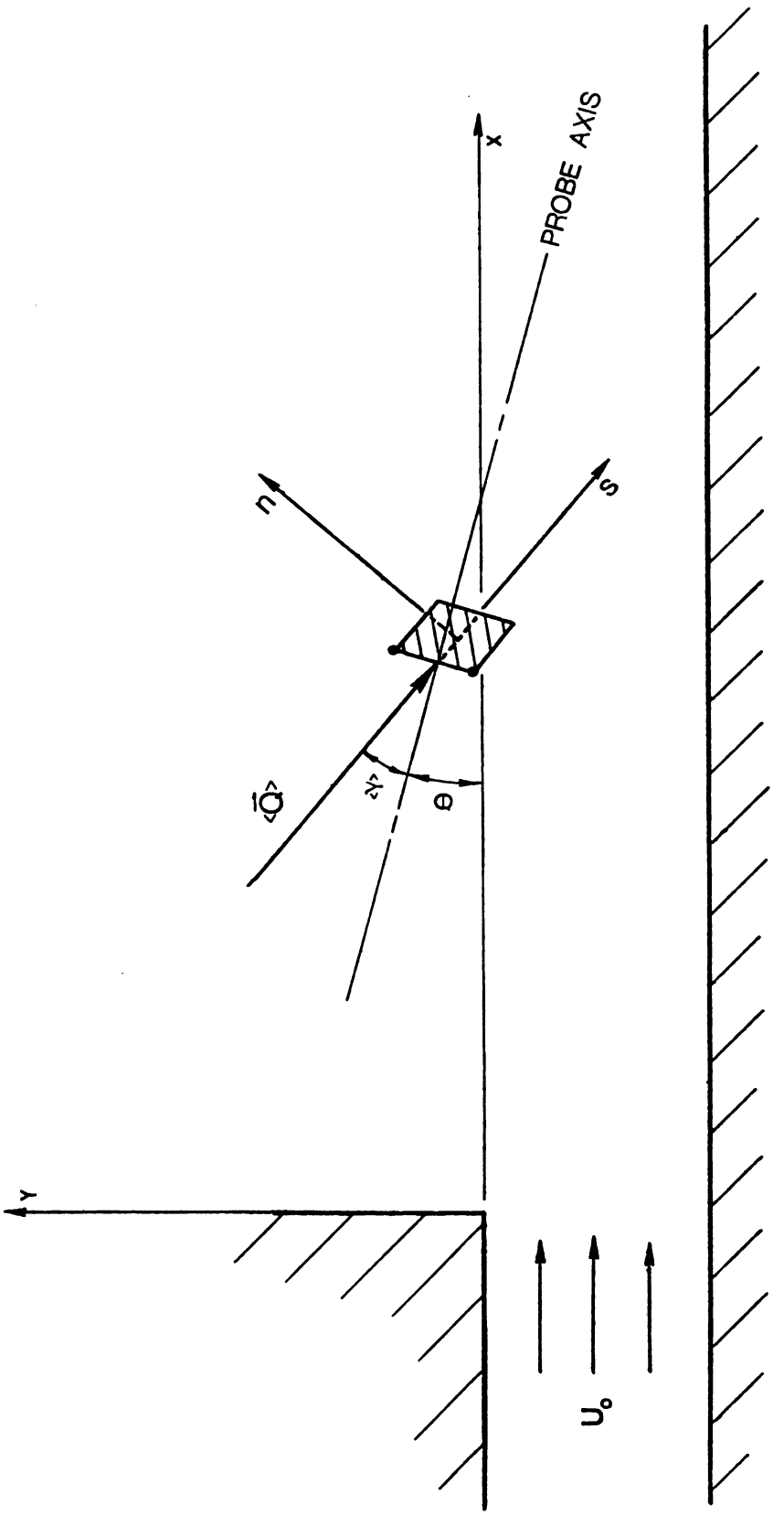

Figure 2.5. Pertinent Coordinate Systems

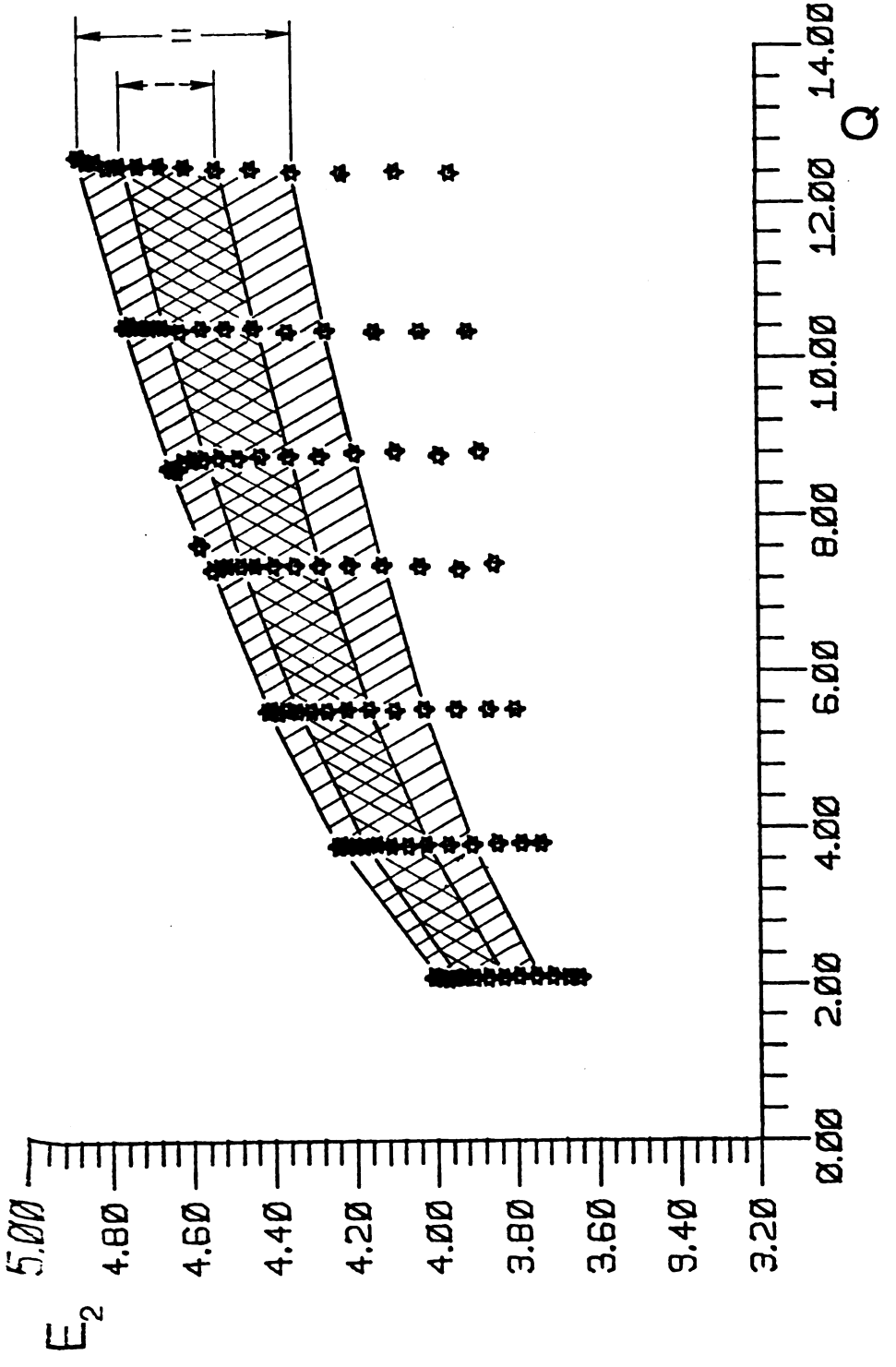

Figure 3.1. Angle Range of Validity for Cosine and Extended Cosine Laws

Notes: (i) Wire 2 calibration data were used for this illustration.
(ii) Range of validity of cosine law (I): $\gamma \leq |12°|$.
(iii) Estimate for the range of validity of the extended cosine law (II): $-24° \leq \gamma \leq \beta$, obtained from processed calibration data of Foss [1979]: see Figure 3 of that reference.

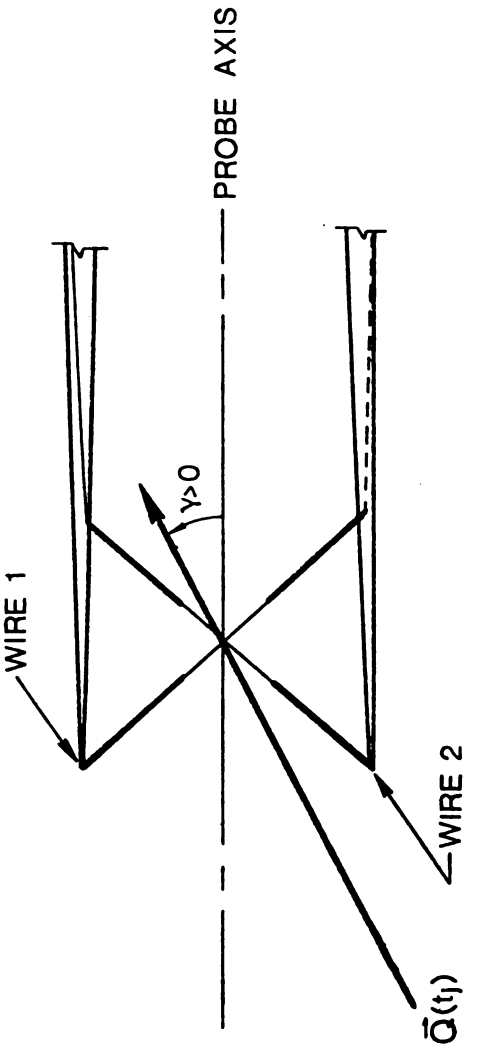

Figure 3.2. Schematic of Typical Velocity Vector/X-Array Orientation

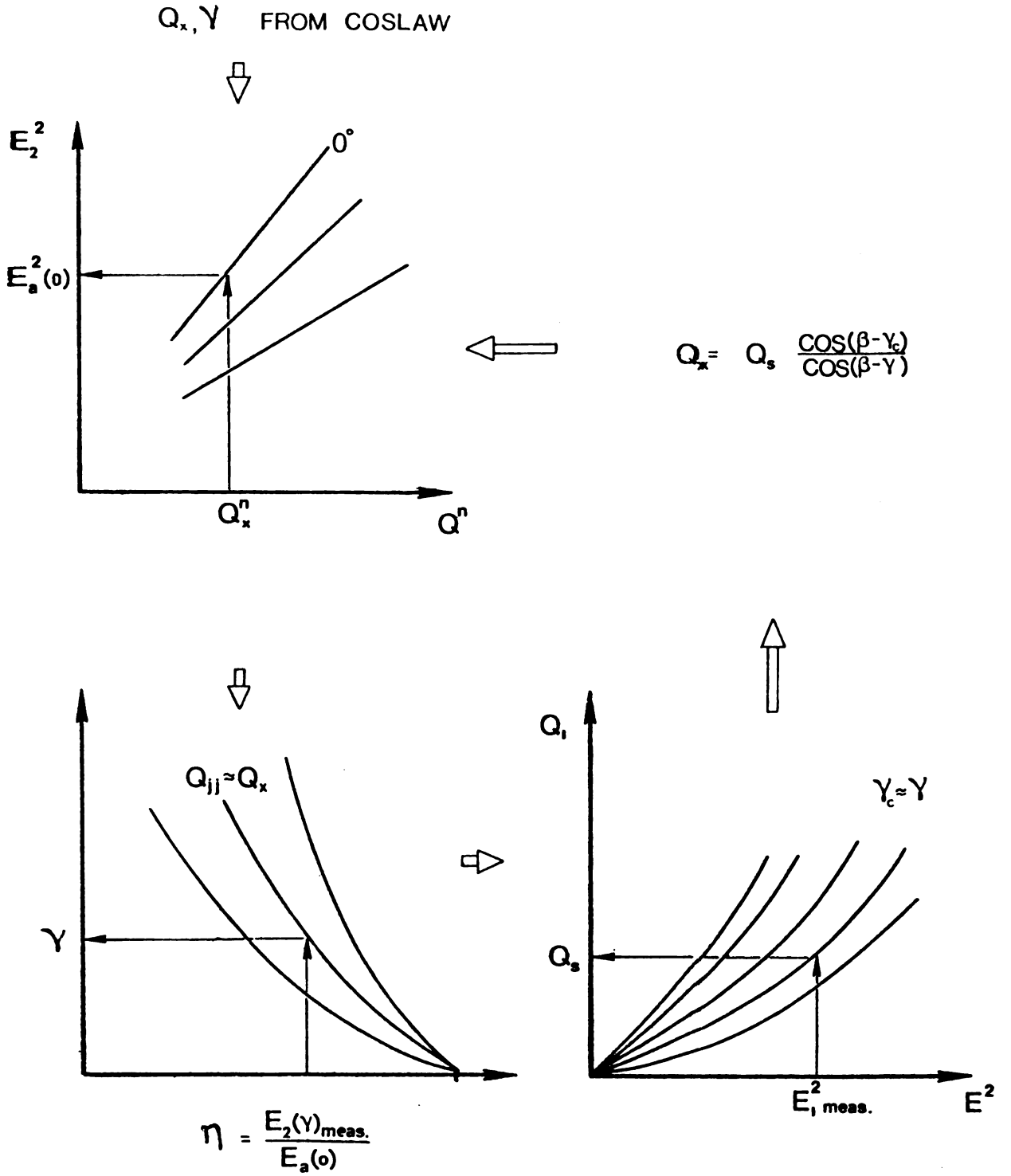

Figure 3.3. Schematic of the Q_x - γ Iteration Scheme

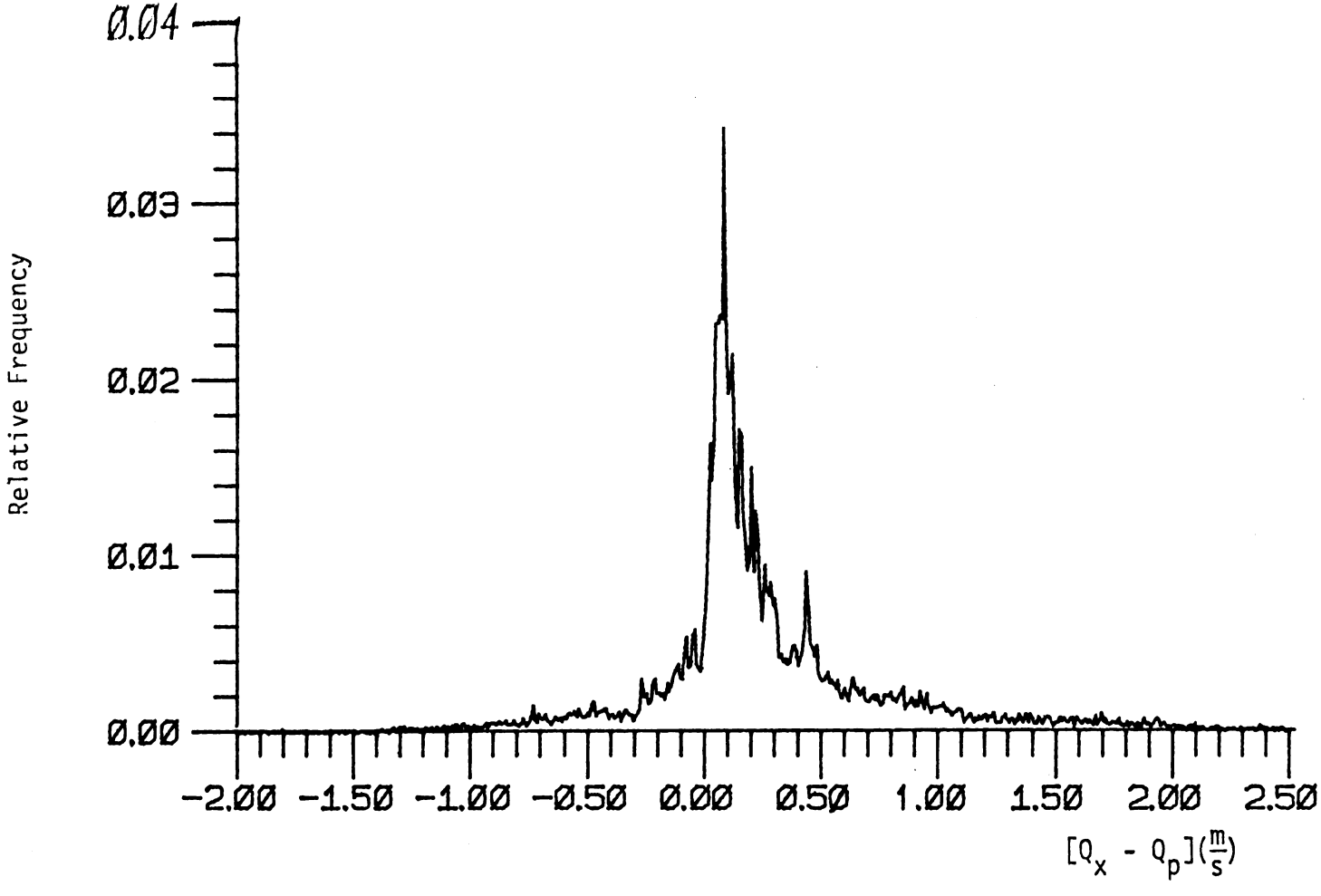

Figure 3.4. Representative Frequency Distribution of $[Q_x - Q_p]$

Notes: Average = .287 $\frac{m}{s}$ Skewness = 1.016
S.T.D. = .554 $\frac{m}{s}$ Flatness = 5.67

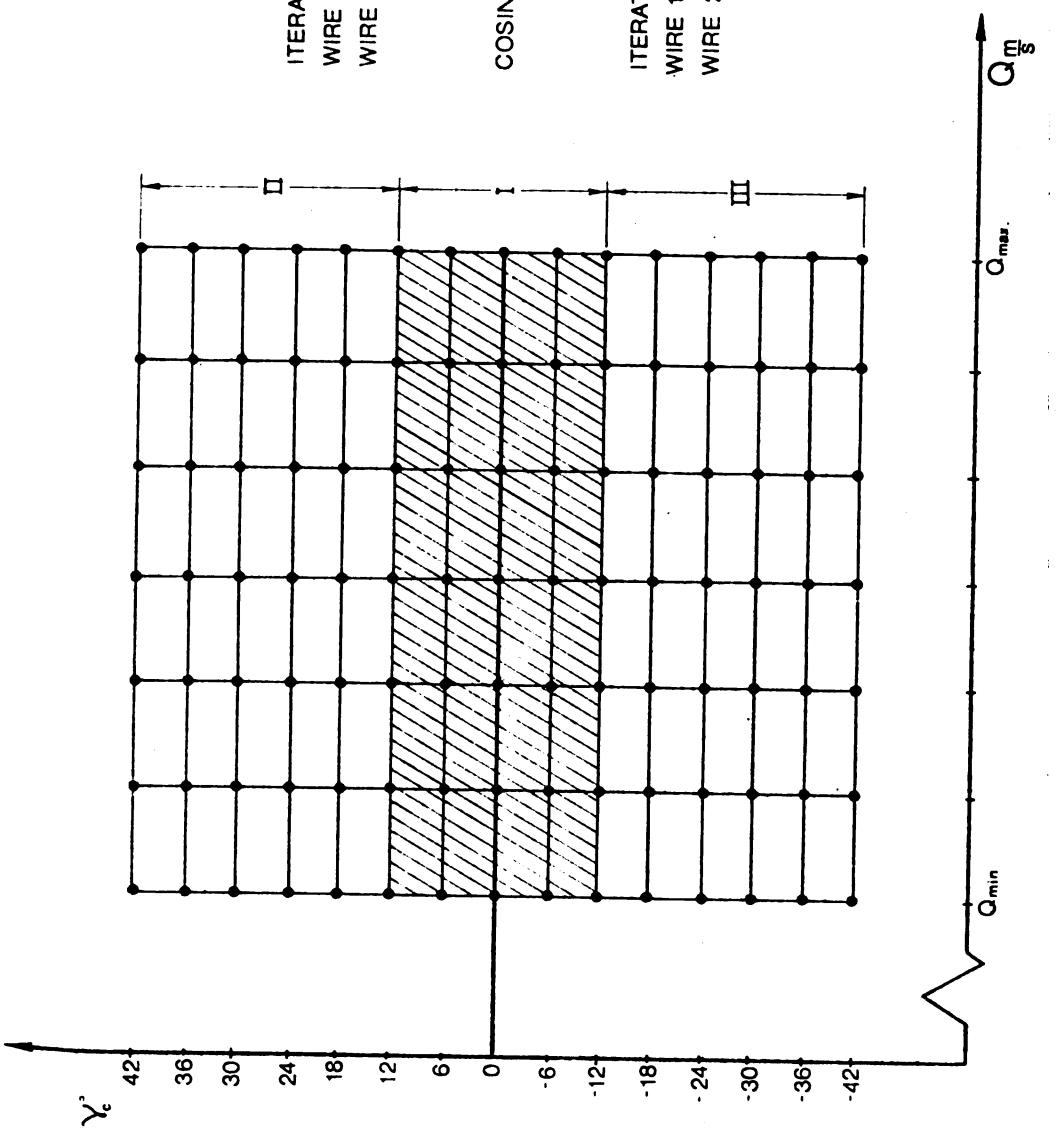

Figure 4.1. Vorticity Probe Calibration Grid

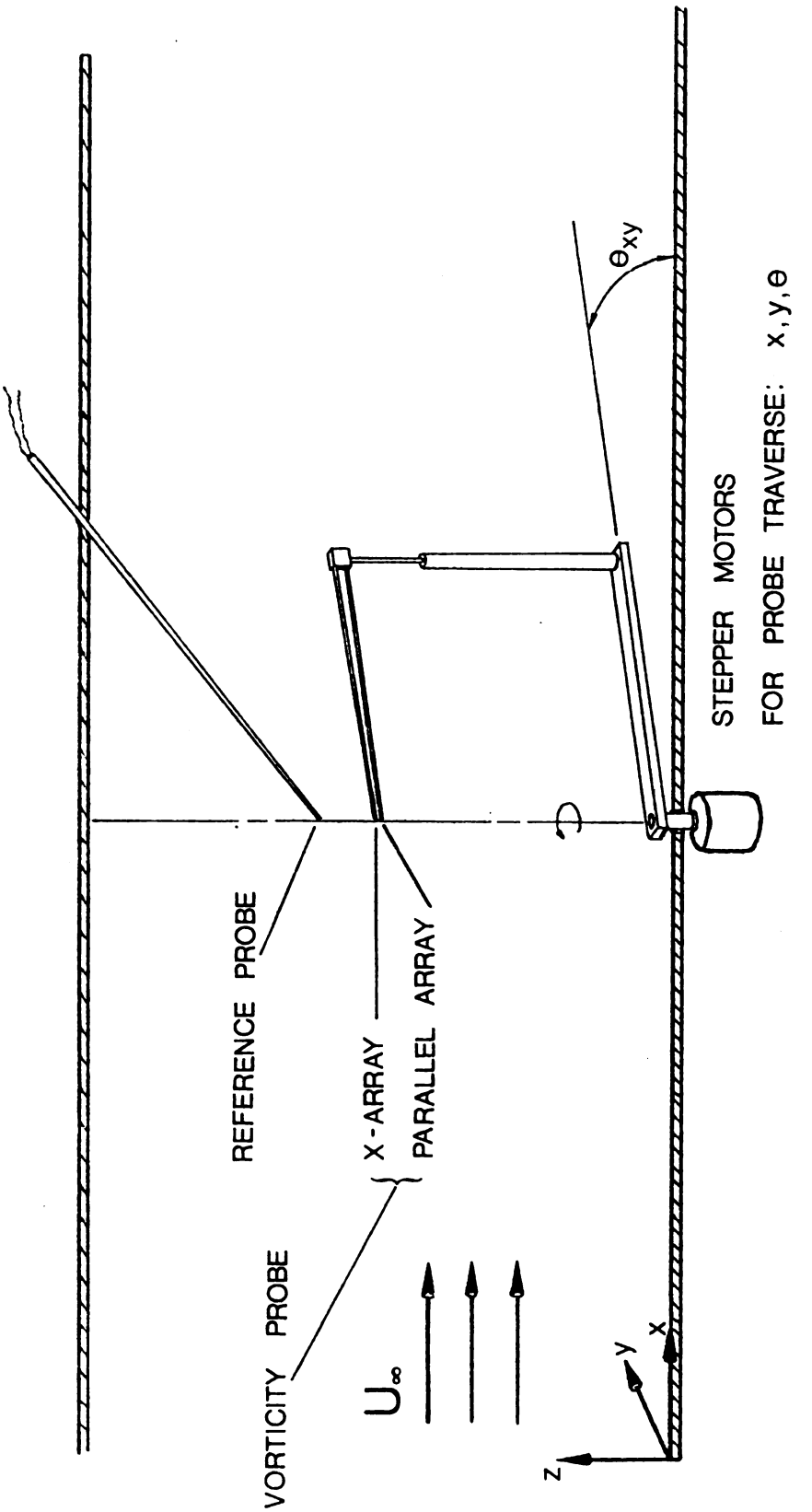

Figure 4.2a. Calibration Facility; Vorticity Probe/Reference Probe Orientation

Notes: (i) θ_{xy} positioning is used to obtain calibration pitch angles (γ_c); + $\gamma_c = -\theta_{xy}$

(ii) Convention for vorticity probe angular position during data-run; cw = $+|\theta_{xy}|$ ccw = $-|\theta_{xy}|$ with respect to x-axis

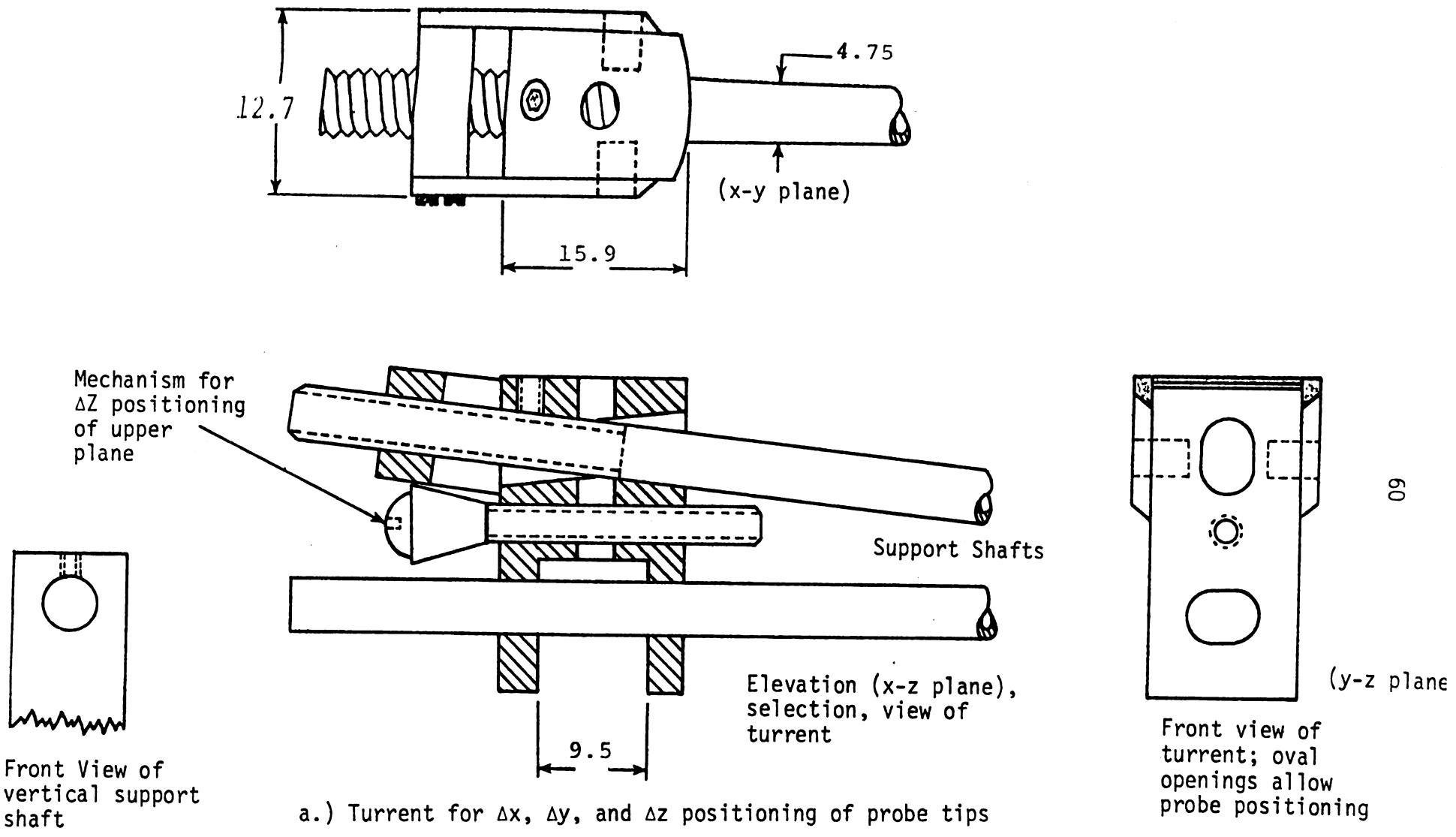

Figure 4.2b. Details of Vorticity Probe Support

Note: all dimensions in mm

Δx adjustment via threaded upper shaft
Δy adjustment via rotation of turret on vertical support shaft

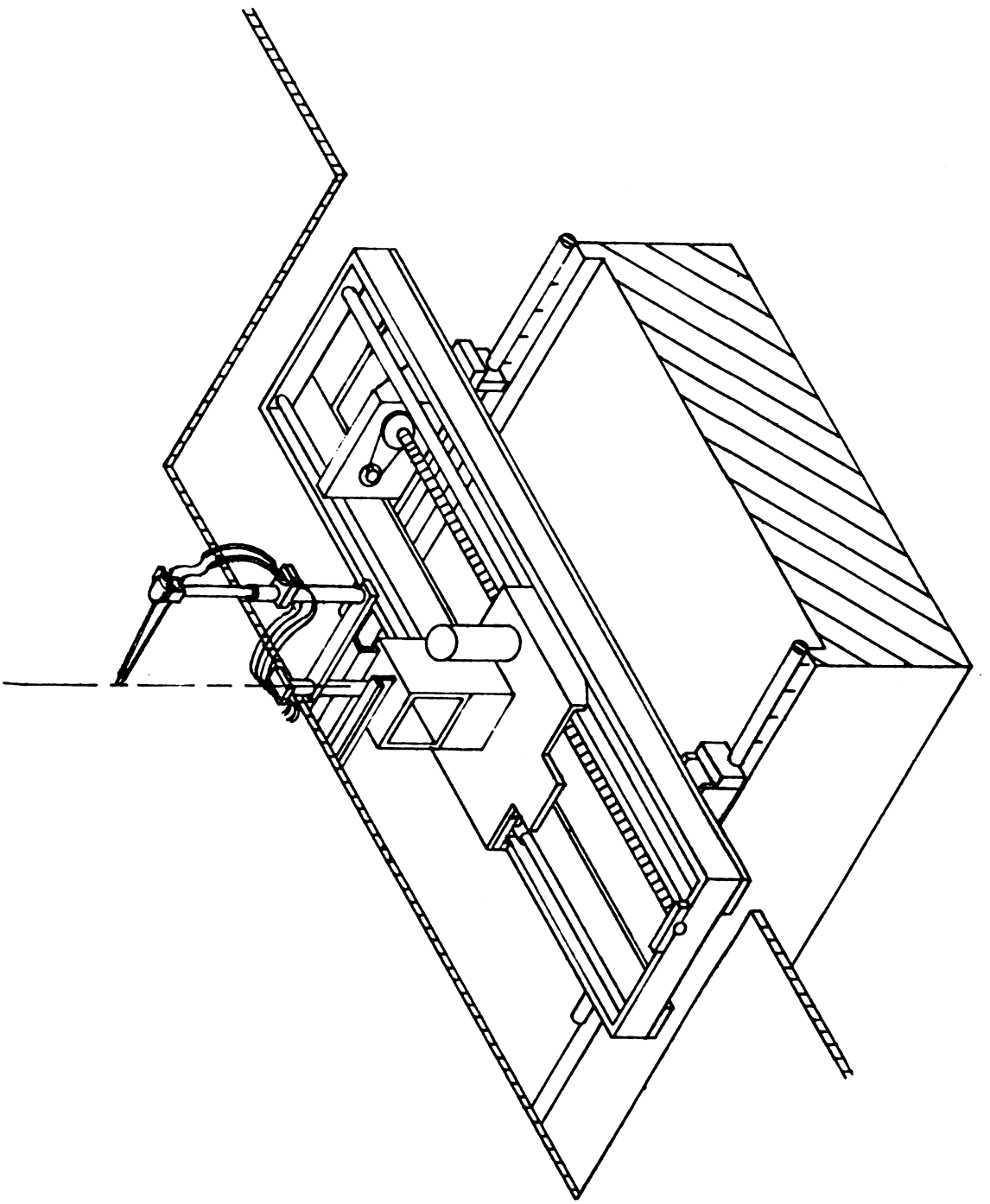

Figure 4.2c. Vorticity Probe Traverse

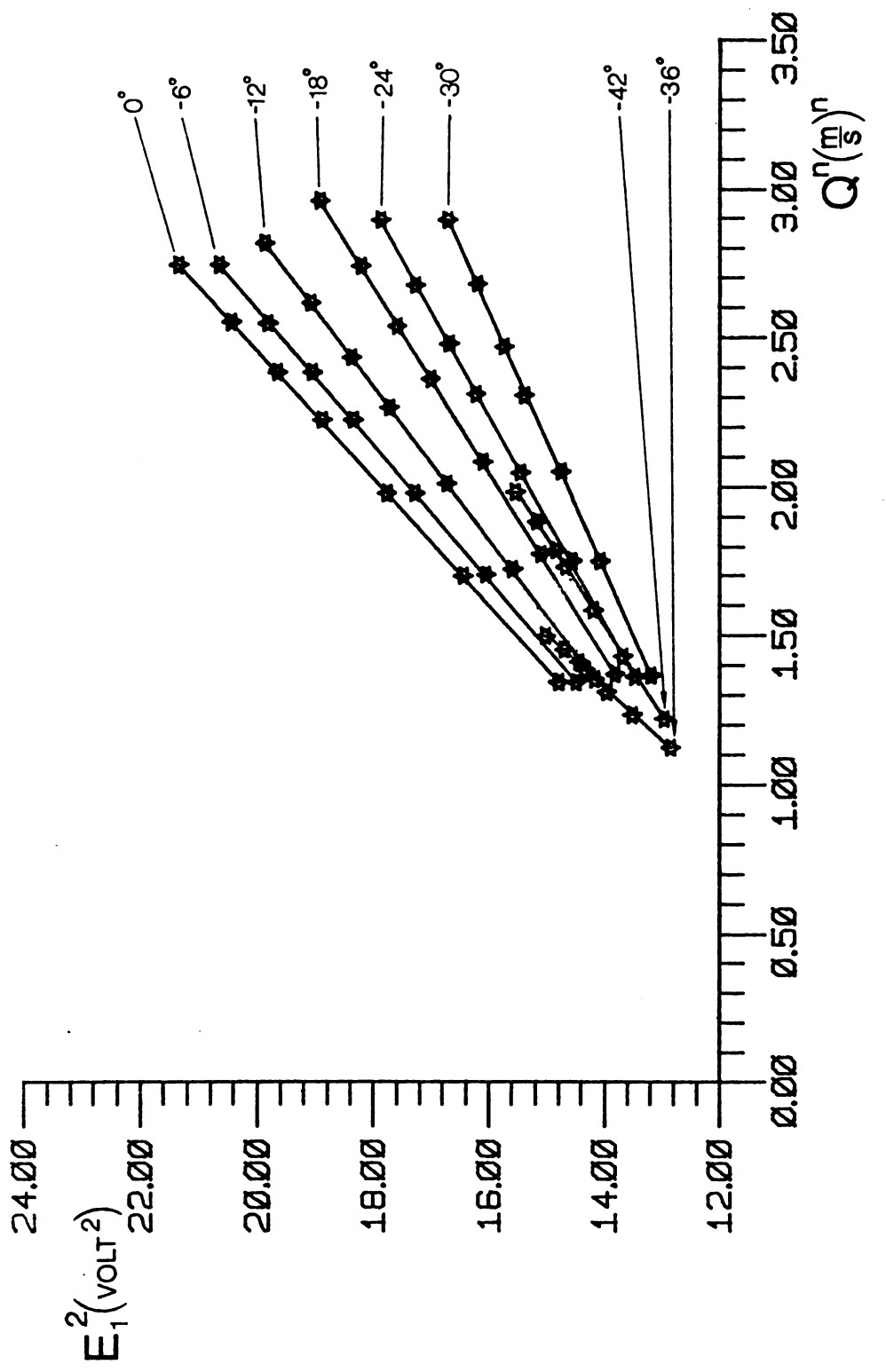

Figure 4.3a. Response Function for Wire 1 = 'Angle - Wire' ($\gamma \leq 0°$)

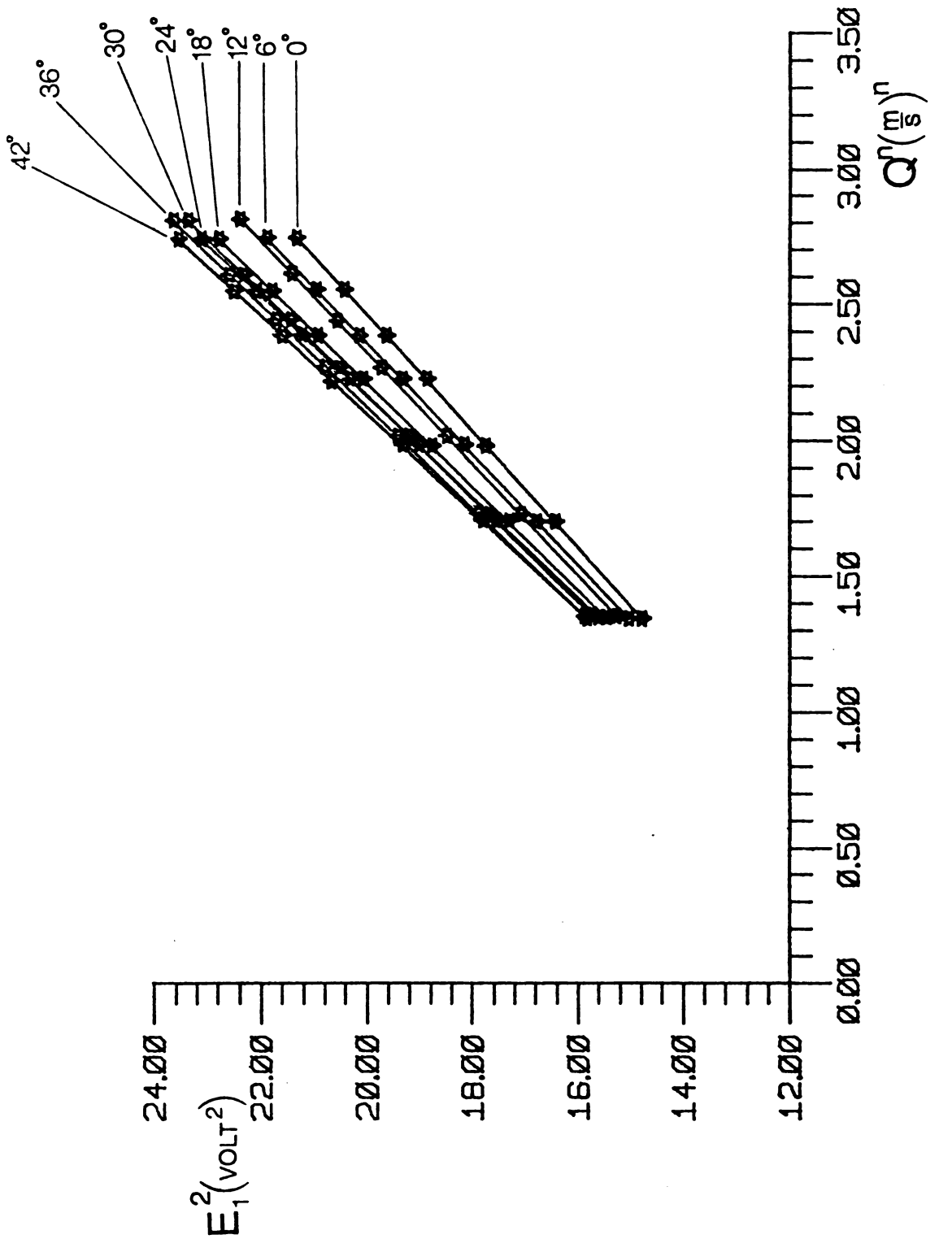

Figure 4.3b. Response Function for Wire 1 ($\gamma \geq 0°$)

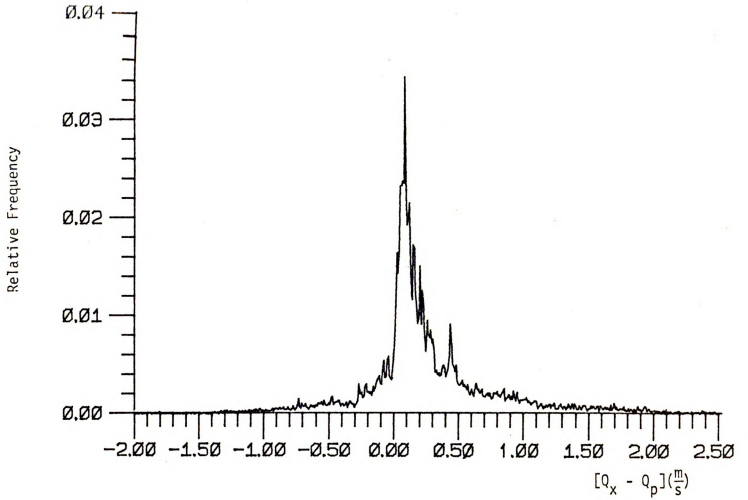

Figure 3.4. Representative Frequency Distribution of $[Q_x - Q_p]$

Notes: Average = .287 $\frac{m}{s}$ Skewness = 1.016
S.T.D. = .554 $\frac{m}{s}$ Flatness = 5.67

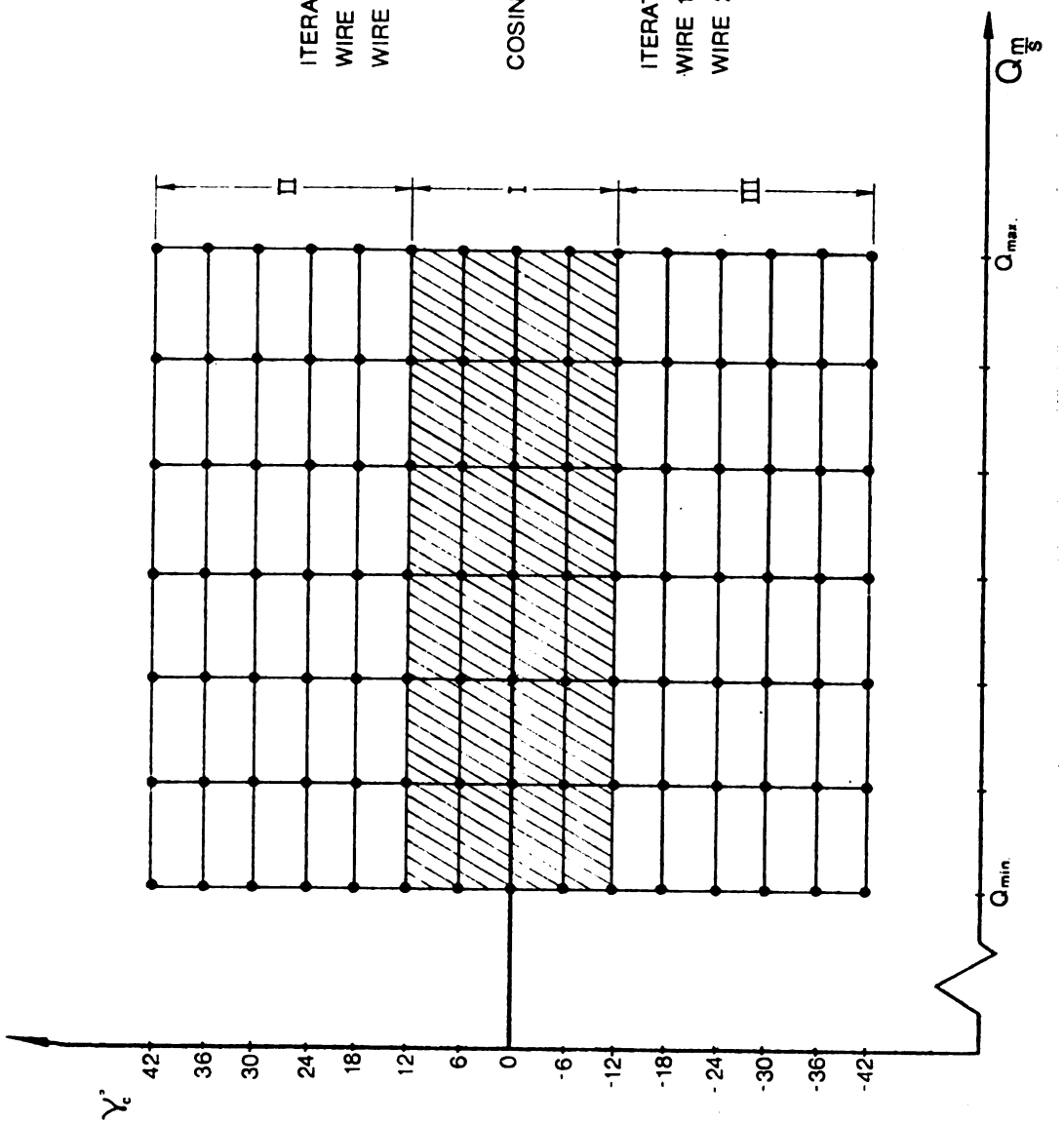

Figure 4.1. Vorticity Probe Calibration Grid

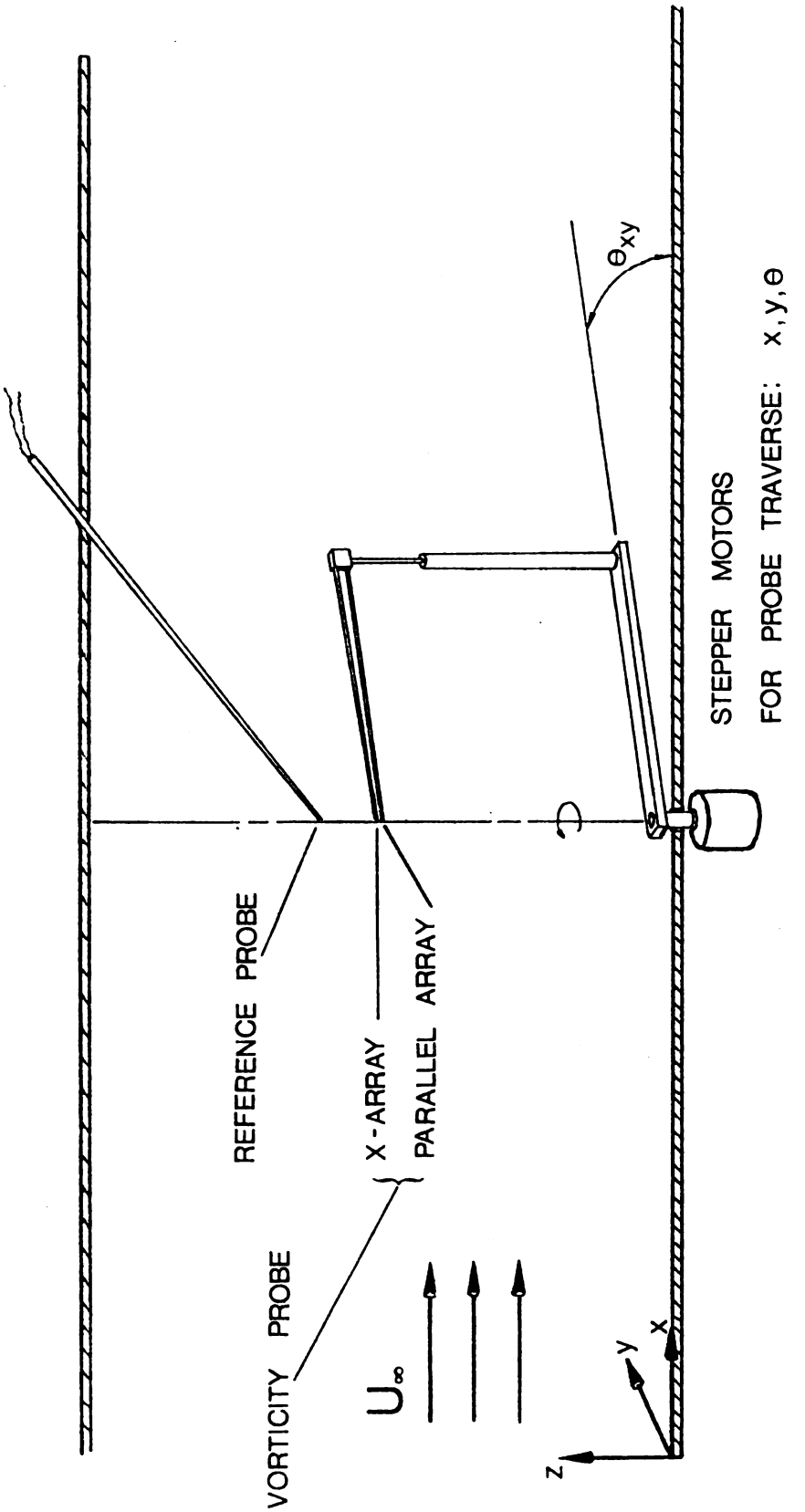

Figure 4.2a. Calibration Facility; Vorticity Probe/Reference Probe Orientation

Notes: (i) θ_{xy} positioning is used to obtain calibration pitch angles (γ_c); + $\gamma_c = -\theta_{xy}$

(ii) Convention for vorticity probe angular position during data-run; cw = $+|\theta_{xy}|$ ccw = $-|\theta_{xy}|$ with respect to x-axis

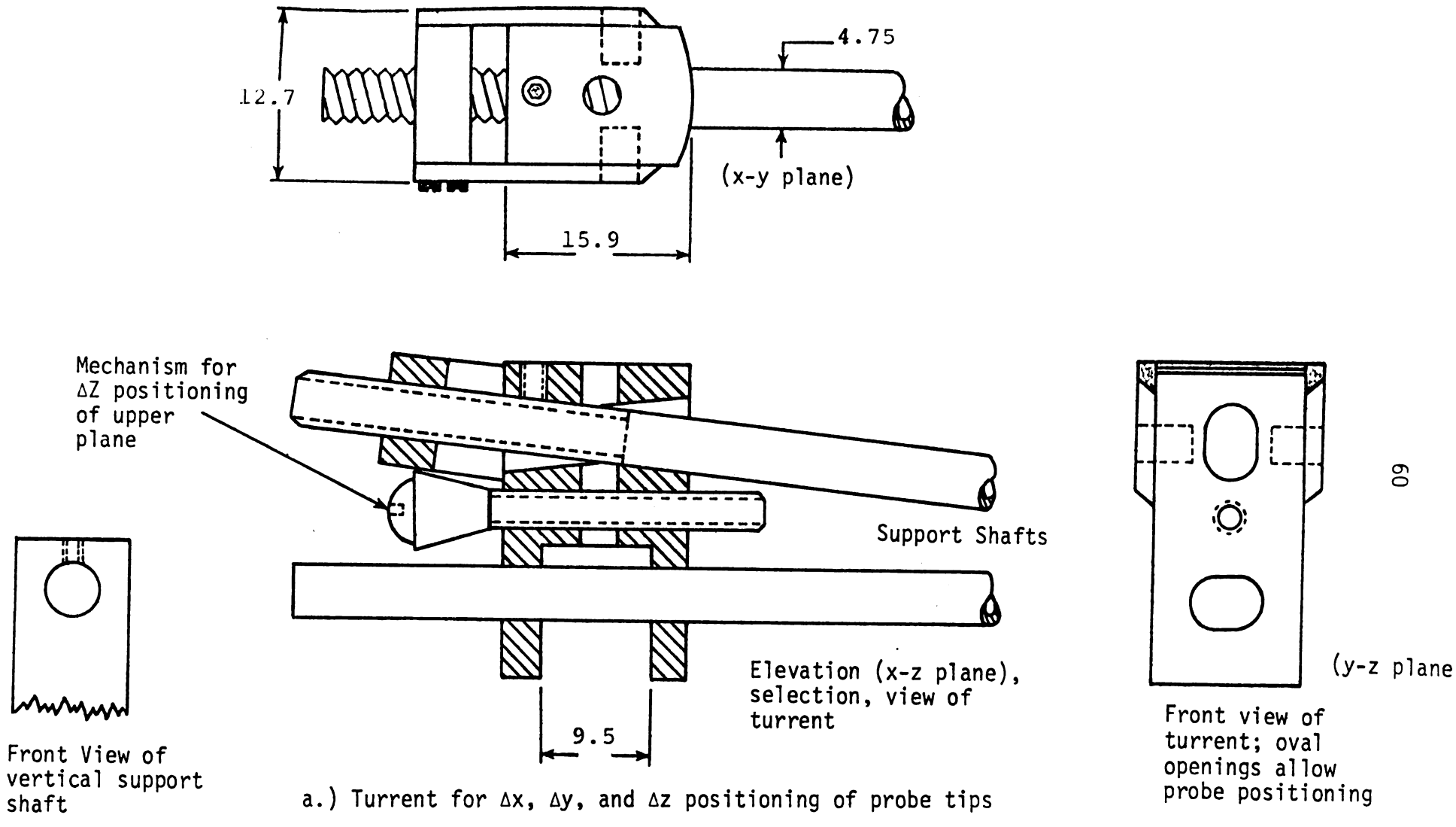

Figure 4.2b. Details of Vorticity Probe Support

Note: all dimensions in mm

Δx adjustment via threaded upper shaft
Δy adjustment via rotation of turret on vertical support shaft

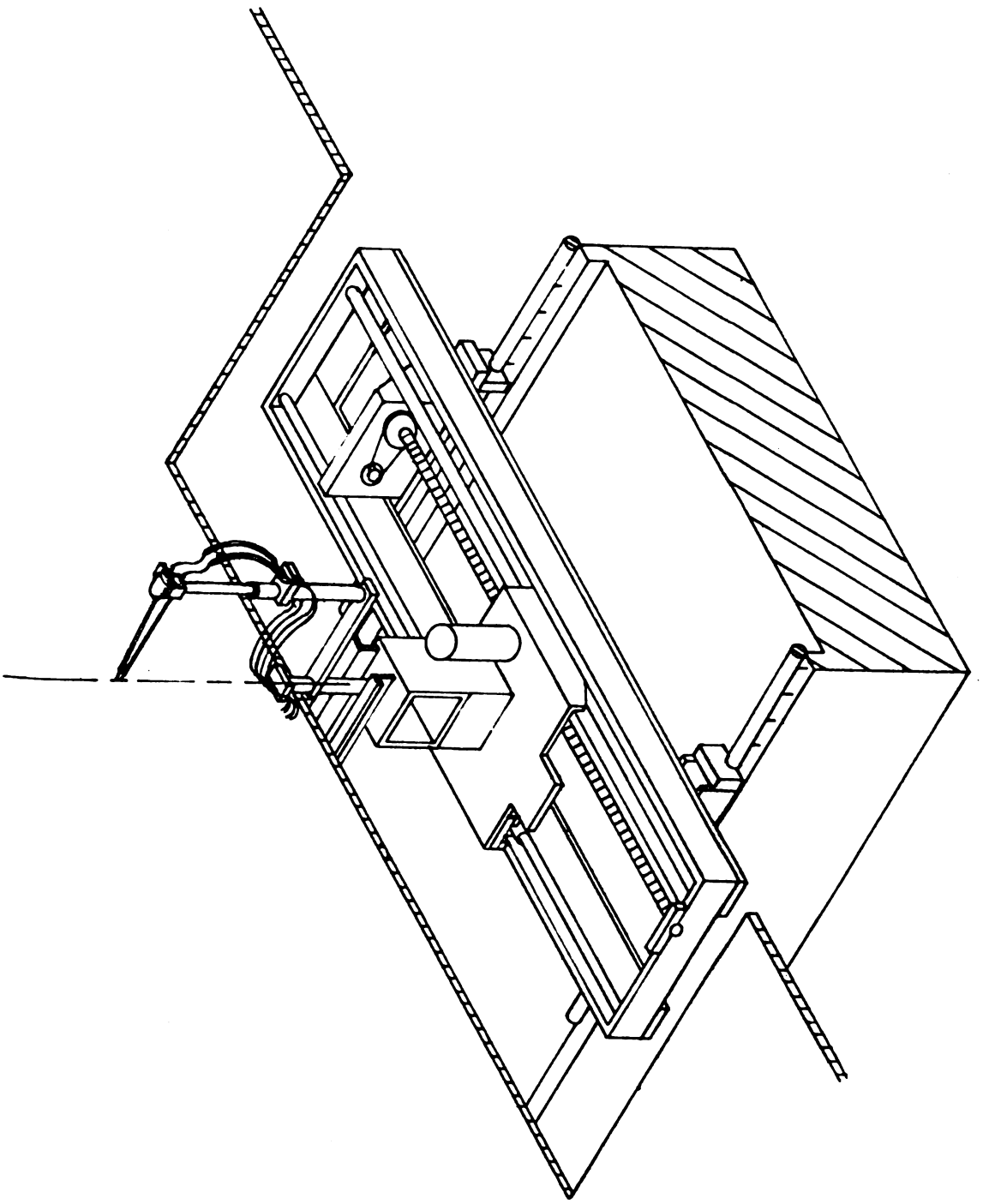

Figure 4.2c. Vorticity Probe Traverse

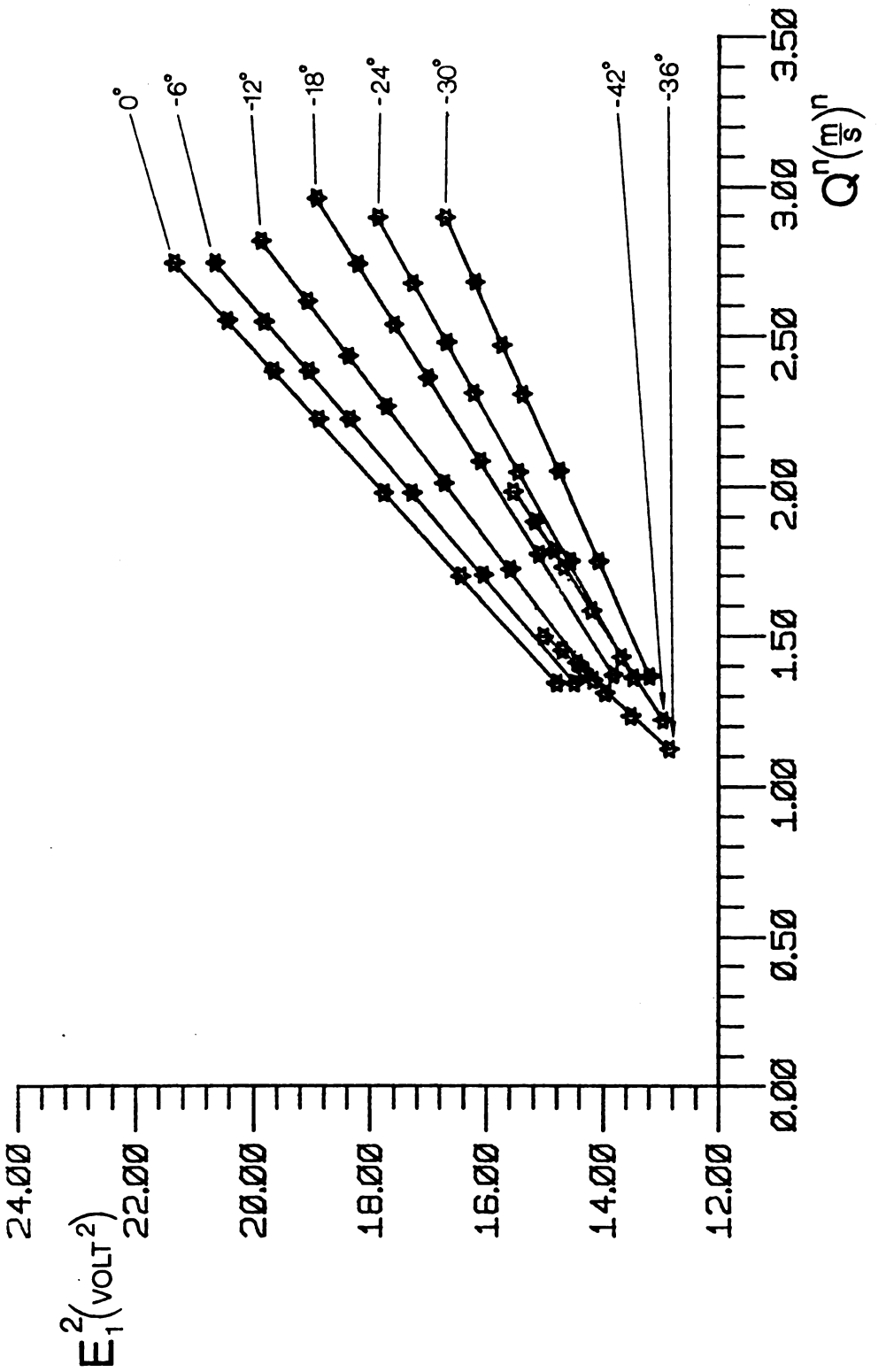

Figure 4.3a. Response Function for Wire 1 = 'Angle - Wire' ($\gamma \leq 0°$)

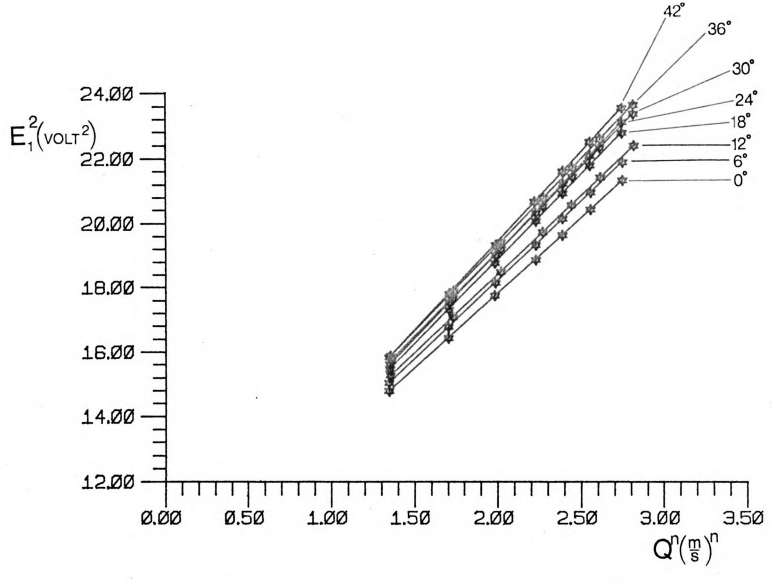

Figure 4.3b. Response Function for Wire 1 ($\gamma \geq 0°$)

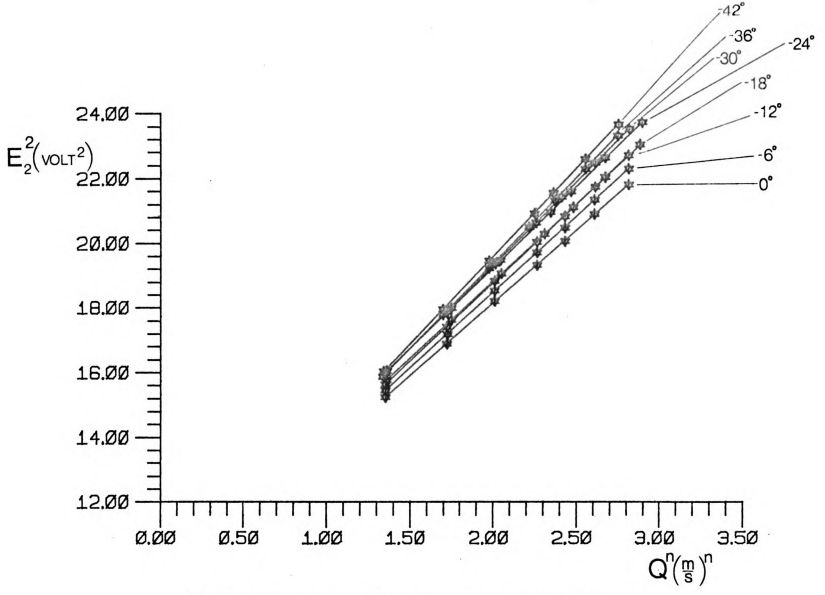

Figure 4.4a. Response Function for Wire 2 ($\gamma \leq 0°$)

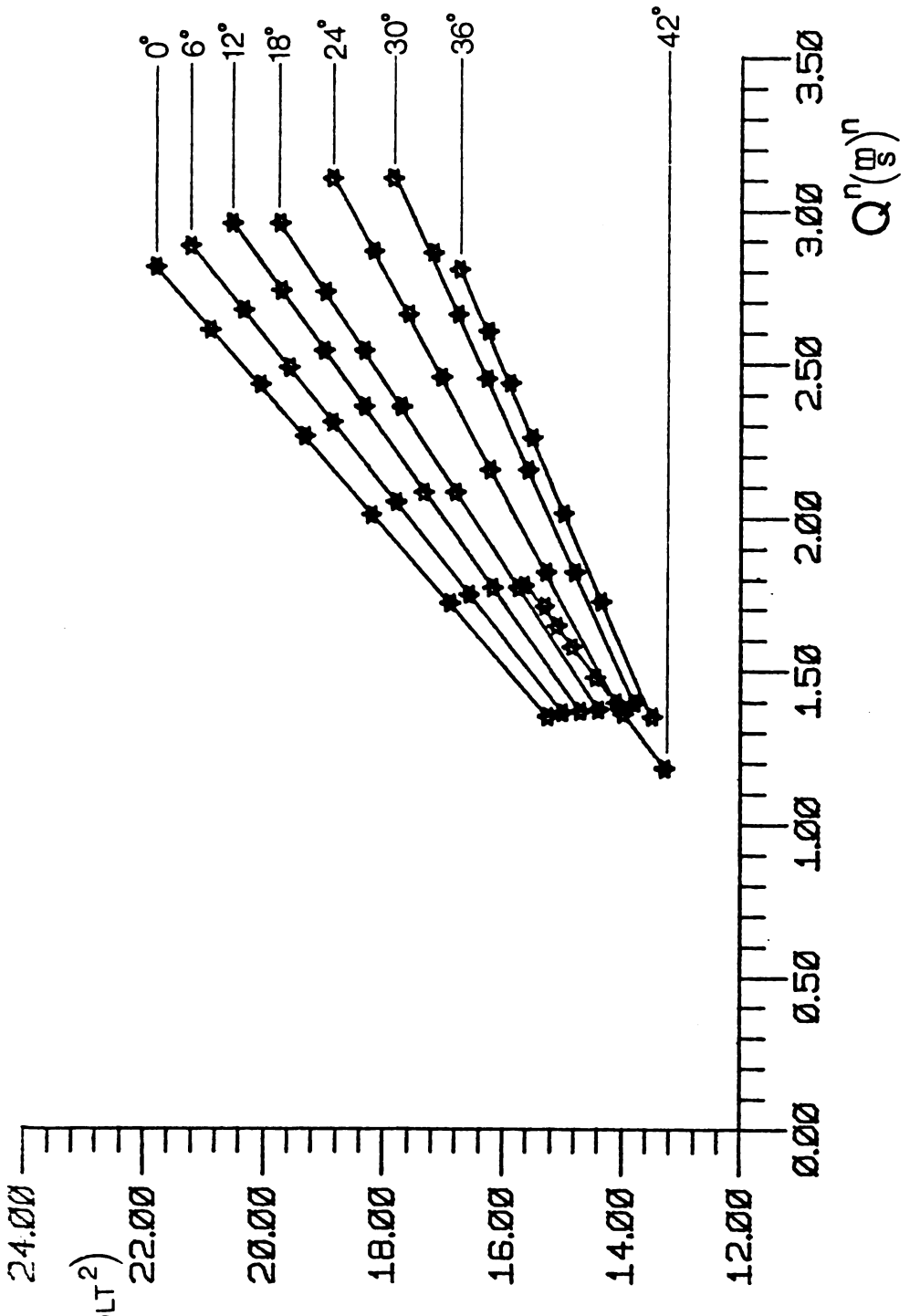

Figure 4.4b. Response Function for Wire 2 = 'Angle Wire' ($\gamma \geq 0°$)

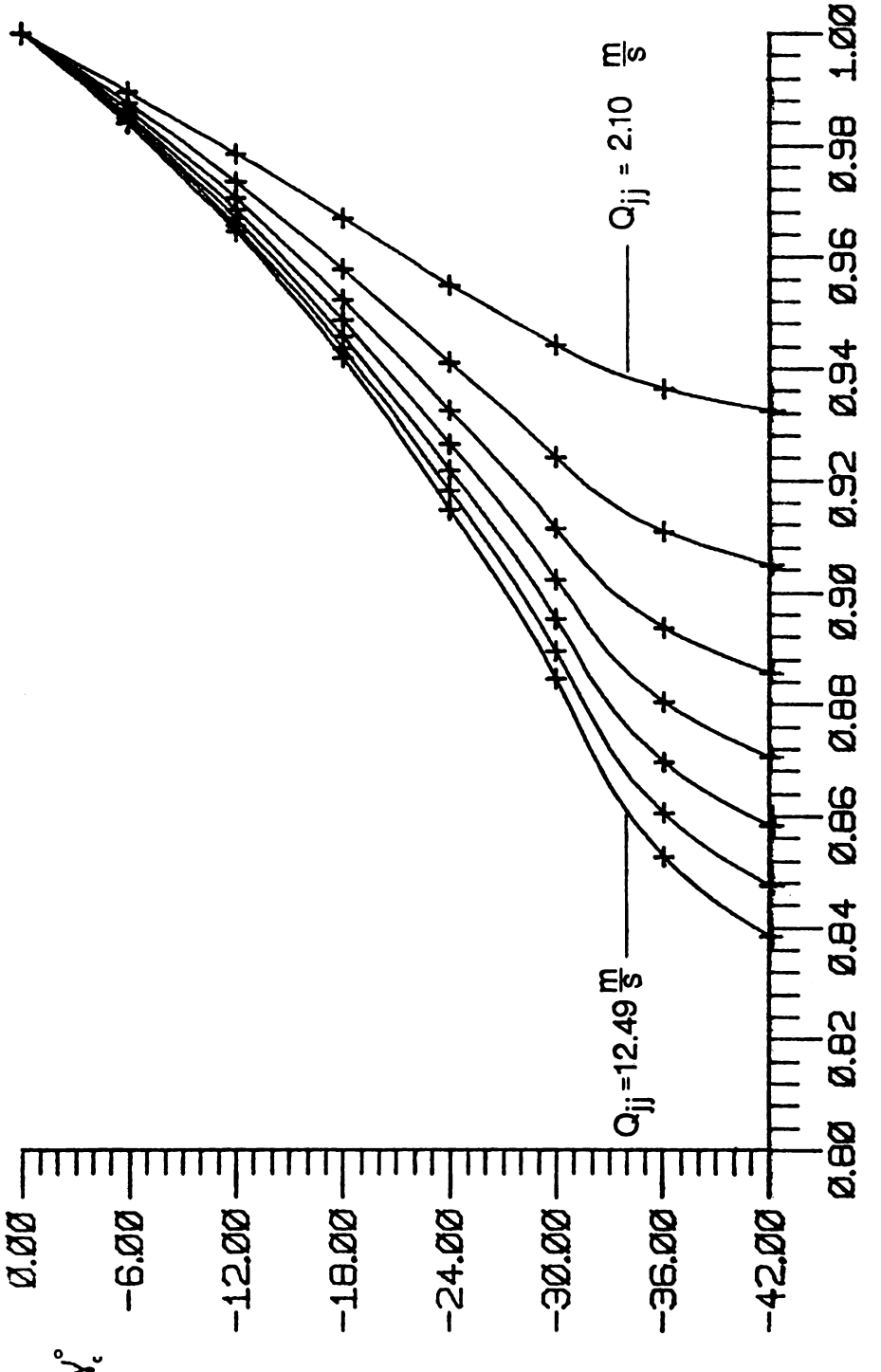

Figure 4.5. Angular Response Function for Wire 1 ($\gamma \leq 0$)

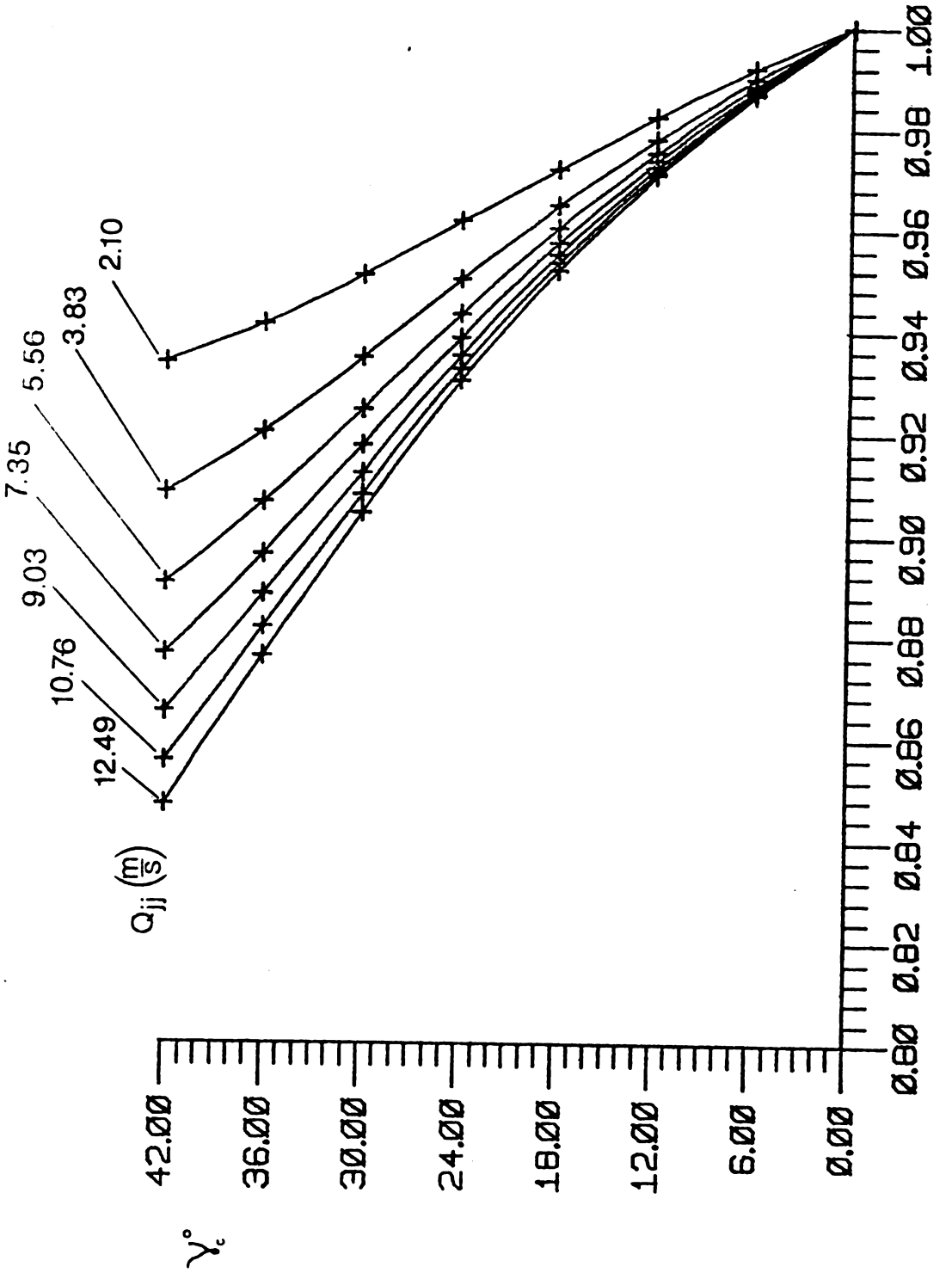

Figure 4.6. Angular Response Function for Wire 2 ($\gamma \geq 0°$)

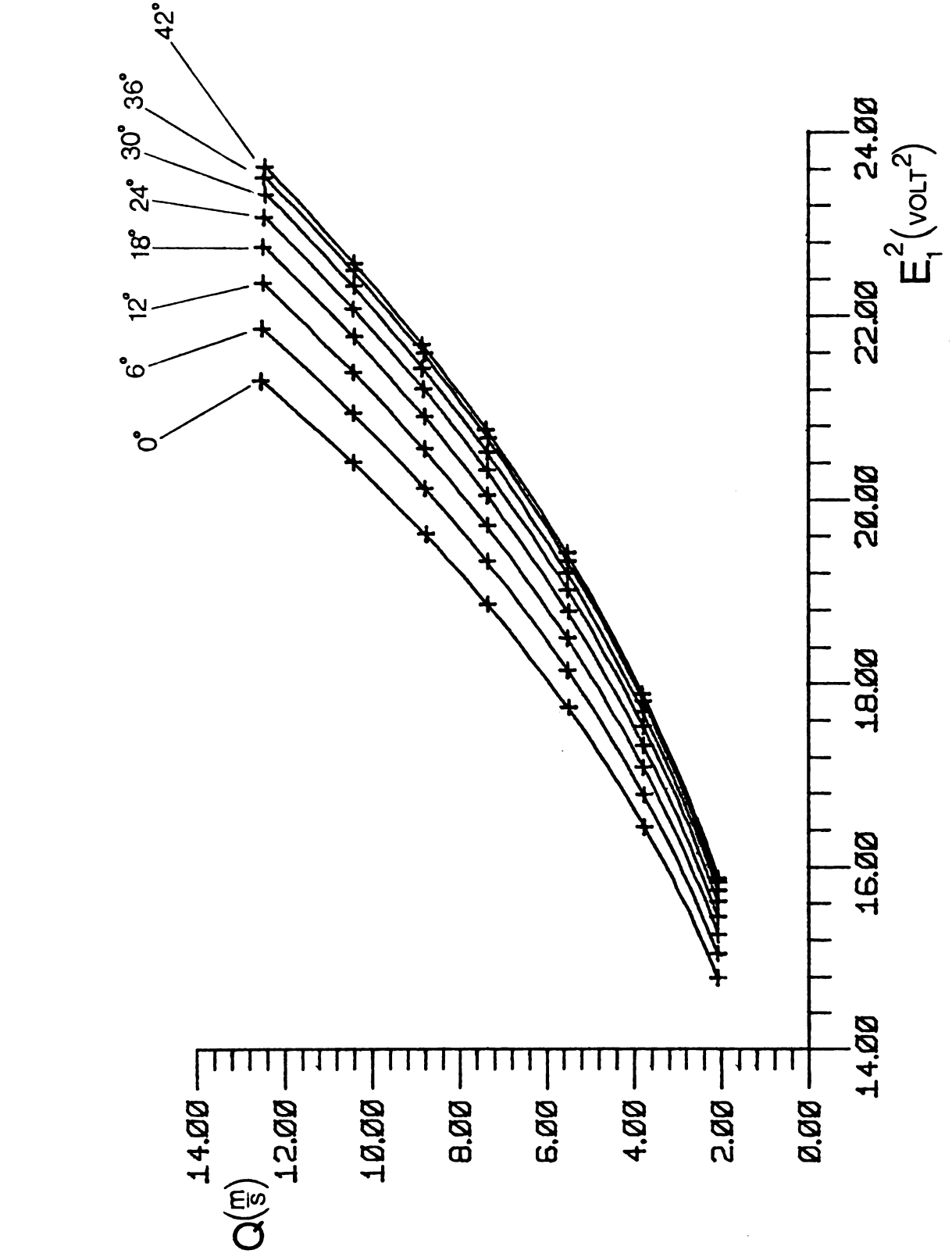

Figure 4.7. Speed Function for Wire 1 = 'Speed-Wire' ($\gamma \geq 0°$)

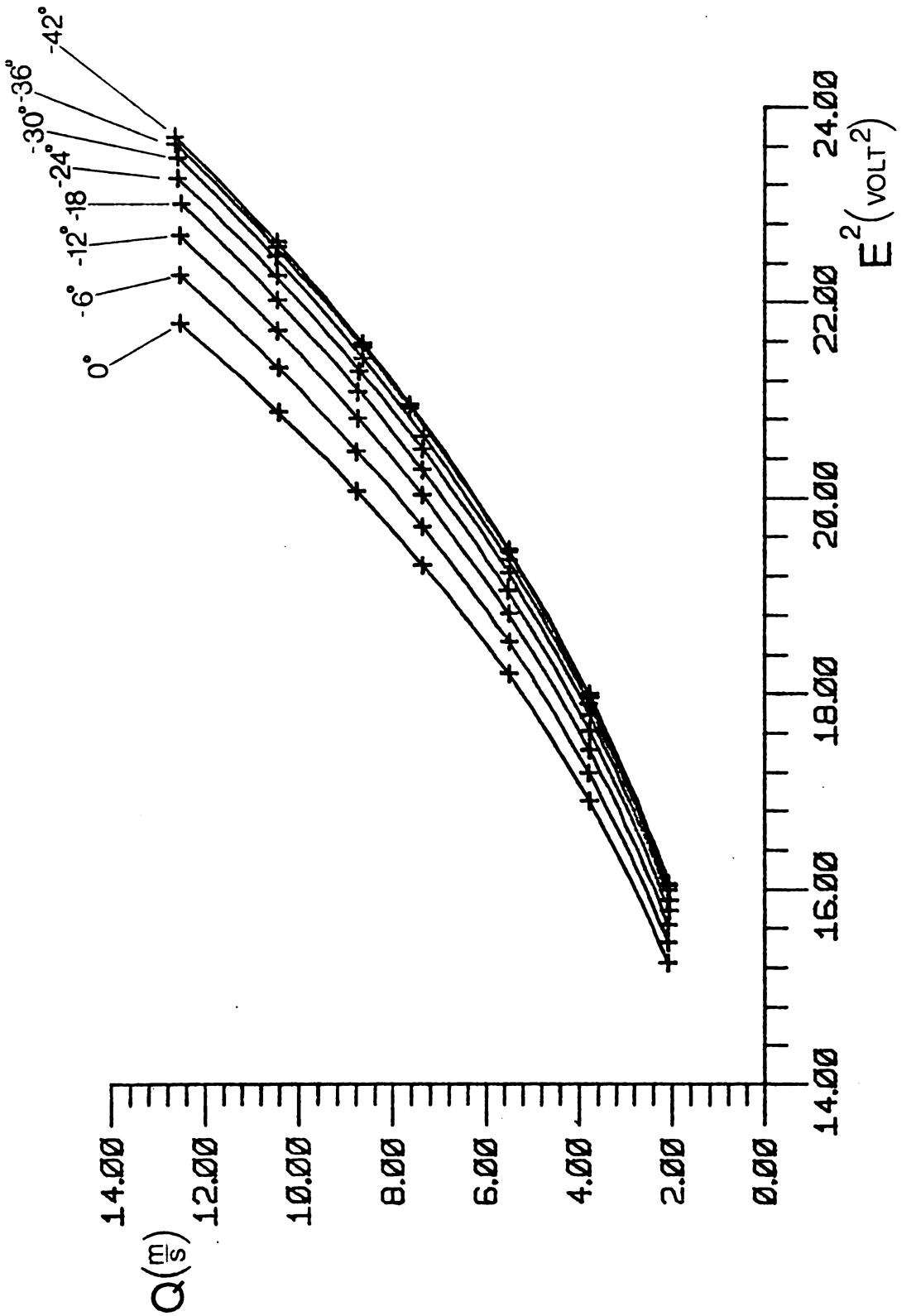

Figure 4.8. Speed Function for Wire 2 = "Speed-Wire' ($\gamma \leq 0°$)

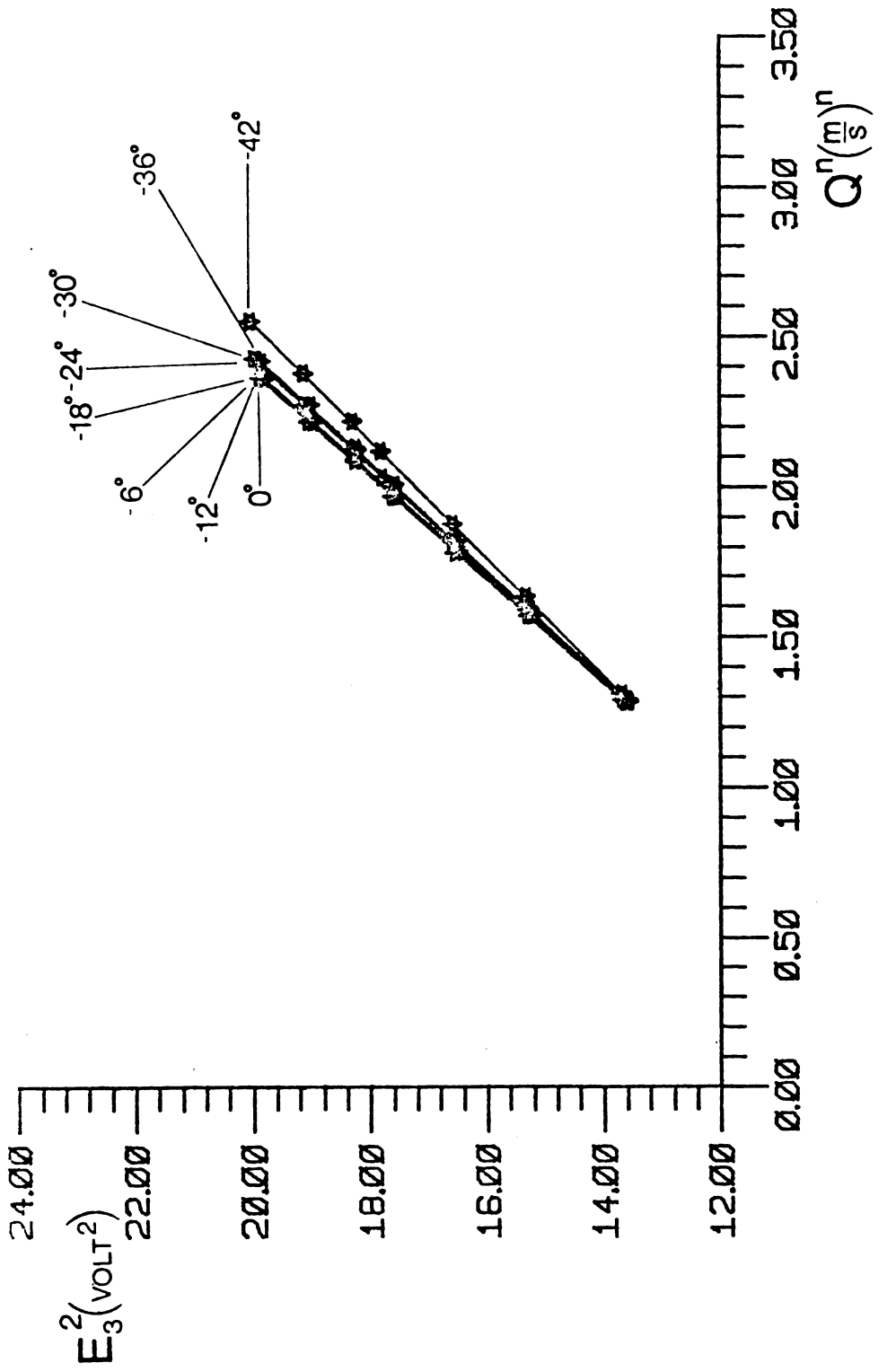

Figure 4.9a. Response Function for Wire 3 ($\gamma \leq 0°$)

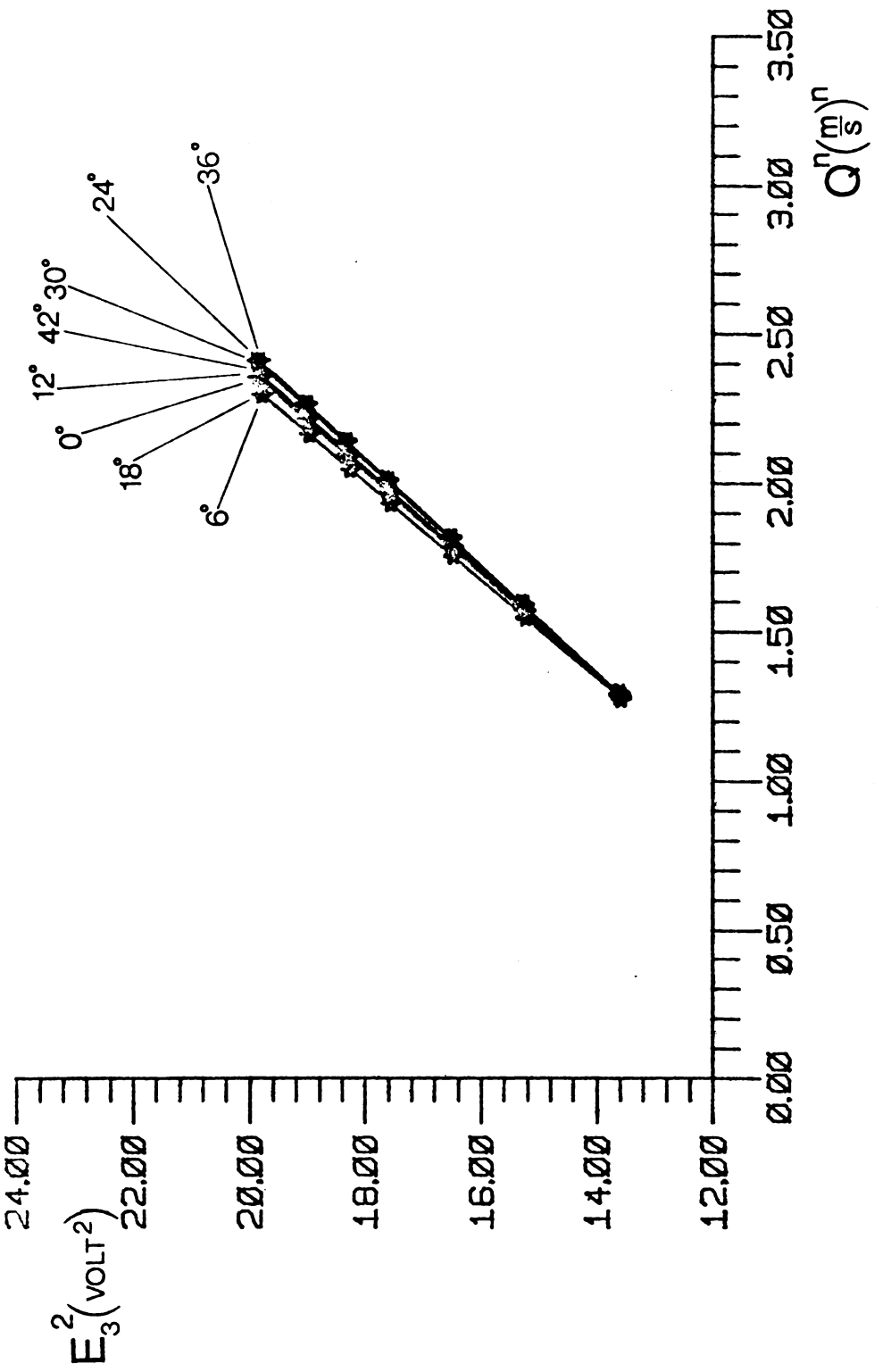

Figure 4.9b. Response Function for Wire 3 ($\gamma \geq 0°$)

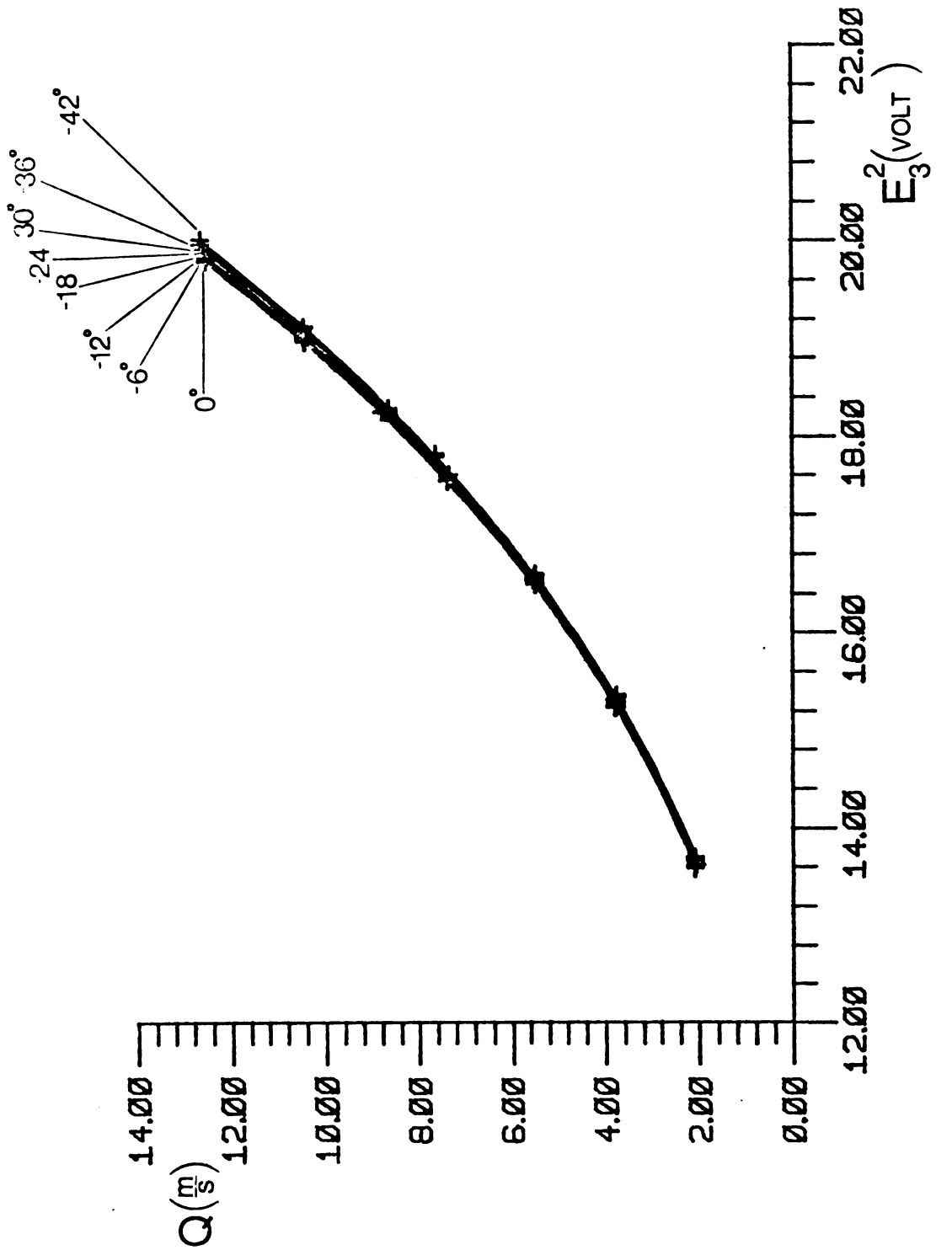

Figure 4.10a. Speed Function for Wire 3 ($\gamma \leq 0$)

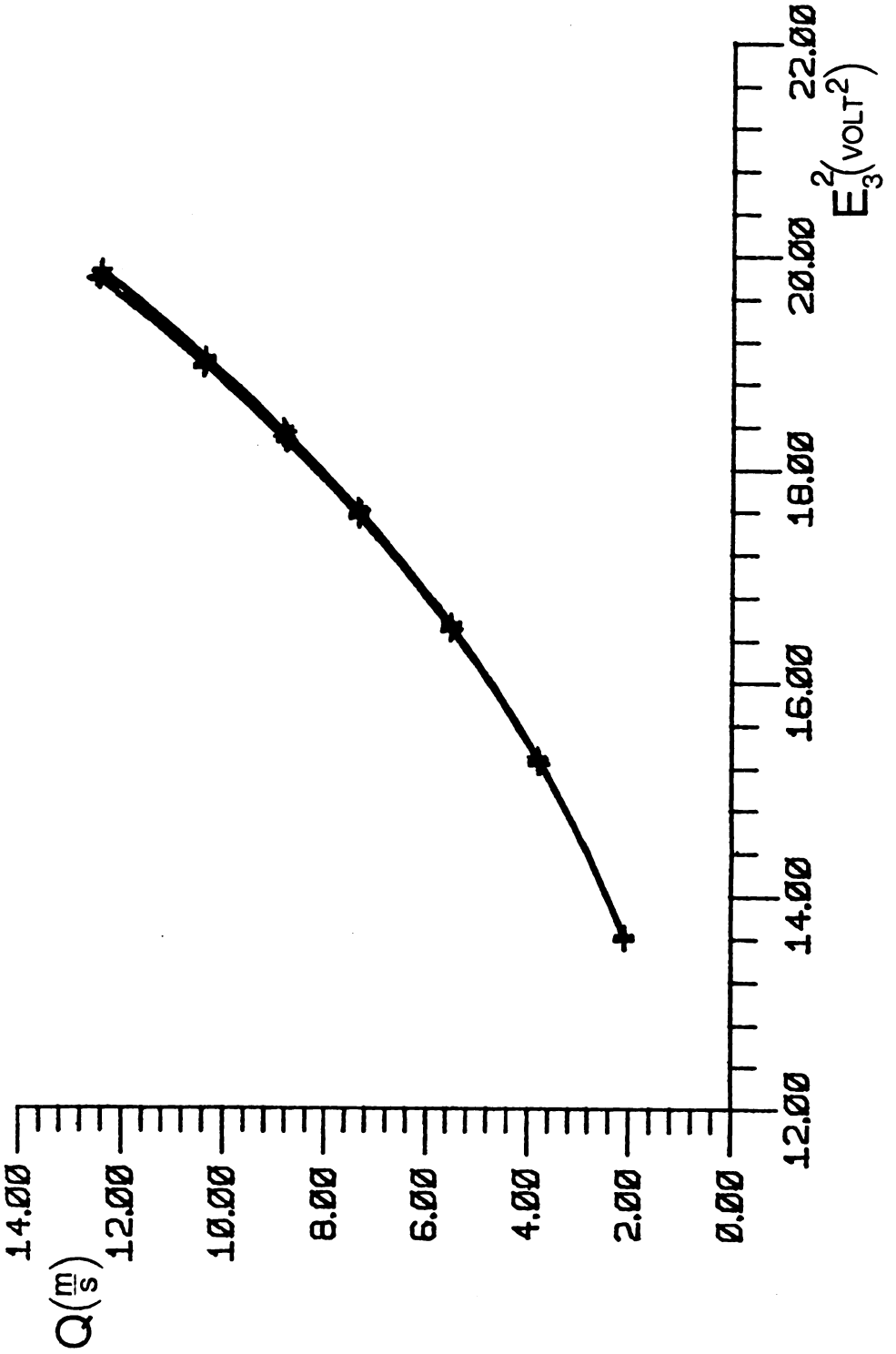

Figure 4.10b. Speed Function for Wire 3 ($\gamma \geq 0$)

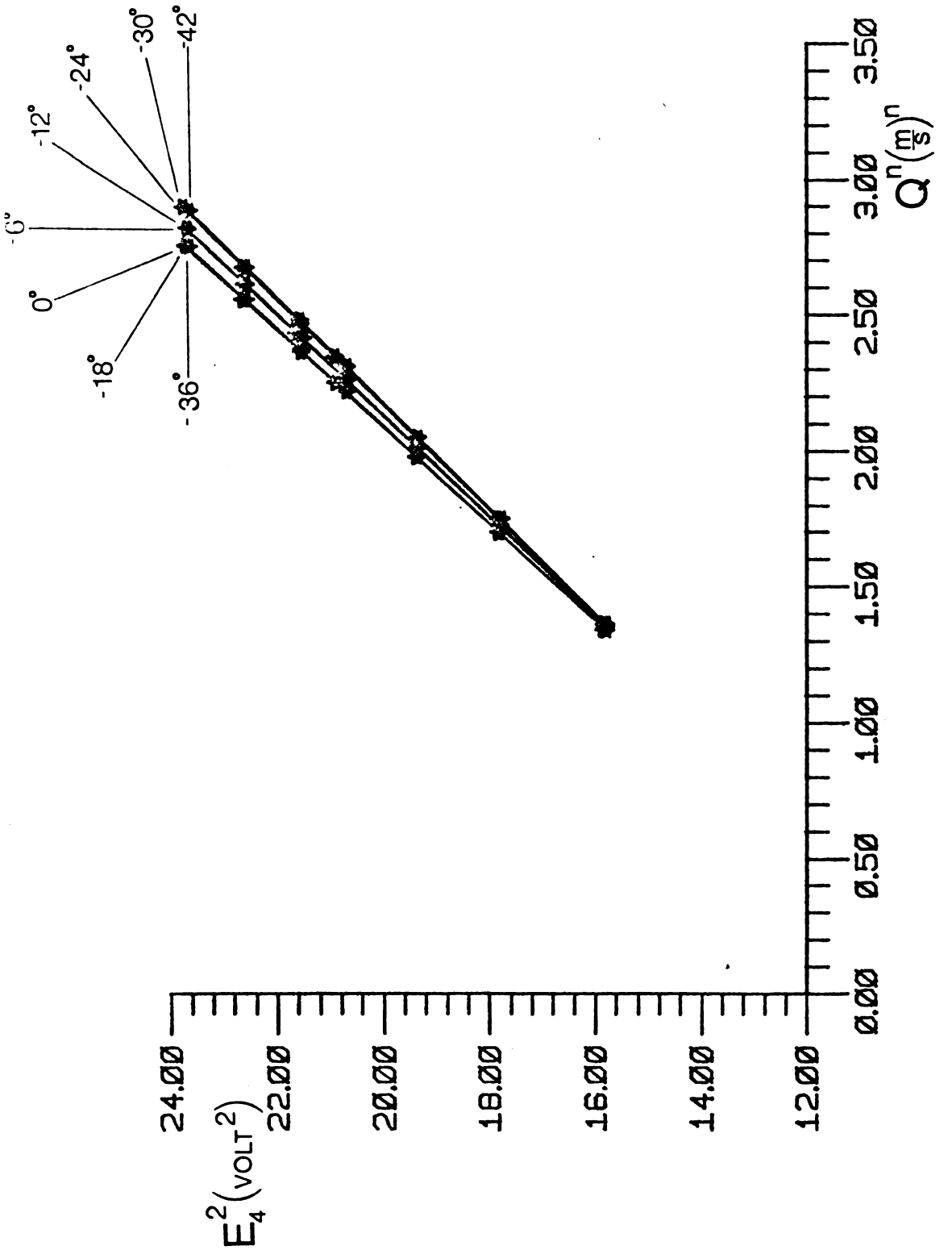

Figure 4.11a. Response Function for Wire 4 ($\gamma \leq 0°$)

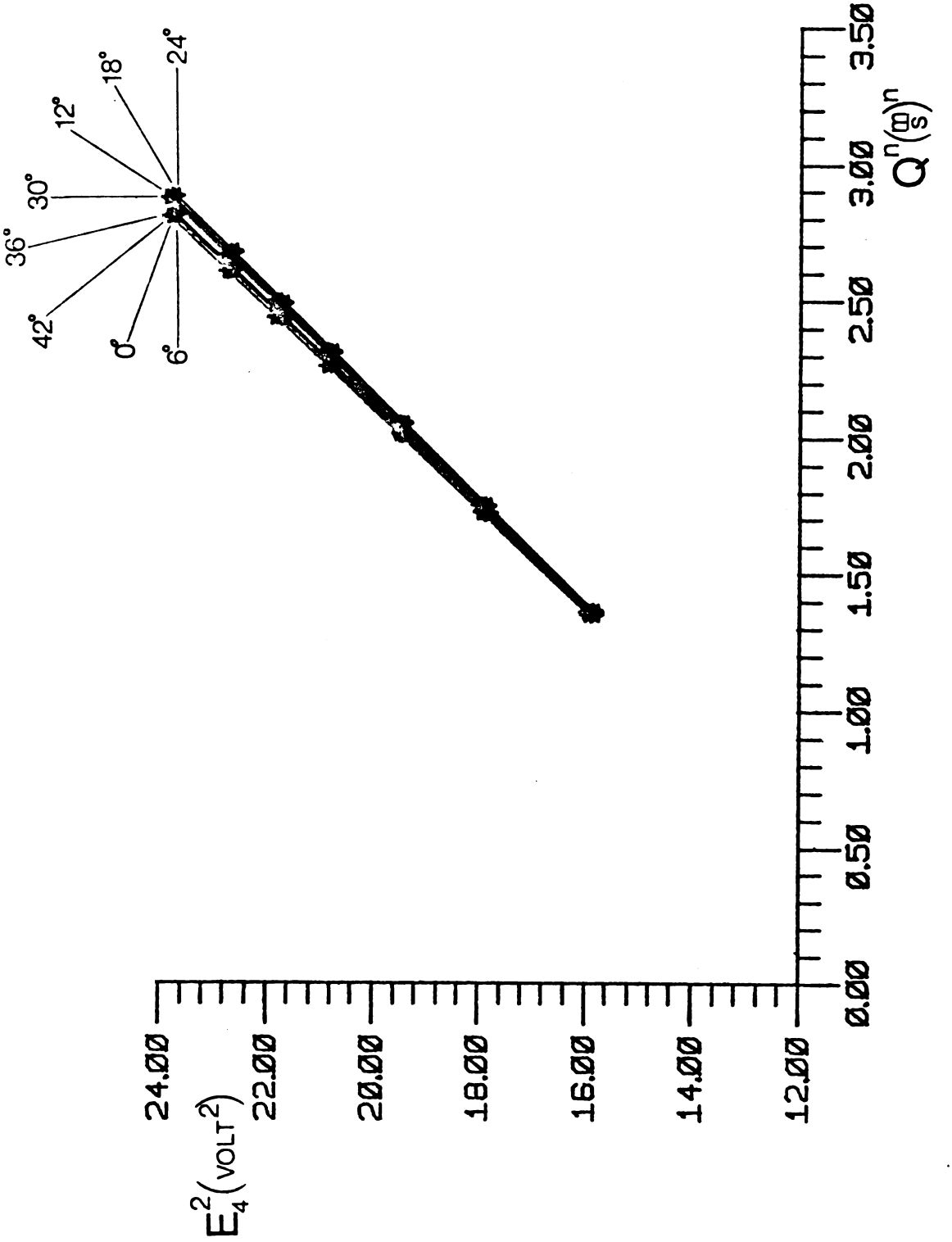

Figure 4.11b. Response Function for Wire 4 ($\gamma \geq 0°$)

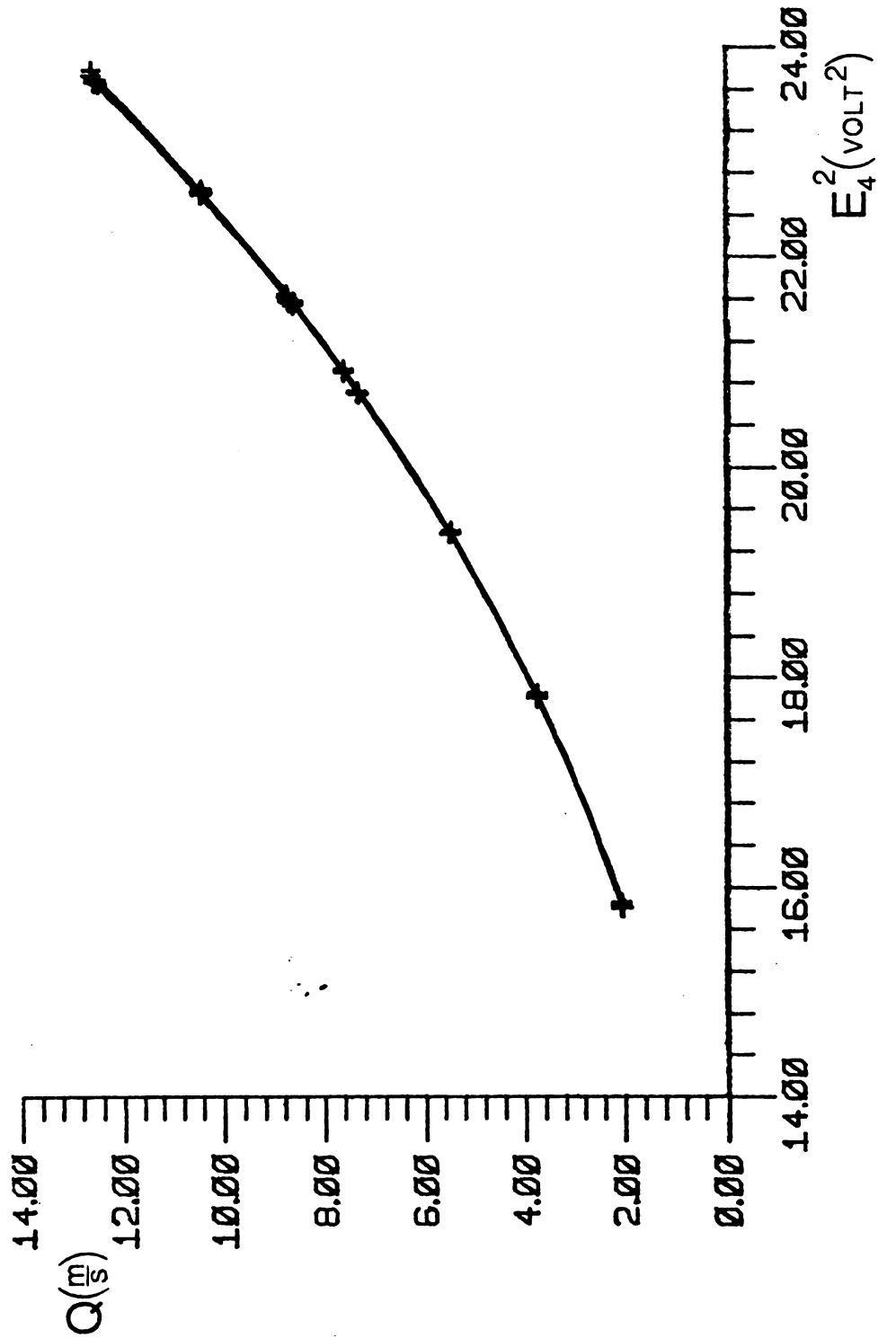

Figure 4.12a. Speed Function for Wire 4 ($\gamma \leq 0$)

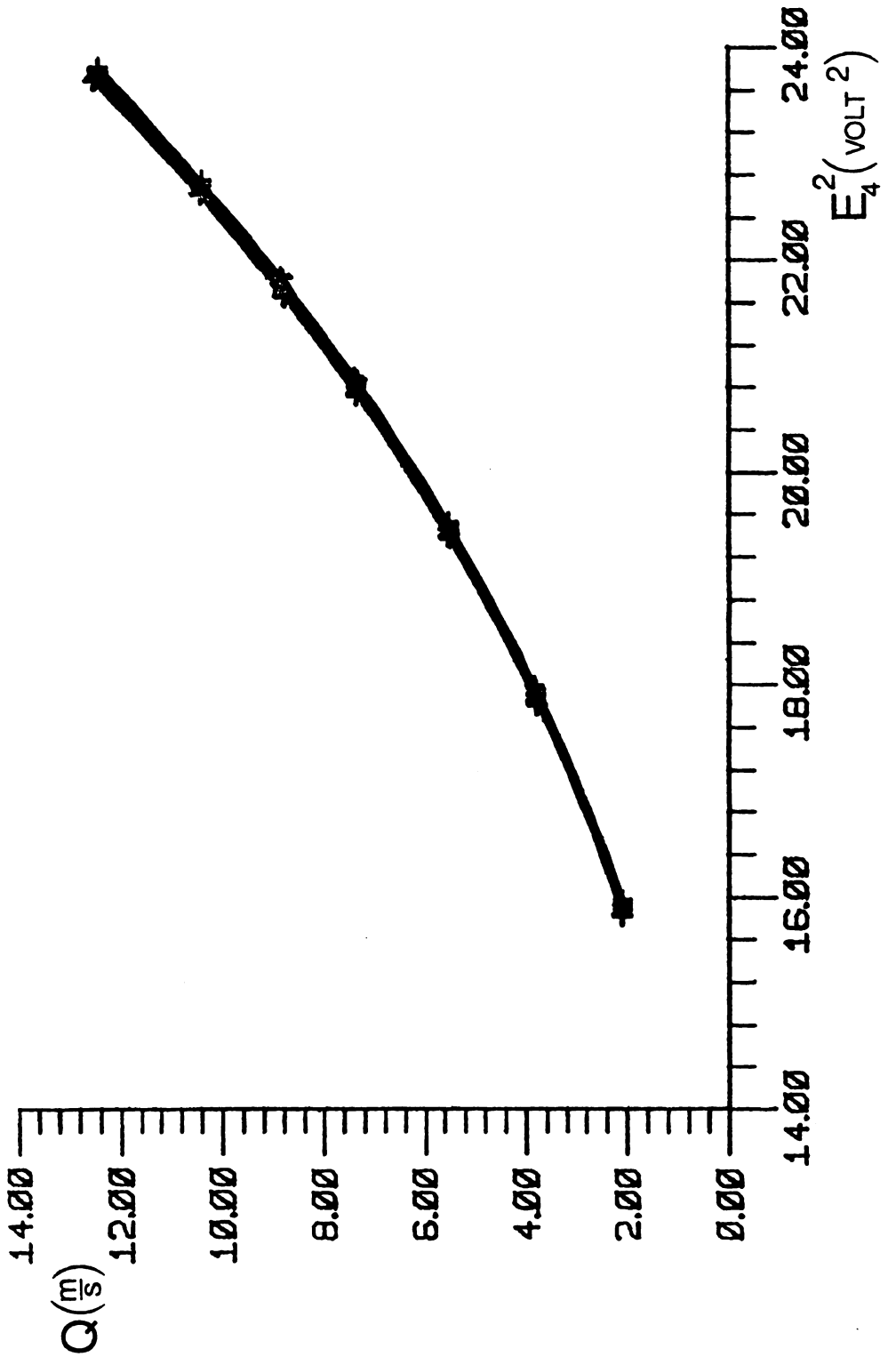

Figure 4.12b. Speed Function for Wire 4 ($\gamma \geq 0$)

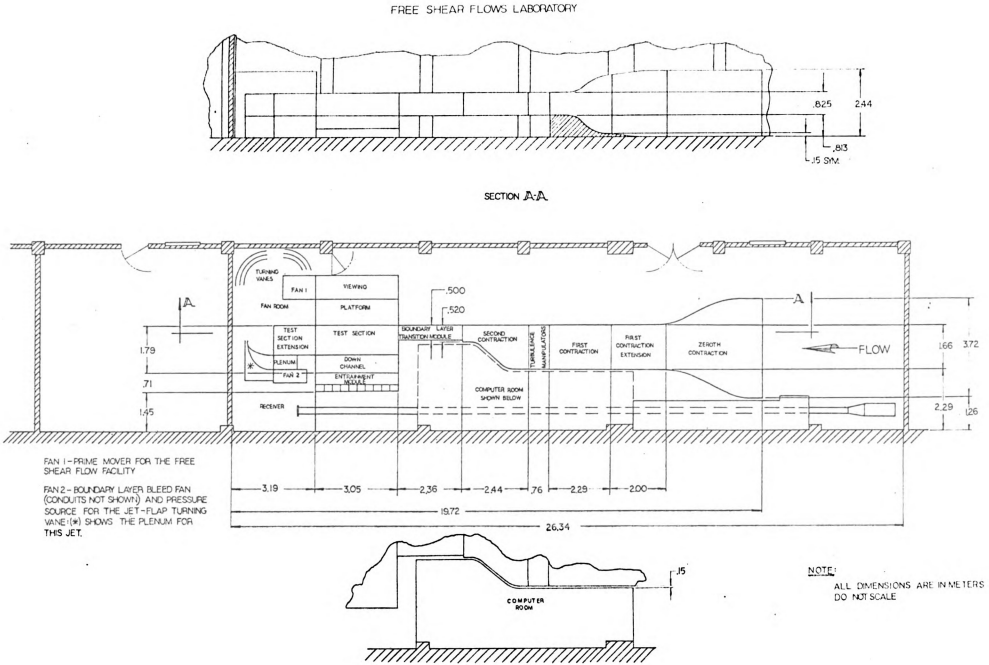

Figure 5.1a The Free Shear Flow Facility

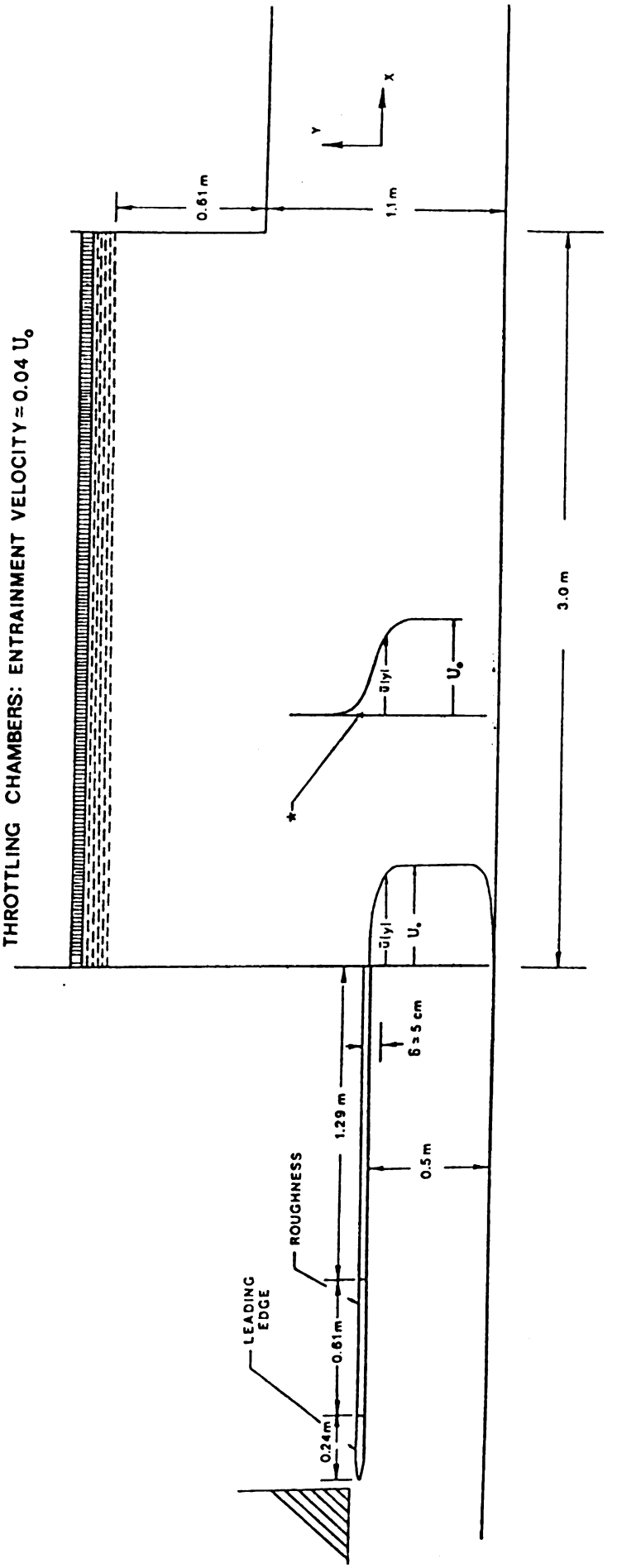

Figure 5.1b Detail view of test section with the initial and shear layer profiles shown schematically.

Note: * - Measurement location

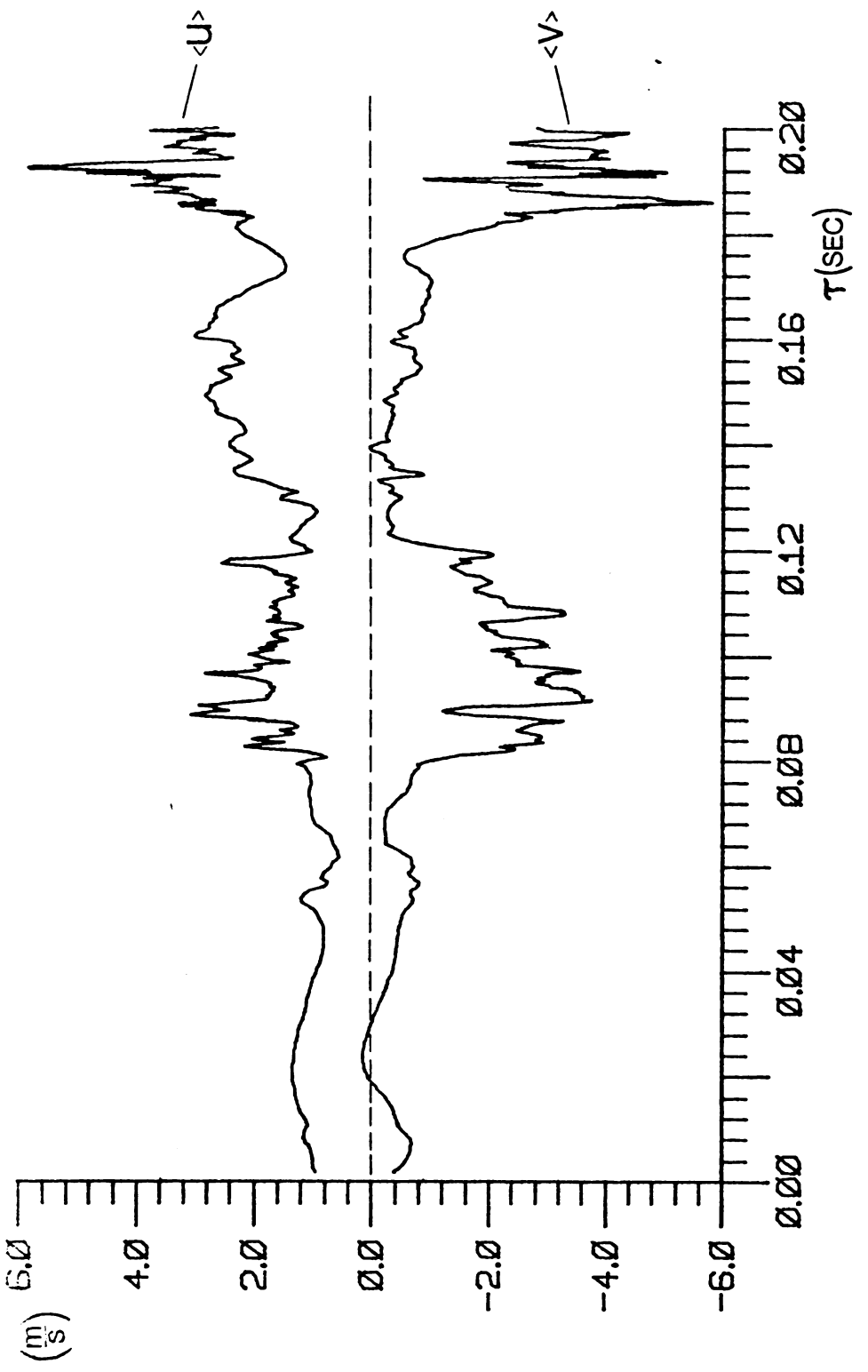

Figure 5.2a. Streamwise and Transverse Velocity Components

Note: Measurement point: x = 1m
y = 9.9 cm
$\eta = \frac{y-y_{\frac{1}{2}}}{x-x_o} = .076$

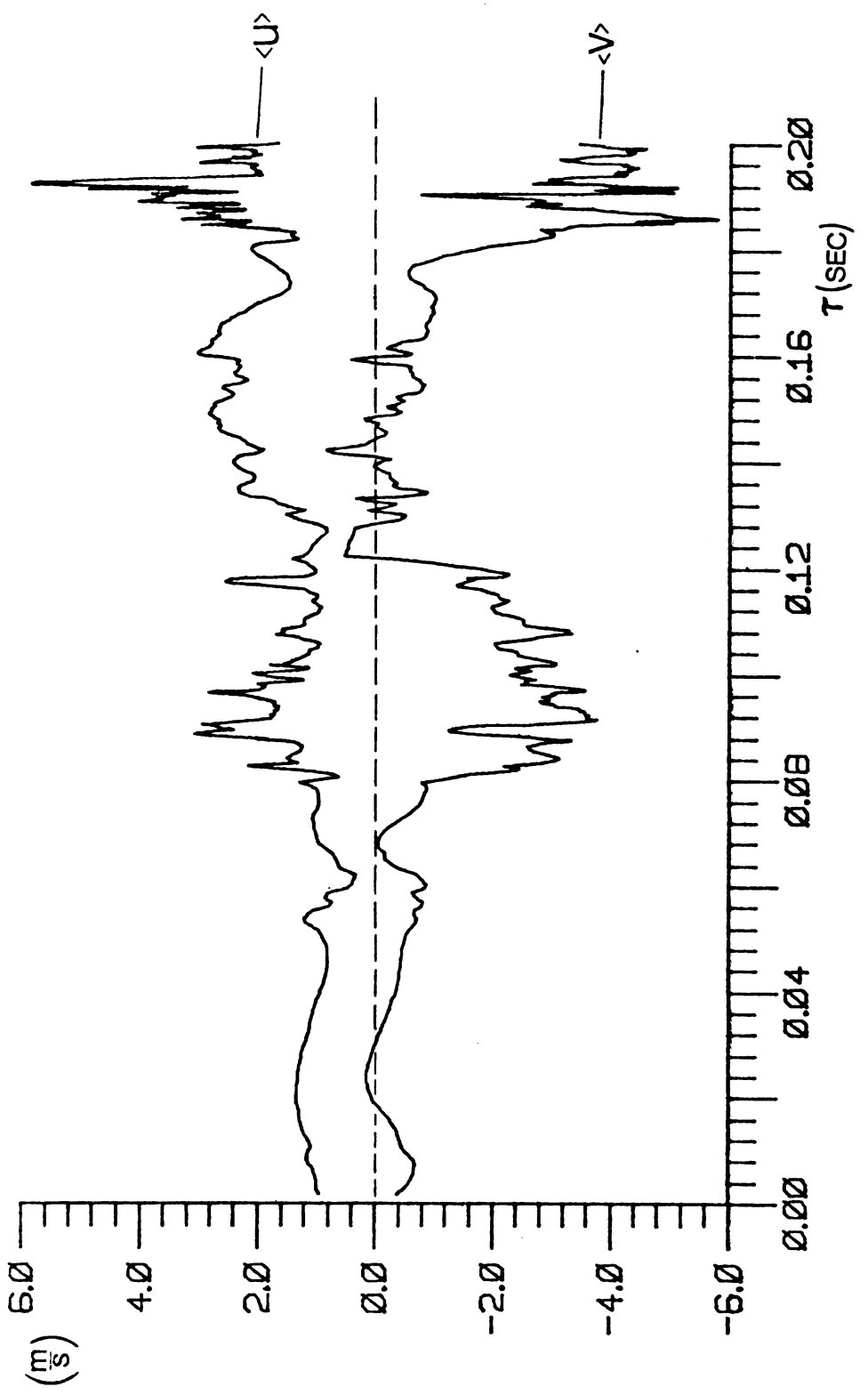

Figure 5.2b. Streamwise and Transverse Velocity Components (see Figure 5.2a. notes)

Note: Values corrected for W^2 Influence

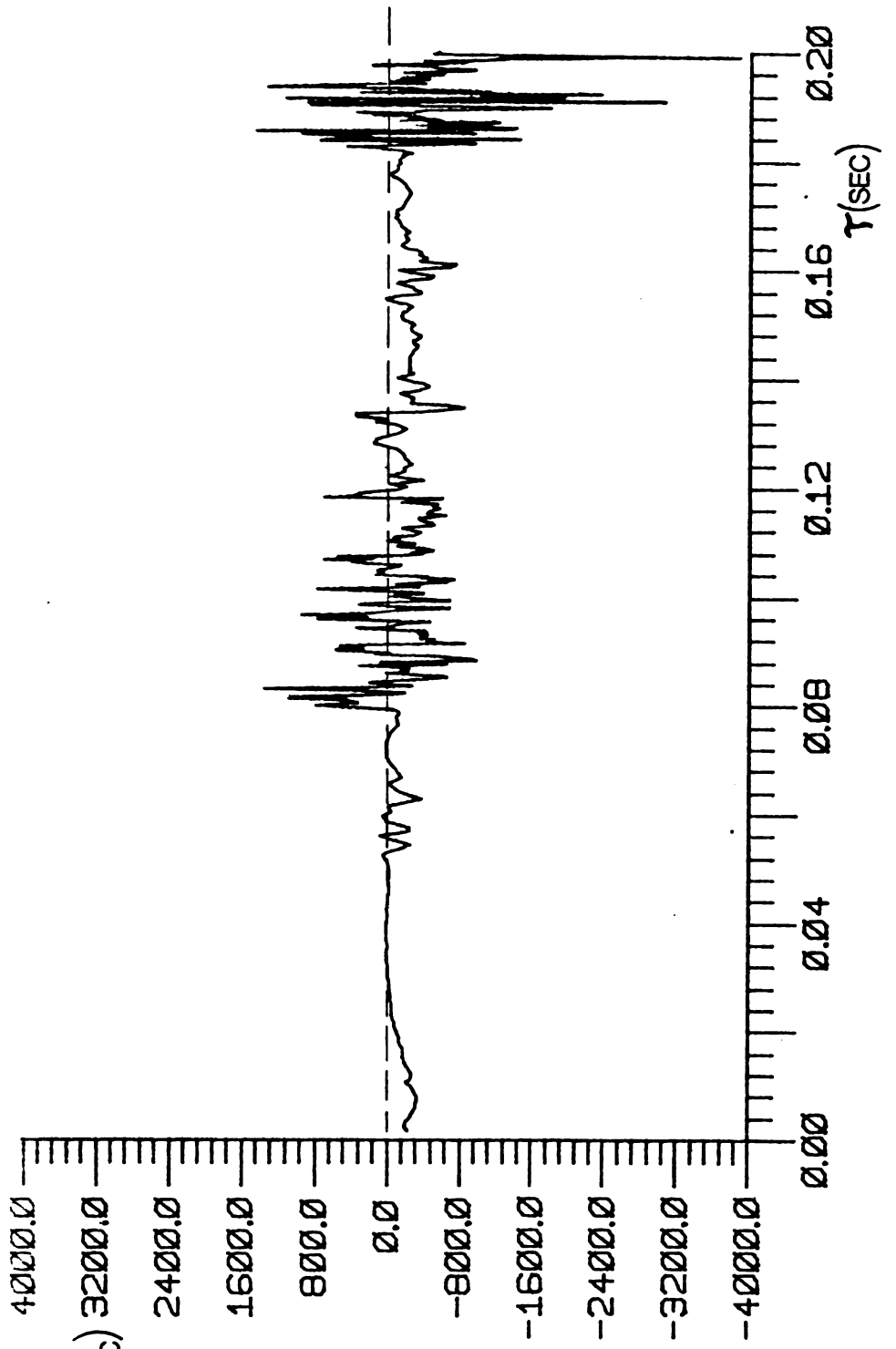

Figure 5.3a. Transverse vorticity time series (see Figure 5.2a. notes)

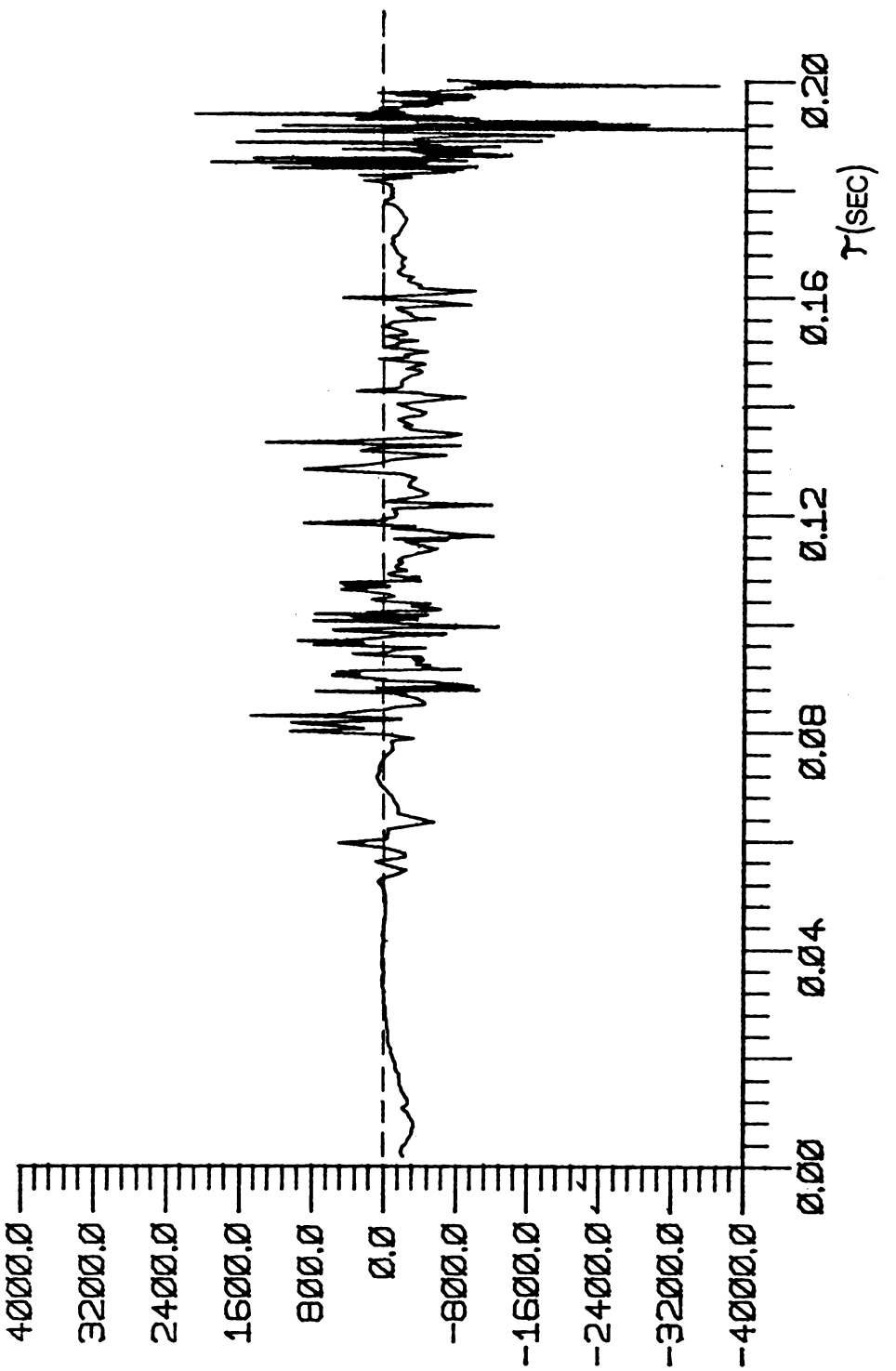

Figure 5.3b. Transverse Vorticity Time Series (see Figure 5.2a. notes)

Note: Values Corrected for W^2 Influence

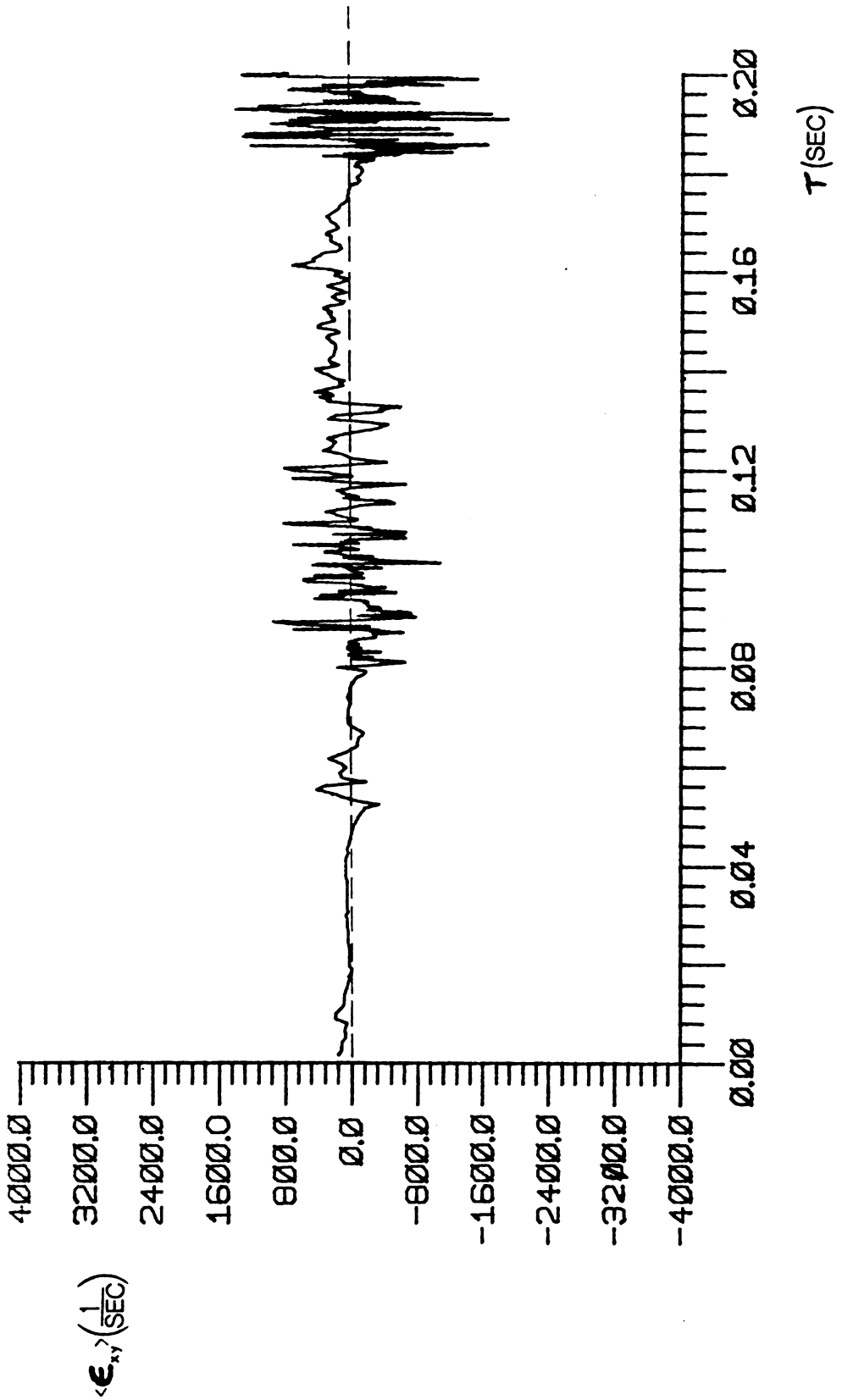

Figure 5.4a. Strain Rate Time Series (see Figure 5.2a. notes)

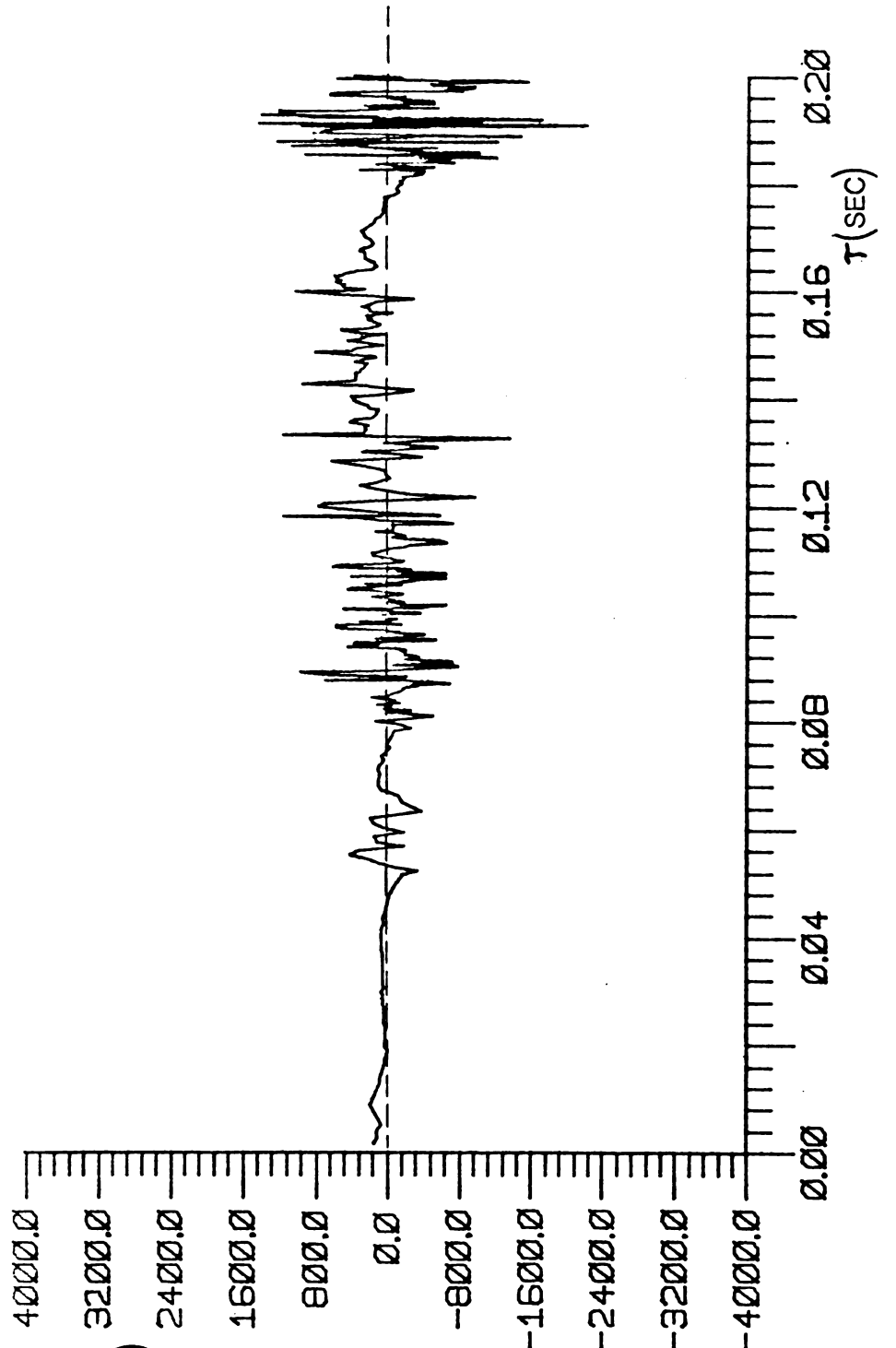

Figure 5.4b. Strain Rate Time Series (see Figure 5.2a. notes)

Note: Values Corrected for W^2 Influence

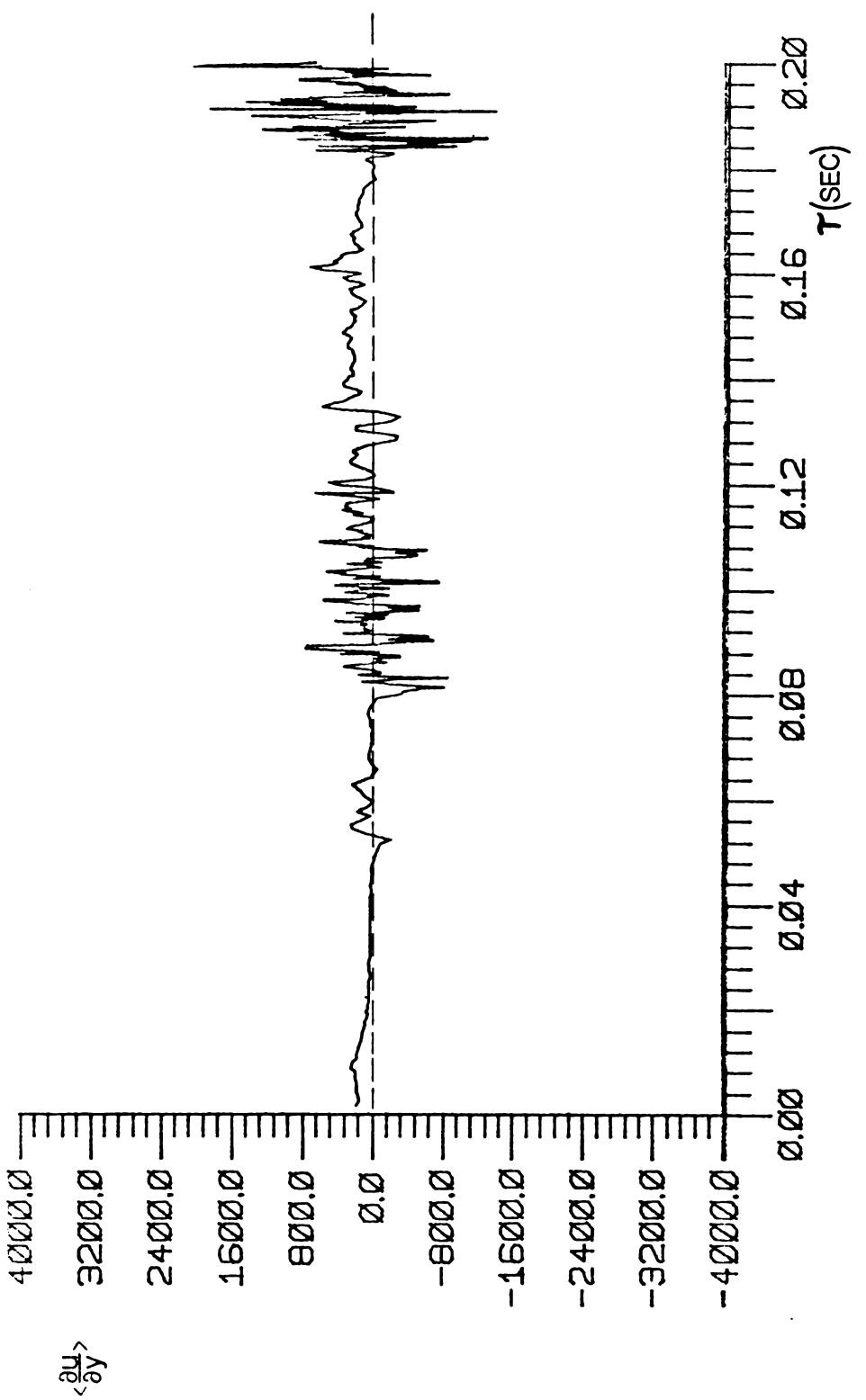

Figure 5.5a. Velocity Gradient $\langle \frac{\partial u}{\partial y} \rangle$ (see Figure 5.2a. notes)

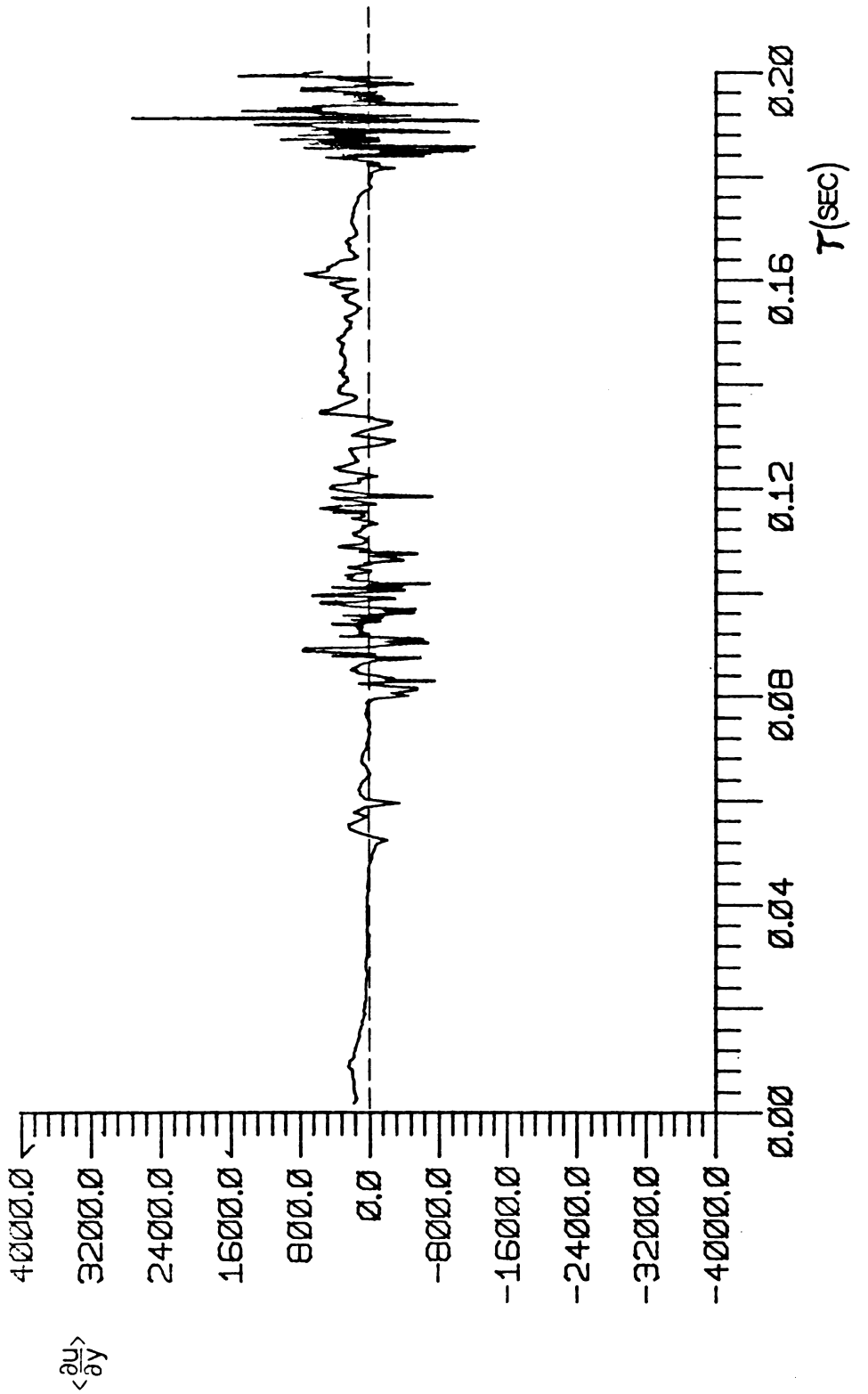

Figure 5.5b. Velocity Gradient $\langle \frac{\partial u}{\partial y} \rangle$ (see Figure 5.2a. notes)

Note: Values Corrected for W^2 Influence

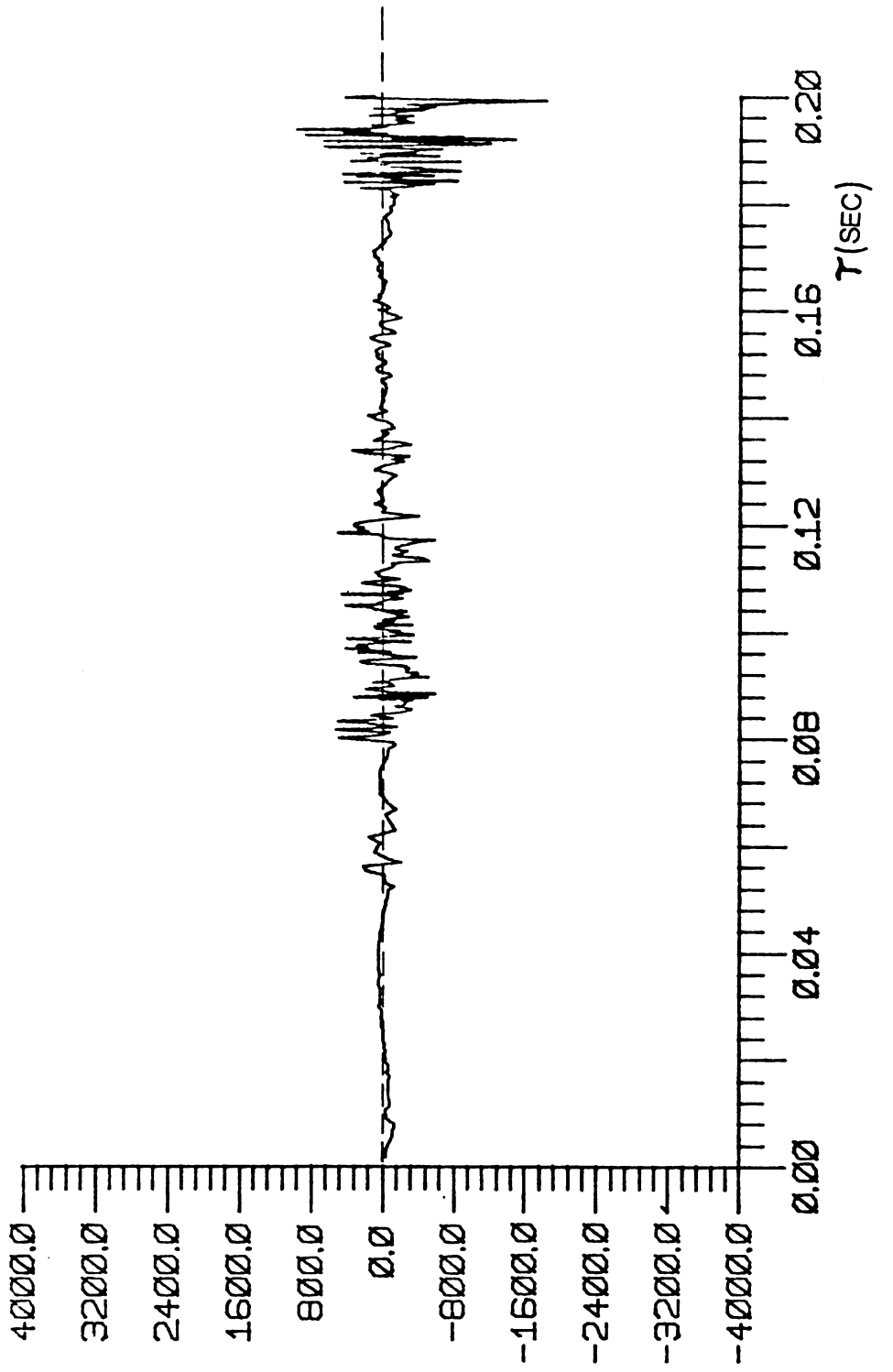

Figure 5.6a. Velocity Gradient $\langle \frac{\partial v}{\partial x} \rangle$ (see Figure 5.2a. notes)

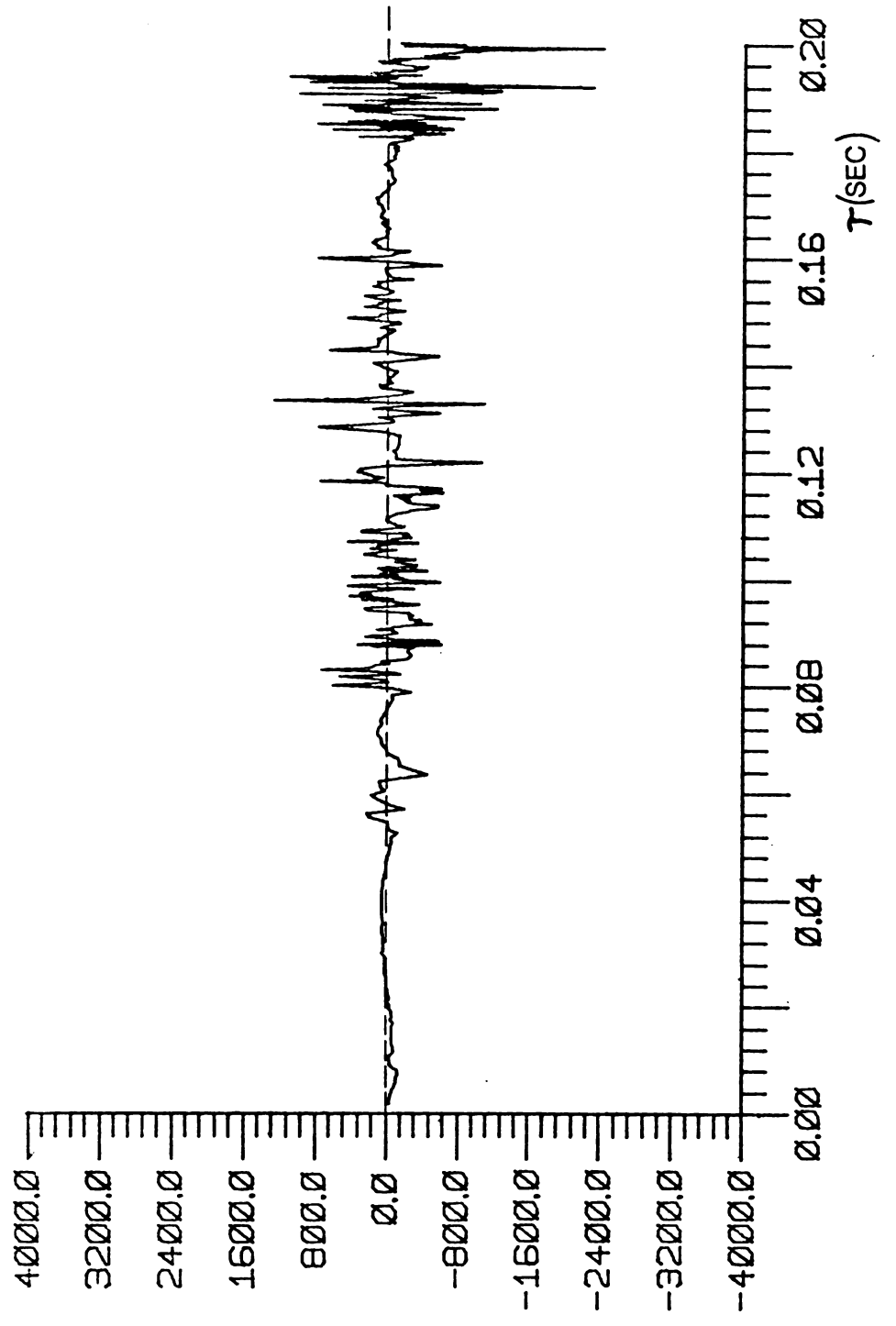

Figure 5.6b. Velocity Gradient $\langle \frac{\partial V}{\partial X} \rangle$ (see Figure 5.2a notes)

Note: Values Corrected for W^2 Influence

APPENDICES

APPENDIX A

COSLAW

The two-equation two-unknown technique, COSLAW, uses the voltages from the x-array to obtain estimates for Q_x and γ. These estimates are either accepted as valid measures of Q_x and γ ($|\gamma| \leq 12^\circ$) or are utilized as initial values for the iterative scheme.

The COSLAW technique employs the following form of the Collis and Williams equation,

$$E^2 = A(0) + b(0) Q_{eff}^{n(o)} \qquad \text{(eq. A.1)}$$

where

$$Q_{eff} = Q_x \cos(\beta - \gamma) \qquad \text{(eq. A.1a)}$$

and

$$b(0) = B(o) / \cos^{n(o)} \beta$$

Note that B(0) is the coefficient determined for the modified Collis and Williams form (eq. 4.4) and the calibration data at $\gamma = 0^\circ$.

Equation A.1 may then be written for both slant wires in an expanded form, as:

$$\left[(E_1^2-A_1(0))/b_1\right]^{1/n(o)} = Q_x\cos(\beta_1-\gamma)$$
$$= Q_x(\cos\beta_1\cos\gamma + \sin\beta_1\sin\gamma) \qquad \text{(eq. A.2)}$$

$$\left[(E_2^2-A_2(0))/b_2\right]^{1/n(o)} = Q_x\cos(\beta_2-\gamma)$$
$$= Q_x(\cos\beta_2\cos\gamma + \sin\beta_2\sin\gamma) \qquad \text{(eq. A.3)}$$

Recognizing that $u=Q_x\cos\gamma$ and $v=Q_x\sin\gamma$ equations A.2 and A.3 may be rewritten as:

$$C_1 = u\cos\beta_1 + v\sin\beta_1 \qquad \text{(eq. A.4)}$$

$$C_2 = u\cos\beta_2 + v\sin\beta_2 \qquad \text{(eq. A.5)}$$

where

$$C_k = \left[(E_k^2-A_k(0))/b_k(0)\right]^{1/n_k(o)} \quad ; \quad \text{for } k=1,2.$$

Equations A.4 and A.5 are then solved simultaneously for the velocity components u and v;

$$u = \Delta^{-1}\left[C_1\sin\beta_2 - C_2\sin\beta_1\right] \qquad \text{(eq. A.6)}$$

and

$$v = \Delta^{-1} [C_2 \cos\beta_1 - C_1 \cos\beta_2] \qquad \text{(eq. A.7)}$$

where

$$\Delta = \cos\beta_1 \sin\beta_2 - \sin\beta_1 \cos\beta_2,$$

from which Q_x and γ are readily determined as:

$$Q_x = [u^2 + v^2]^{1/2}$$

$$\gamma = \text{TAN}^{-1} (v/u).$$

The COSLAW technique is considered to adequately determine Q_x and γ for values of $\gamma \leq |12^\circ|$. Figures A.1 and A.2 show the difference between calculated values of γ (using COSLAW) and the γ_c value of the calibration data. Note that this difference is both speed and angle dependent. Tables 1 and 2 present the numerical values of these differences as well as the percent difference between the calculated and measured speed values for both slant wires. For $\gamma < |12^\circ|$ these differences for both wires are relatively constant and adequately close to zero at all flow speeds. This is the angle-range for which the COSLAW technique is considered valid in determining values for Q_x and γ. It is interesting to note that the COSLAW probides a relatively accurate Q_x value for a much larger range of γ values; the relative errors in the u and v calculations are self-compensating since

$$Q=(u^2+v^2)^{1/2}.$$

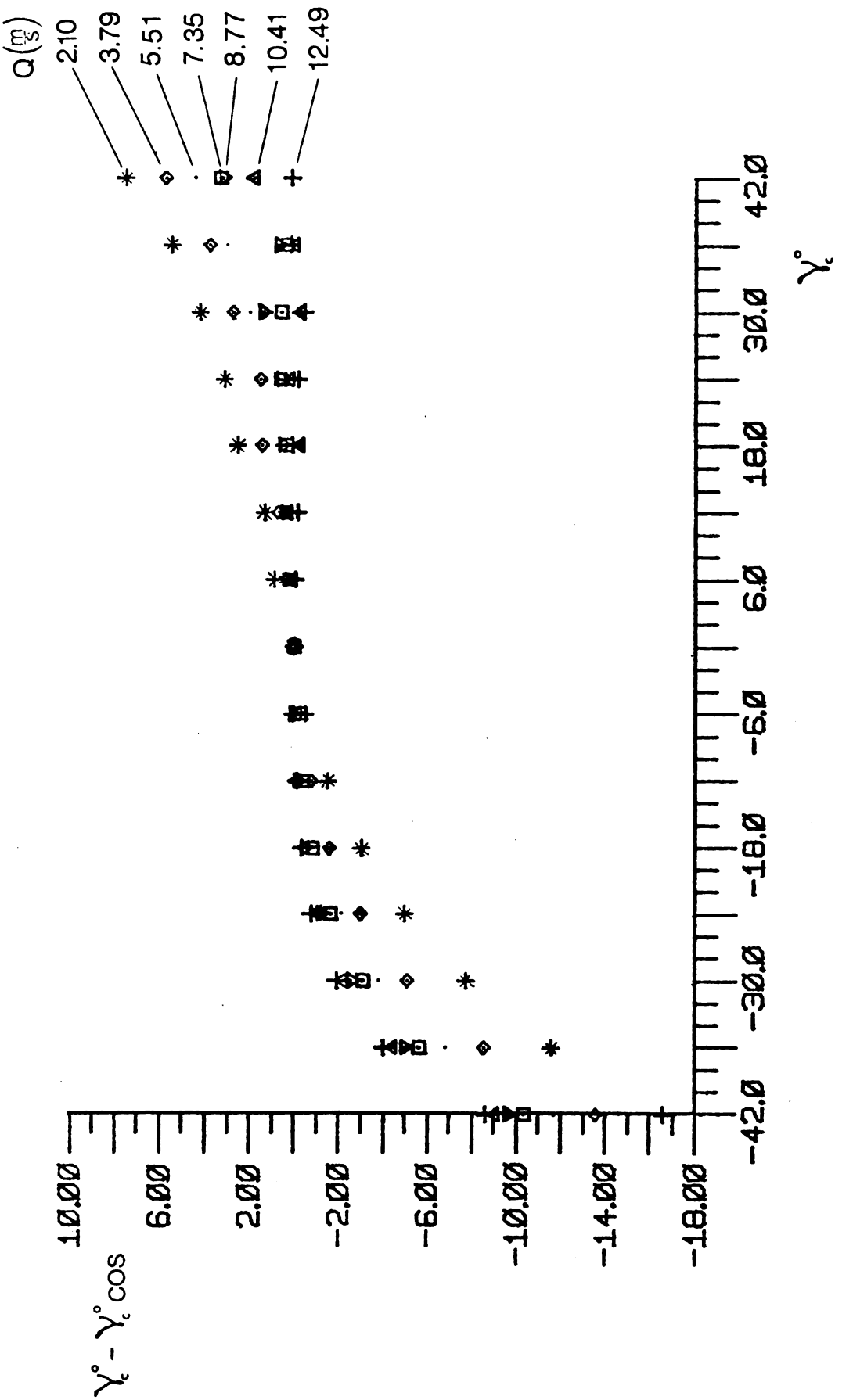

Figure A.1. Difference between True Angle and Angle Calculated using the COSLAW for Wire 1

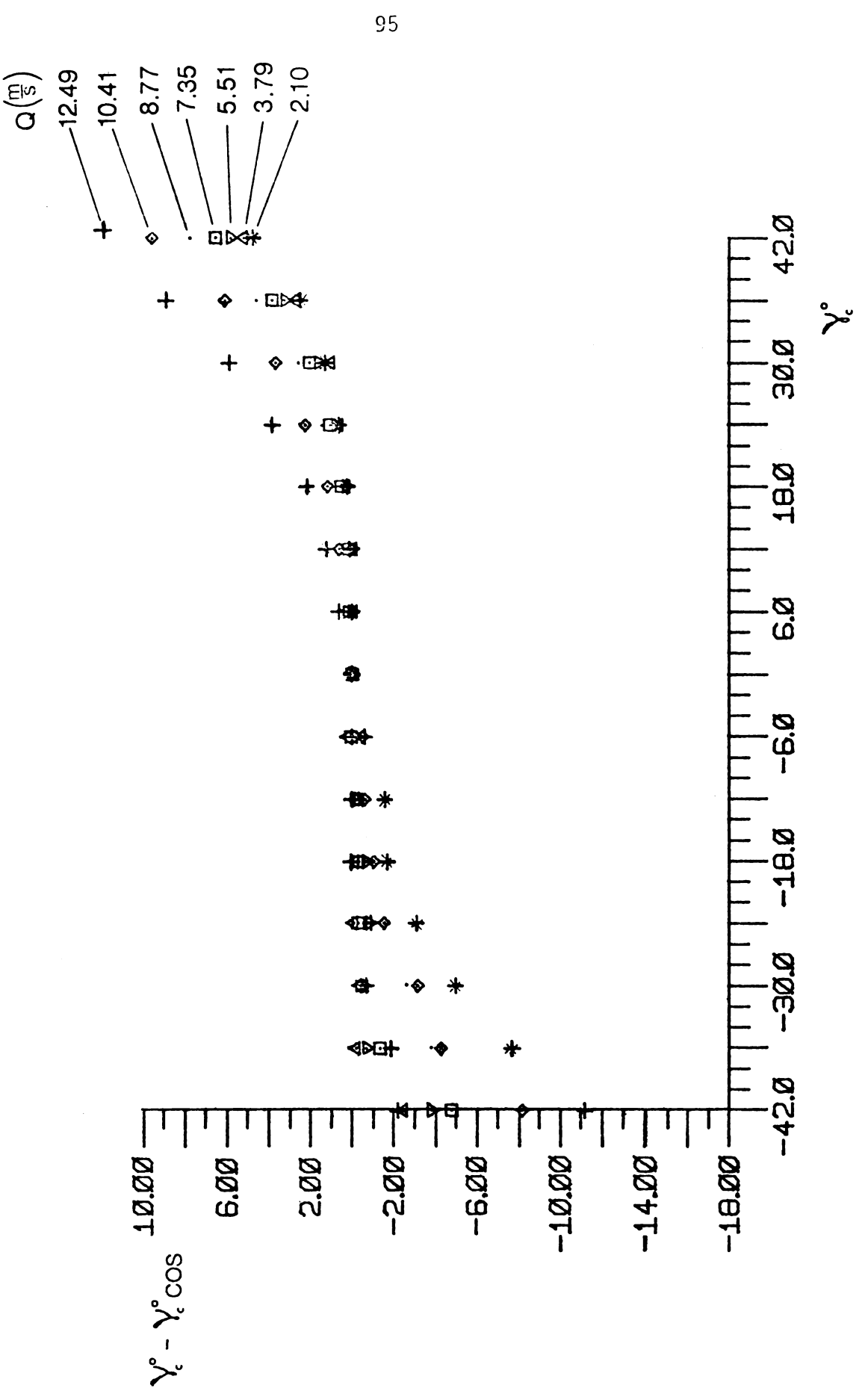

Figure A.2. Difference between True Angle and Angle Calculated using COSLAW for Wire 2

TABLE 1
ACCURACY OF COSLAW (slant wire 1)

a. $[(Q_c - Q_{cos})/Q_c] * 100.$

γ \ m/s	12.489	10.405	8.755	7.357	5.503	3.779	2.100
-42.0	-469.914	-494.155	-527.021	-562.641	-639.027	-735.523	-902.556
-36.0	94.331	105.821	119.238	132.778	162.127	200.397	272.802
-30.0	18.240	21.143	25.156	29.918	36.607	48.257	73.879
-24.0	4.533	6.206	7.563	9.685	12.847	17.368	29.623
-18.0	1.345	1.926	2.378	3.434	4.271	6.363	13.032
-12.0	0.263	0.483	0.881	1.136	1.592	2.169	5.004
-6.0	-0.269	0.420	0.123	0.590	0.347	0.143	1.448
0.0	-0.160	0.048	0.282	-0.074	0.098	-0.342	0.146
6.0	-0.064	-0.029	-0.098	-0.396	-0.466	-0.926	-1.250
12.0	0.094	-0.289	-0.214	-0.529	-0.759	-1.239	-1.612
18.0	-0.220	0.327	-0.234	-0.414	-0.739	-1.853	-2.585
24.0	0.025	-0.076	-0.185	-0.552	-1.024	-1.606	-2.577
30.0	0.149	0.248	-0.576	-0.400	-1.184	-2.112	-2.733
36.0	-0.189	0.079	0.015	-0.214	-1.288	-2.136	-2.596
42.0	-0.164	-0.408	-0.609	-1.005	-1.223	-2.165	-2.464

b. $\gamma_c - \gamma_{cos}$

-42.0	-8.580	-9.011	-9.595	-10.279	-11.671	-13.509	-16.570
-36.0	-3.976	-4.443	-4.989	-5.595	-6.823	-8.511	-11.562
-30.0	-1.902	-2.177	-2.563	-3.104	-3.778	-5.064	-7.690
-24.0	-0.783	-1.026	-1.211	-1.630	-2.129	-2.978	-4.961
-18.0	-0.353	-0.439	-0.489	-0.822	-0.977	-1.581	-3.040
-12.0	-0.130	-0.133	-0.183	-0.372	-0.459	-0.776	-1.500
-6.0	0.042	-0.145	0.062	-0.259	-0.097	-0.189	-0.507
0.0	0.000	0.000	0.000	0.000	0.000	0.000	0.000
6.0	-0.057	0.046	0.226	0.192	0.335	0.349	0.826
12.0	-0.188	0.248	0.364	0.335	0.627	0.659	1.277
18.0	0.055	-0.259	0.472	0.313	0.764	1.374	2.436
24.0	-0.220	0.146	0.547	0.561	1.297	1.464	3.054
30.0	-0.498	-0.321	1.319	0.512	1.944	2.654	4.155
36.0	0.069	-0.072	0.608	0.323	2.923	3.708	5.365
42.0	0.017	1.713	3.099	3.227	4.323	5.629	7.410

TABLE 2
ACCURACY OF COSLAW (slant wire 2)

a. $[(Q_c - Q_{cos})/Q_c] * 100.$

γ \ m/s	12.489	10.405	8.755	7.357	5.503	3.779	2.100
-42.0	-0.121	-0.216	-0.720	-1.046	-1.272	-1.619	-2.806
-36.0	-0.418	0.021	-0.382	-0.690	-0.862	-1.370	-2.949
-30.0	-0.182	-0.102	-0.457	-0.534	-0.947	-1.541	-2.661
-24.0	-0.445	0.025	-0.768	-0.513	-0.271	-1.011	-2.181
-18.0	0.154	-0.035	-0.774	-0.555	-0.540	-0.907	-1.547
-12.0	0.113	-0.106	-0.529	-0.569	-0.223	-0.637	-1.801
-6.0	0.112	0.318	-0.477	-0.239	-0.130	-0.660	-0.895
0.0	0.125	0.064	-0.203	-0.325	0.350	0.028	-0.030
6.0	0.118	-0.034	-0.282	-0.154	0.371	0.649	1.150
12.0	0.303	-0.073	-0.240	0.060	0.780	1.502	3.016
18.0	0.762	0.929	0.722	1.330	2.720	3.834	6.867
24.0	2.748	2.675	3.101	4.240	6.454	9.706	16.391
30.0	7.950	6.015	9.450	12.230	16.398	22.673	36.206
36.0	25.541	27.844	32.855	38.611	47.778	62.488	90.421
42.0	137.173	148.778	167.202	187.173	223.572	273.954	363.872

b. $\gamma_c - \gamma_{cos}$

-42.0	-2.189	-2.418	-3.793	-4.775	-8.041	-8.135	-11.185
-36.0	-1.858	-0.164	-0.657	-1.292	-3.764	-4.259	-7.688
-30.0	-0.661	-0.360	-0.550	-0.456	-2.616	-3.126	-4.972
-24.0	-0.852	-0.059	-0.847	-0.286	-0.924	-1.531	-3.065
-18.0	0.033	-0.113	-0.648	-0.263	-0.998	-1.051	-1.688
-12.0	-0.011	-0.152	-0.291	-0.218	-0.508	-0.591	-1.555
-6.0	-0.010	0.182	-0.197	0.062	-0.342	-0.491	-0.617
0.0	-0.000	-0.000	-0.000	-0.000	-0.000	-0.000	-0.000
6.0	-0.003	-0.046	-0.037	0.081	0.010	0.293	0.558
12.0	0.067	-0.052	-0.014	0.146	0.162	0.559	1.159
18.0	0.189	0.257	0.276	0.494	0.704	1.136	2.070
24.0	0.590	0.587	0.746	1.032	1.373	2.190	3.741
30.0	1.238	0.941	1.533	1.999	2.542	3.609	5.815
36.0	2.419	2.647	3.161	3.732	4.522	5.992	8.735
42.0	4.689	5.094	5.753	6.457	7.647	9.437	12.610

APPENDIX B

COORDINATE TRANSFORMATION

The spatially averaged values, associated with a given micro-domain, are in terms of the local s-n (micro-domain) coordinates. A coordinate transformation is used to express the values in terms of the laboratory coordinates; x-y. From Spencer[29], the transformation for the velocity components in tensor notation is given by;

$$x_i^* = x_j \, e_{ji} \qquad \text{(eq. B.1)}$$

where * quantities represent the value in the new corrdinates; x-y, non-starred values are in terms of the original coordinates; s-n,
and e_{ki} and e_{lk} are direction cosines.

By setting i=1 and i=2, the velocity components u and v may be expressed in terms of u_s and v_n as;

$$u^* = u_s \cos\alpha + u_n \sin\alpha \qquad \text{(eq. B.2)}$$

$$v^* = -u_s \sin\alpha + u_n \cos\alpha. \qquad \text{(eq. B.3)}$$

Similarly, the transformation for the spatial derivatives in tensor notation is given by;

$$A^*_{i,j} = e_{ki}\, e_{lj}\, A_{k,l} \qquad \text{(eq. B.4)}$$

To express one spatial derivative in the new coordinates, four spatial derivatives in the s-n system must be converted to x-y corrdinates. The following sequence presents the transformations to obtain $\partial u/\partial y$ and $\partial v/\partial x$. Specifically, $\partial u/\partial y$ may be written as;

$$\partial u_1/\partial x_2 = e_{11}e_{12}\,\partial u_1/\partial x_1 + e_{21}e_{12}\,\partial u_2/\partial x_1 + e_{11}e_{22}\,\partial u_1/\partial x_2 + e_{21}e_{22}\,\partial u_2/\partial x_2 \qquad \text{(eq. B.5)}$$

which is determined from setting i=1 and j=2 in eq. B.4.

$$\partial u/\partial y = -\cos\alpha \sin\alpha\, \partial u_s/\partial s - \sin^2\alpha\, \partial u_n/\partial s + \cos^2\alpha\, \partial u_s/\partial n + \sin\alpha \cos\alpha\, \partial u_n/\partial n \qquad \text{(eq. B.6)}$$

$$\partial u/\partial y = \cos^2\alpha\, \partial u_s/\partial n - \sin^2\alpha\, \partial u_n/\partial s + \sin\alpha \cos\alpha\, (\partial u_n/\partial n - \partial u_s/\partial s) \qquad \text{(eq. B.7)}$$

Similarly by setting i=2 and j=1 in eq. B.4 the equation for $\partial v/\partial x$ is

$$\partial u_2/\partial x_1 = e_{12}e_{11}\partial u_1/\partial x_1 + e_{22}e_{11}\partial u_2/\partial x_1 +$$

$$e_{12}e_{21}\partial u_1/\partial x_2 + e_{22}e_{21}\partial u_2/\partial x_2 \qquad \text{(eq. B.8)}$$

$$\partial v/\partial x = -\sin\alpha\cos\alpha\,\partial u_s/\partial s + \cos^2\alpha\,\partial u_n/\partial s - \sin^2\alpha\,\partial u_s/\partial n + \cos\alpha\sin\alpha\,\partial u_n/\partial n \qquad \text{(eq. B.9)}$$

$$\partial v/\partial x = \cos^2\alpha\,\partial u_n/\partial s - \sin^2\alpha\,\partial u_s/\partial n + \sin\alpha\cos\alpha\,(\partial u_n/\partial n - \partial u_s/\partial s) \qquad \text{(eq. B.10)}$$

where

$$\alpha = \theta + \gamma. \qquad \text{(eq. B.11)}$$

Since the vorticity is coordinate independent (perpendicular to the x-y plane), the equation for its value should be the same in terms of s-n and x-y. By the addition of eqs. B.7 and B.10, it can be shown that the vorticity vectors in the s-n and x-y coordinates, to have the same form:

$$\partial v/\partial x - \partial u/\partial y = \partial u_n/\partial s - \partial u_s/\partial n. \qquad \text{(eq. B.12)}$$

APPENDIX C

RESPONSE FUNCTION COEFFICIENTS

For each of the four wires of the vorticity probe the response function, i.e. modified Collis and Williams equation, was determined at every calibration pitch angle γ_c. The set of coefficients, [ABn], from each of these functions are presented in Figures C.1–C.4 as a function of γ_c, for each of the wires.

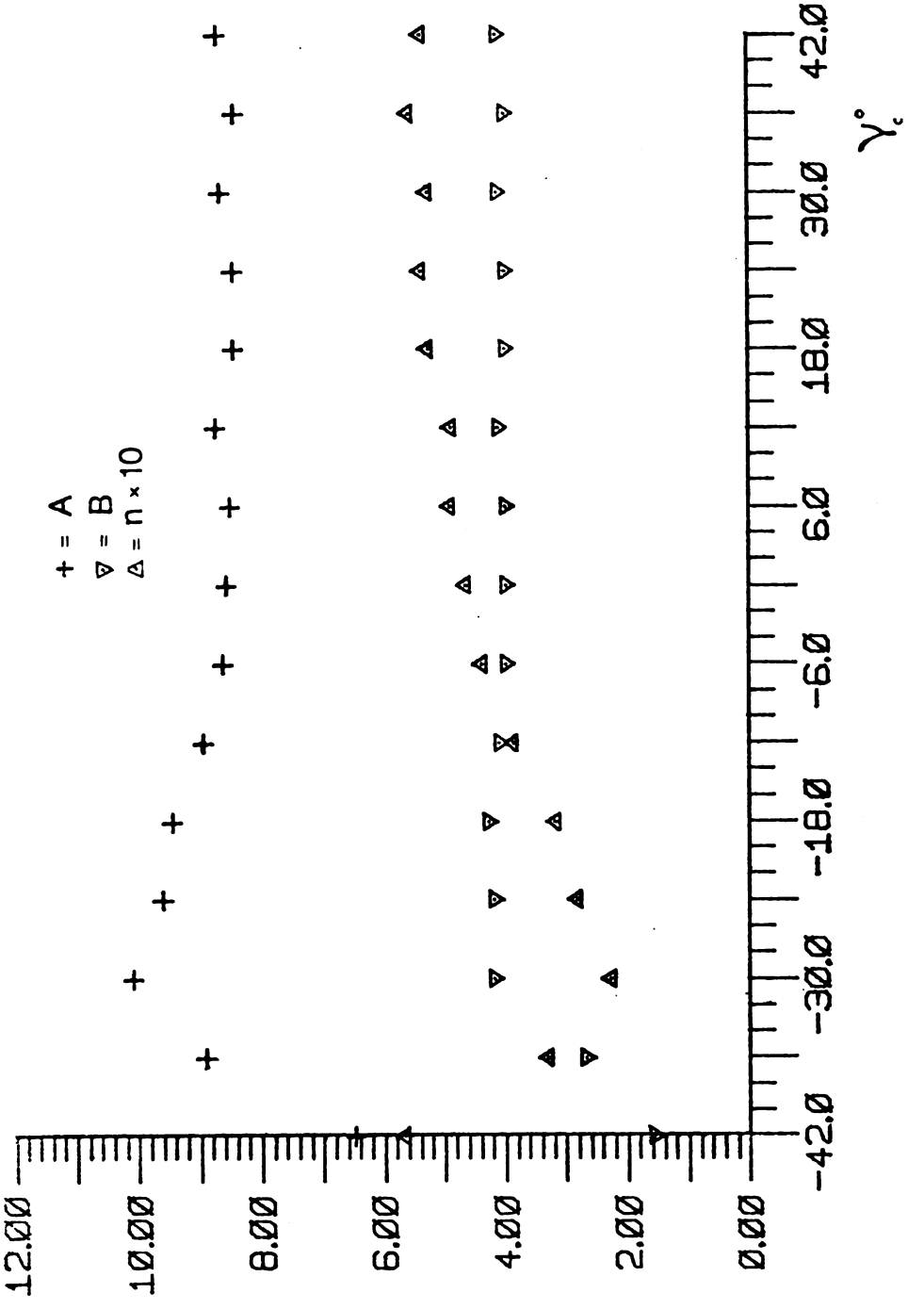

Figure C.1. Variation of ABn Coefficients with γ for Wire 1

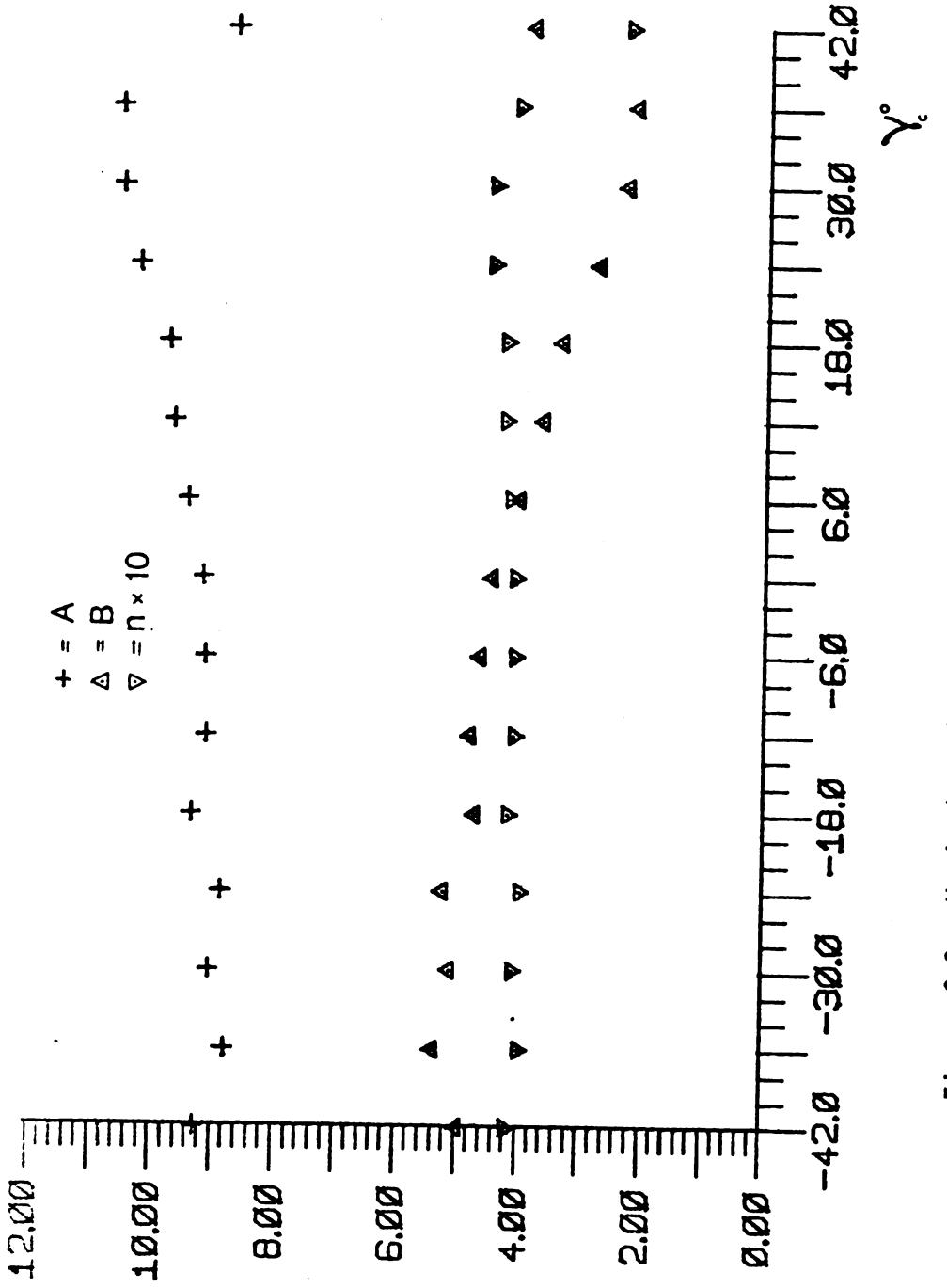

Figure C.2. Variation of ABn in Coefficients with γ for Wire 2.

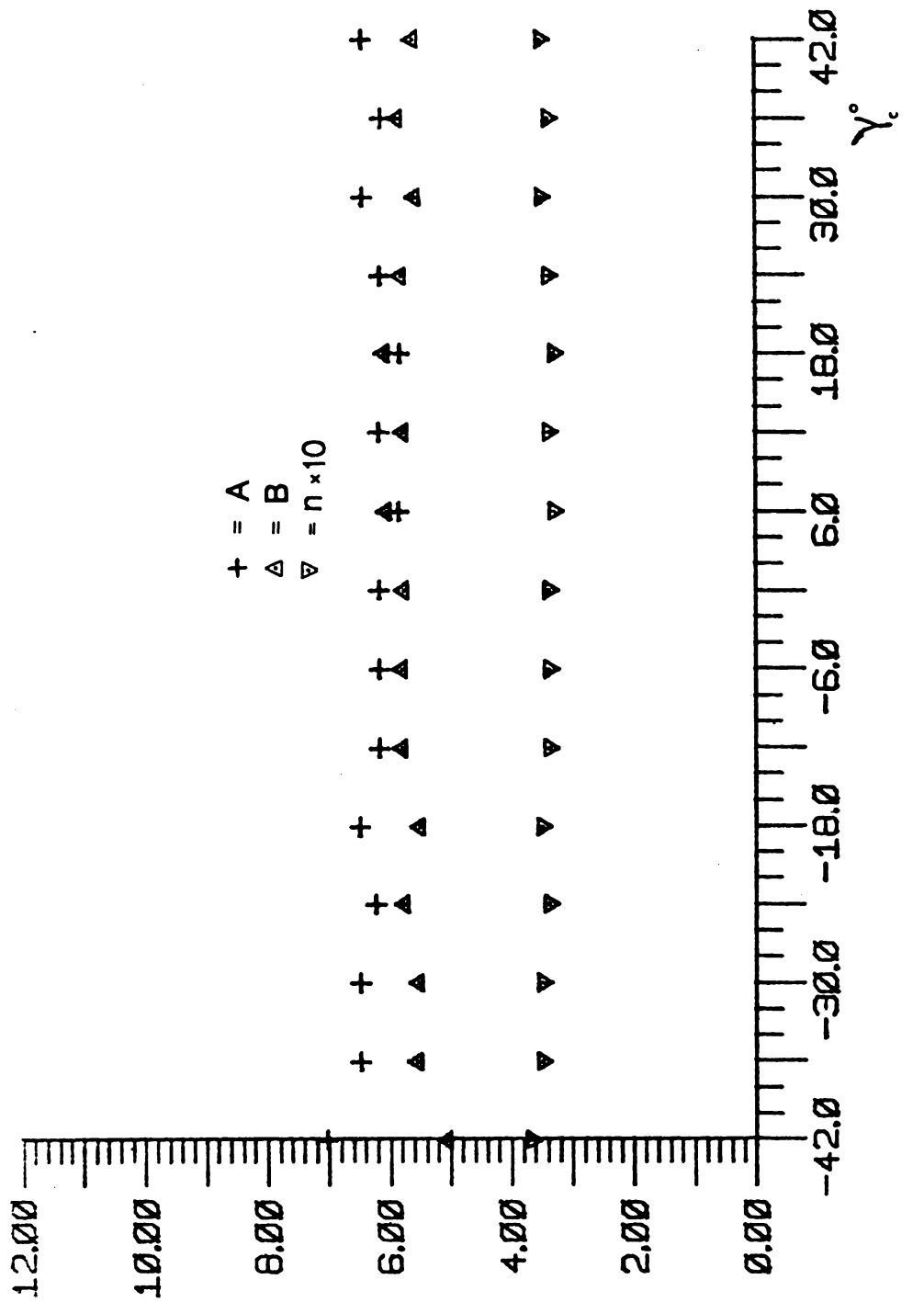

Figure C.3. Variation of ABn Coefficients with γ for Wire 3.

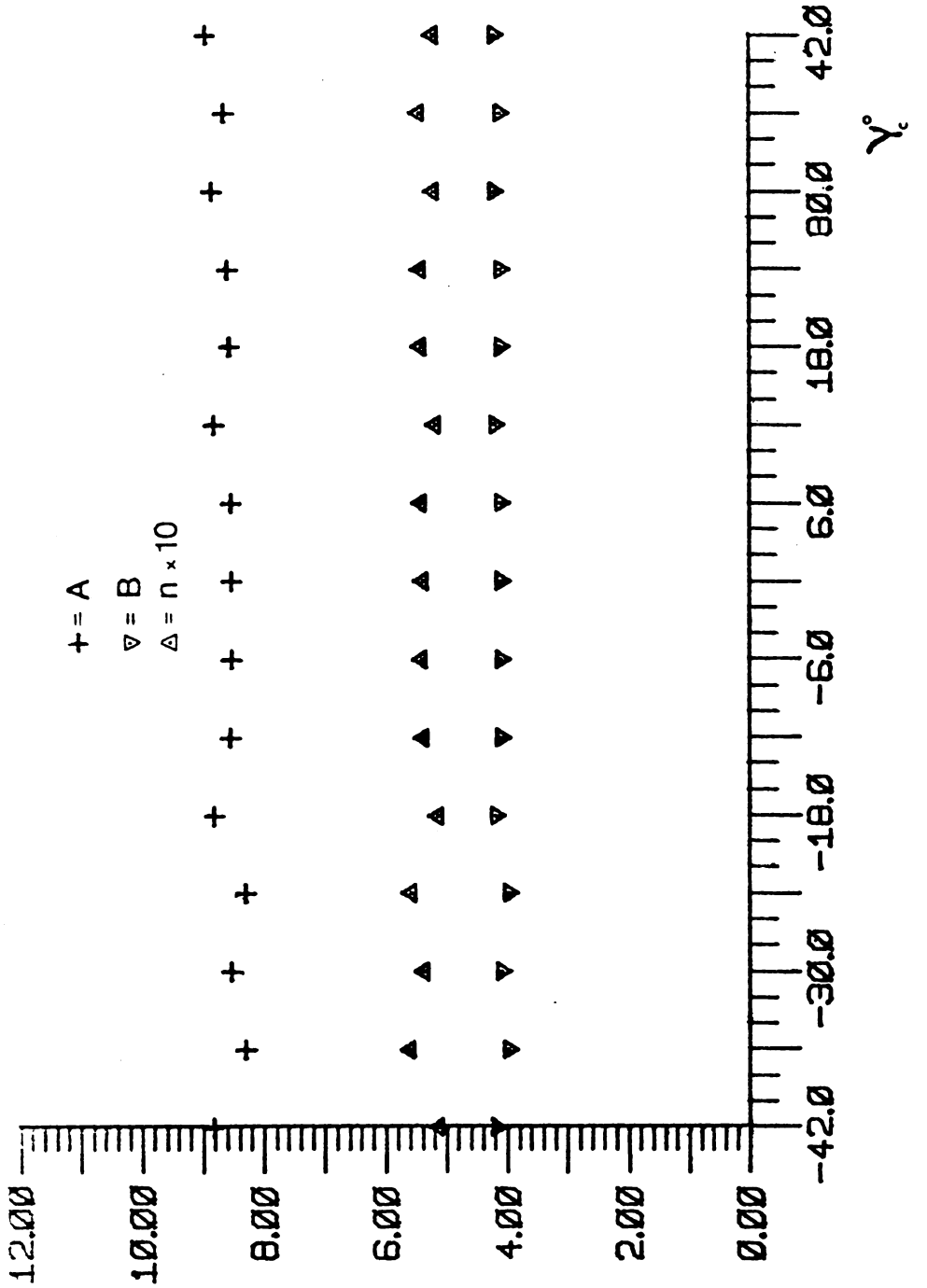

Figure C.4. Variation of ABn Coefficients with γ for Wire 4

REFERENCES

REFERENCES

1. Corrsin, S. and Kistler, A.L. NACA Report No. 1244, 1955.

2. Kibens, V., Kovasznay, S. G. and Oswald, L. J. "Turbulent - Nonturbulent Interface Detector." Rev. Sci. Instrum. 45, No. 9 (1974).

3. Hardin, J. C. "Analysis of Noise Production by an Orderly Structure of Turbulent Jets." NASA TND-7242, L8843 (1973).

4. Willmarth, W. W. and Bogar, T. J., "Survey and New Measurements of Turbulent structure near the wall," Physics of Fluids 20 (1977).

5. Brown, G. L. and Roshko, A. "On Density Effects and Large Structure in Turbulent Mixing Layers." J. of Fluid Mech. Vol 64 (1974):775-816.

6. Blackwelder R. F. and Eckelmann H. "Streamwise Vortices Associated with the Bursting Phenomenon" J. of Fluid Mech. Vol 94 (1979):577-594.

7. Signor, D. B. and Falco, R. E. "Reynolds Number Scaling of Coherent Motions in Turbulent Boundary Layers," APS Bulletin, Vol 27, No. 9 , GA1, November 1982.

8. Falco, R. E. and Lovett, J. A. "The Turbulence Production Process Near Walls," APS Bulletin, Vol 27, No 9, GA2, November 1982.

9. Eckelmann, H., Nychas, S., Brodkey, R. and Wallace, J. "Vorticity and Turbulence Production in Patterns Recognized Turbulent Flow Structures" Physics of Fluids 20 (1977):5225-5231.

10. Kovasznay, L. S. G. High Speed Aerodynamics and Jet Propulsion. Princeton: Princeton University Press, 1954, Vol 9, 1954.

11. Uberoi, M. S. and Corrsin S. Progress Report for Contract NAW 5504 for NACA, The Johns Hopkins University, 1951.

12. Kastrinakis, E. G., Eckelmann, H. and Willmarth, W. W. "Influence of the Flow Velocity on a Kovasznay Type Vorticity Probe." Rev. Sci. Instrum. 50(6) (June 1979).

13. Vukoslavcevic, P. and Wallace, J. M. "Influence of Velocity Gradients on Measurements of Velocity and Streamwise Vorticity with Hot-Wire X-Array Probes." Rev. Sci. Instrum. 52(6) (June 1981).

14. Frish, M. B. and Webb, W. W. "Direct Measurement of Vorticity by Optical Probe." J. Fluid Mech. Vol 107 (1981):173-200.

15. Lang, D. B. and Dimotakis, P. E. "Measuring Vorticity Using the Laser Doppler Velocimeter," APS Bulletin, Vol 27, No 9, AD5, November 1982.

16. Foss, J. F. "Transverse Vorticity Measurements," Dynamic Flow Conference, B. W. Hansen, Ed. Skovlunde, Denmark 1979.

17. ____. "Accuracy and Uncertainty of Transverse Vorticity Measurements," APS Bulletin, Vol 21, No 10, EB4, November 1976.

18. ____. "Advanced Techniques for Transverse Vorticity Measurements." Proceedings, 7th Biennial Symposium on Turbulence, J. L. Zakin and G. K. Patterson, Ed. University of Missouri-Rolla, pp. 29-1,12, 1981.

19. Wyngaard, J. C. "Spatial Resolution of the Vorticity Meter and Other Hot-Wire Arrays." J. of Sci. Instrum. Series 2, Vol 2 (1969).

20. Collis, D. C. and Williams, M. J. "Two-Dimensional Convection from Heated Wires at Low Reynolds Numbers." J. of Fluid Mech., 16 (1959):357-358.

21. Bradshaw, P. An Introduction to Turbulence and its Measurements. Pergamon Press, 1971.

22. Drubka, R. E. and Wlezian, R. W. "Efficient Velocity Calibration and Yaw-Relation Truncation Errors in Hot-Wire Measurements of Turbulence," APS Bulletin, 24, No 8, DC6, October, 1979.

23. Bruun, H. H. "Hot-wire Data Corrections in a Low and High Turbulence Intensity Flows." Journal of Physics E: Scientific Instrum. 5, (1972):812-818.

24. Friehe, C. A. and Schwarz, W. H. "Deviations from the Cosine Law for Yawed Cylindrical Anemometer Sensors." Trans. ASME E. J. Appl. Mech. 35 (1968).

25. Burden, B. L. Numerical Analysis (Second Edition). Boston: Brindle, Weber and Schmidt, 1981.

26. VanAtta, C. W. "Multi-Channel Measurements and High-Order Statistics," Proceedings of the Dynamic Flow Conference, pp. 919-914, 1978.

27. Comte-Bellot, G. "Hot-Wire Anemometry." Ann. Rev. Fluid Mech. Vol 8 (1976):209-231.

28. Comte-Bellot, G., Strohl, A., Alcaraz, E. "On Aerodynamic Disturbances Caused by Single Hot-Wire Probes." J. of Applied Mechanics Vol 38 (December 1971):767-774.

30. Spencer, A. J. M., Continuum Mechanics London and New York: Longman, Inc.,;.20, 1980.